Hybrid Power Systems Energy Management Based on Artificial Intelligence

Emad Maher Natsheh

A thesis submitted for the fulfilment of the requirements of the Manchester Metropolitan

University for the degree of Doctor of Philosophy

School of Engineering

Manchester Metropolitan University

July 2013

Abstract

This thesis presents a novel adaptive scheme for energy management in stand-alone hybrid power systems. The proposed management system is designed to manage the power flow between the hybrid power system and energy storage elements in order to satisfy the load requirements based on artificial neural network (ANN) and fuzzy logic controllers.

- The neural network controller is employed to achieve the maximum power point (MPP) for different types of photovoltaic (PV) panels, based on Levenberg Marquardt learning algorithm. The statistical analysis of the results indicates that the R^2 value for the testing set was 0.99.

- The advance fuzzy logic controller is developed to distribute the power among the hybrid system and to manage the charge and discharge current flow for performance optimization.

The developed management system performance was assessed using a hybrid system comprises PV panels, wind turbine, battery storage, and proton exchange membrane fuel cell (PEMFC). To improve the generating performance of the PEMFC and prolong its life, stack temperature is controlled by a fuzzy logic controller.

Moreover, perturb and observe (P&O) algorithm with two different controller techniques - the linear PI and the non-linear passivity-based controller (PBC) - are provided for a comparison with the proposed MPPT controller system. The comparison revealed the robustness of the proposed PV control system for solar irradiance and load resistance changes.

Real-time measured parameters and practical load profiles are used as inputs for the developed management system. The proposed model and its control strategy offer a proper tool for optimizing the hybrid power system performance, such as the one used in smart-house applications.

The research work also led to a new approach in monitoring PV power stations. The monitoring system enables system degradation early detection by calculating the residual difference between the model predicted and the actual measured power parameters. Measurements were taken over 21 month's period; using hourly average irradiance and cell temperature. Good agreement was achieved between the theoretical simulation and the real time measurement taken the online grid connected solar power plant.

Declaration

No portion of the work referred in this thesis has been submitted in support of an application for another degree or qualification at this, or any other university, or institute of learning.

Date: _____

Signed: _____

This dissertation is dedicated to my parents.

Acknowledgements

The printed pages of this dissertation hold far more than the culmination of years of study. These pages also reflect the relationships with many generous and inspiring people I have met since the beginning of my postgraduate work. The list is long, but I cherish each contribution to my development as a scholar and teacher. It is to them that I owe my deepest gratitude.

First of all, to my loving parents, Maher and Nawal, who raised me with a love of science and supported me in all my pursuits. To my brother, Abdel Razzak, who have always supported, encouraged and believed in me.

To my loving and supportive wife Rola, who loved and supported me during the final critical month of my dissertation, and made me feel like anything was possible.

To my director of study Dr. Alhussein Albarbar, his wisdom, knowledge and commitment to the highest standard inspired and motivated me.

To my invaluable network of supportive, forgiving, generous and loving friends without whom I could not have survived the process: Dalil, Ghalib, Fayad, Mahmoud, Khattab, Laith, Thanandorn, and Amer. Thank you for everything.

And finally, to An-Najah National University and Manchester Metropolitan University for their partial financially support.

Table of Contents

Nomenclature

AFC	Alkaline Fuel Cell
AI	Artificial intelligence
ANN	Artificial neural network
BS	Battery Status
BJTs	Bipolar Junction Transistors
CdTe	Cadmium Telluride
CO	Charge Only
CD	Charge or Discharge
CIGS	Copper Indium Gallium di-Selenide
CIS	Copper Indium Selenide
CST	Crystalline Silicon Cells
DMFC	Direct Methanol Fuel Cell
DO	Discharge Only
EERE	Energy Efficiency and Renewable Energy
EMS	Energy Management Strategy
FLC	Fuzzy Logic Controller
GTO	Gate Turn-Off
HAWT	Horizontal Axis Wind Turbines
HOGA	Hybrid Optimization by Genetic Algorithms
HOMER	Hybrid Optimization Model for Electric Renewables
HSWPS	Hybrid Solar-Wind Power System
HSWSO	Hybrid Solar-Wind System Optimization
IGBTs	Insulated Gate Bipolar Transistors
IGCT	Integrated Gate Commutated Thyristors
JRC	Joint Research Centre
LCE	Levelised Cost of Energy
Li-Ion	Lithium-Ion
LPSP	Loss of Power Supply Probability
MOSFETs	Metal Oxide Semiconductor Field Effect Transistors
MCFC	Molten Carbonate Fuel Cell
MCT	MOS Controlled Thyristors

MPP	Maximum power point
MPPT	Maximum power point tracking
NiCd	Nickel Cadmium
NiMH	Nickel Metal Hydride
OCV	Open Circuit Voltage
PBC	Passivity Based Controller
PMDC	Permanent Magnet DC
P&O	Perturb and Observe
PAFC	Phosphoric Acid Fuel Cell
PV	Photovoltaic
P	Proportional Action
Pb	Proportional Band
PI	Proportional Integral
PEMFC	Proton Exchange Membrane Fuel Cell
REN21	Renewable Energy Policy Network for the 21st Century
RERL	Renewable Energy Research Laboratory
SCR	Silicon Controlled Rectifier
SOFC	Solid Oxide Fuel Cell
SOC	State Of Charge
SMPS	Switching Mode Power Supply
TRIAC	Triode AC
USDE	United States Department of Education
VAWT	Vertical Axis Wind Turbines
WT	Wind Turbine

List of Figures

List of Tables

List of Publications Based on this Work

Natsheh, E.M., Natsheh, A.-R., & Albarbar, A. (2013) *Intelligent Controller for Managing Power Flow within Standalone Hybrid Power Systems*, IET Science, Measurement & Technology, In Press.

Natsheh, E.M., & Albarbar, A. (2013) *Hybrid Power Systems Energy Controller Based on Neural Network and Fuzzy Logic*, Smart Grid and Renewable Energy, 4, (2), pp. 187-197.

Natsheh, E.M., & Albarbar, A. (2012) *Solar Power Plant Performance Evaluation: Simulation and Experimental Validation*, Journal of Physics: Conference Series, 364, (1), pp. 1-13.

Natsheh, E.M., & Albarbar, A. (2011) *Photovoltaic Model with MPP Tracker for Standalone /Grid-Connected Applications*, IET Conference on Renewable Power Generation, Edinburgh, UK.

Natsheh, E.M., & Albarbar, A. (2011) *PV System Monitoring and Performance of a Grid Connected PV Power Station Located in Manchester-UK*, IET Conference on Renewable Power Generation, Edinburgh, UK.

Natsheh, E.M., Albarbar, A., & Yazdani, J. (2011) *Modelling and Control for Smart Grid Integration of Solar/Wind Energy Conversion System*, 2nd IEEE PES International Conference and Exhibition on Innovative Smart Grid Technologies, Manchester, UK.

Chapter 1

Introduction

*This **chapter** provides an overview of **renewable energy sources** (solar and wind energy), **power conditioner units**, and then discuss the **aim and objectives** of the thesis.*

1.1 Motivation

The global warming caused by the abundance of CO_2 in the atmosphere and the limitations of global resources of fossil and nuclear fuel has necessitated an urgent search for alternative sources of energy to meet the future demand. It is also important to find alternative energy sources to minimize the negative environmental impact and to cover the continuously increasing demand of power supply. Figure 1.1 shows the projected availability of fossil and nuclear fuels.
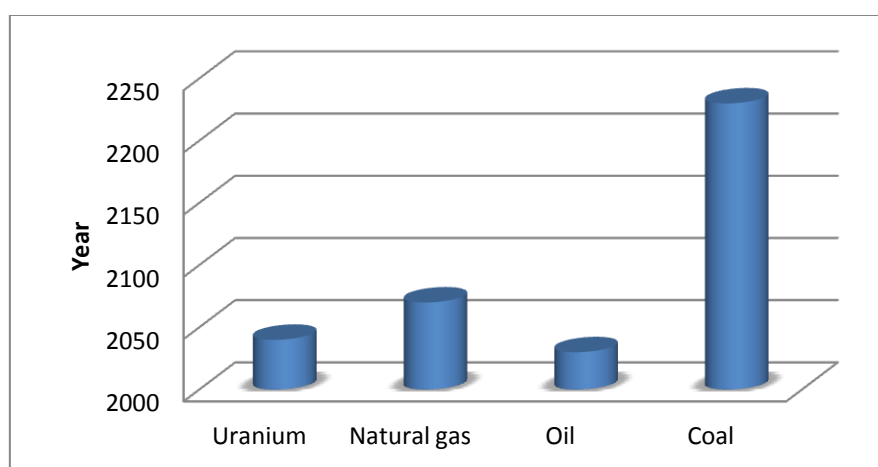
Figure 1.1- Projected availability of fossil and nuclear fuels (based on today's rate consumption (HTE 2012)

Wind, solar and water energy which are non-pollution, free in their availability and renewable are considered as a promising power sources. However, due to their unpredictability and weather dependency, the integration of renewable energy sources to form a hybrid system is an excellent option for distributed energy production. A hybrid power system augments the photovoltaic (PV), wind turbine and fuel cell with a reversible energy storage system so that the overall system can cope with the power demands. The energy storage system can be implemented with either an ultra-capacitor or a rechargeable battery banks. The chief merit of this architecture is that the power-capacity rating of the hybrid system is required to meet the average

demand only, rather than the peak demand. This makes the hybrid power system more cost-effective and energy-efficient than using the fuel cell alone in supplying the required power.

However, one main problem for the hybrid system is related to the management and control of the energy distribution. The dynamic interaction between the load demand and the renewable energy source can lead to critical problems of stability and power quality that are not very common in conventional power systems. Therefore, managing flow of energy throughout the hybrid system is essential to ensure the continuous power supply for the load demand.

In the literature, there are a few studies related to energy management of hybrid power system (Dursun & Kilic 2012). Beside the conventional approaches (Dursun & Kilic 2012; Onar et al. 2008; Mohamed & Koivo 2010; Ahmed et al. 2008; Ipsakis et al. 2009); which have afterwards been proven it's instability in handling various changes in weather conditions (Zhou et al. 2010). Some advanced controlling techniques (such as genetic algorithms, fuzzy logic, and artificial neural networks) exist, which can readily incorporate human intelligence in complicated control system based on human knowledge and experience. The question is can these controlling techniques improve the system performance further (handle various changes dynamically without any major problems) (Zhou et al. 2010), and what's the best application that it can be applied on.

According to the World Bank, more than 2 billion people live in villages that are not yet connected to utility lines (Patel 2006). These villages are the largest potential market for stand-alone hybrid systems for meeting their energy needs.

More, stand-alone hybrid system is technically more challenging to design than the grid-connected system because the use of fuel cells and battery. Accordingly, this

thesis presents an optimized adaptive management strategy for power flow in stand-alone hybrid power systems, based on neural networks and fuzzy logic. The intended study will start by looking into design and evaluation parameters of individual systems. The system consists of solar photovoltaic panels, wind turbine, fuel cell system and batteries for energy storage. System components will be studied and modelled using MatLab/Simulink software packages to verify the I-V and power outputs characteristic.

A major important for the theoretical study of hybrid system is the availability of models, which can be used to study the behaviour of hybrid system and software environment. Therefore, a solar-wind hybrid power system model will be presented. The system will consists of (a) PV panels, to convert the sunlight into direct current, (b) wind turbine, to convert the kinetic energy from the wind into mechanical energy, (c) DC generator, to convert the mechanical energy from the turbine into electrical energy, (d) MPPT, to operate the PV at the maximum power point (MPP), (e) fuel cells, which performs as a backup power source, (f) battery bank, to supply energy to the system when is needed and store it when is not needed, (g) DC/DC converters, to steps-up the voltage to a higher DC voltage, (h) DC/AC inverters, to generate AC waveform from the DC signal, (i) main controller, to ensure the continuous power supply for the load demand. A schematic diagram of a basic hybrid system is shown in Figure 1.2.
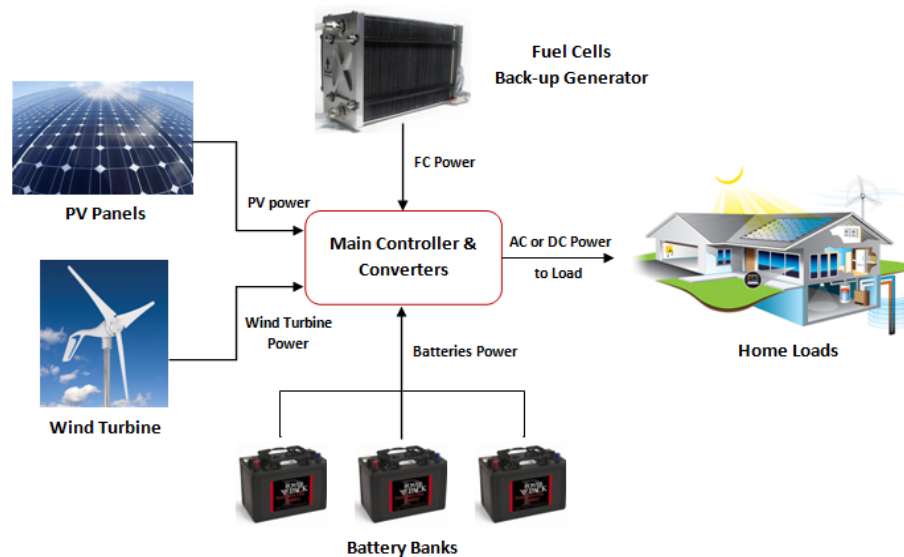
Figure 1.2 - Block diagram of a hybrid power generation system

1.2 Renewable energy sources

Energy is a fundamental aspect to people's life, and is essential not only for individuals but also for various sectors. It can be supplied from various resources which can be divided into two categories; renewable and non-renewable. Typical examples of non-renewable energy sources are petroleum, coal, and natural gas. As for renewable sources, these include energy generated from wind, solar, wave, geothermal, biomass and hydro. Both renewable and non-renewable energy sources can be used to produce secondary energy sources including electricity and hydrogen.

According to the report by the Renewable Energy Policy Network for the 21st Century (REN21) (REN21 2012), about 81% of the world's energy consumption is supplied by fossil fuels, 16% from renewable sources and the rest from nuclear, as illustrated in Figure 1.3. The report indicates that renewable energy replaces fossil and nuclear fuels in four distinct markets: power generation, heating and cooling, transport fuels, and rural/off-grid energy services.
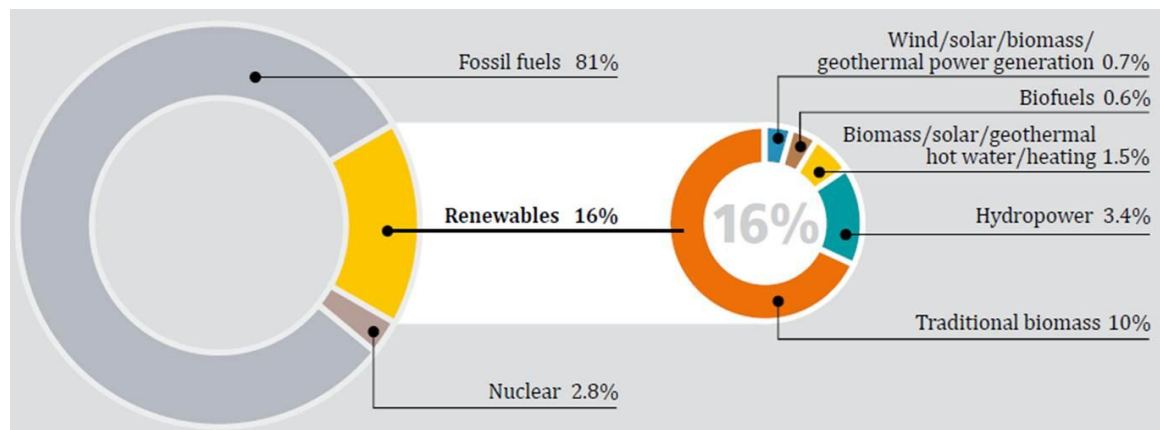
Figure 1.3 - Renewable energy share of global final energy consumption (REN21 2012)

In this work our interest will be in the solar and wind energy.

1.2.1 Solar energy

Solar energy is produced from the sun. The sun forms its energy through thermonuclear reactions that converts hydrogen to helium. This process creates electromagnetic radiation and heat. The electromagnetic radiation (including infra-red light, visible light and ultra-violet radiation) streams out into space in all directions. While the heat remains in the sun, and is instrumental in maintaining the thermonuclear reaction (Miller 2002).

Solar energy can be applied in different applications such as: heating, and cooling. Heating is the business for which solar energy is best suited. Solar heating has a very high efficiency because it requires no energy transformation.

Solar energy can be converted to electricity, besides being used for heating and cooling, so most of our tools can be operated through solar power. The solar collectors that convert radiation into electricity can be either flat-plane collectors or focusing collectors, and the silicon components of these collectors are photovoltaic cells.

Photovoltaic solar cell is made of semiconductor material which converts the solar radiation into direct current electricity. In 1839, a French physicist Alexander discovered the PV effect while he was experimenting with an electrolytic cell made up of two metal electrodes (NREL 2012). Then Bell Laboratories produce the first silicon cell in 1954 (Rivera 2008). Previously due to the high power generation capacity per unit weight, PV technology was used to converts the sunlight into electricity for earth-orbiting satellites. After that matured in space applications, PV technology is now used in different applications ranging from powering remotes sites to feeding utility grids around the world. In the past the photovoltaic application has been limited to remote site and not connected to utility grid, due to the high cost of PV technology. But with the decreasing of PV cost, the PV module marketing has been growing at 25 to 30% annually during the last 5 years. In 2010 solar photovoltaic power (PV) was the leading renewable energy technology in terms of new capacity growth by almost 13,000 MW in Europe (EPIA 2012). The energy output of these new PV installations corresponds to the electricity production of two large coal-fired power plants. At the end of 2010, the cumulative installed capacity of PV in the EU amounted to more than 28,000MW, with an energy output that equals the electricity consumption of around 10 million households in Europe. "The growth of PV has simply been impressive in 2010. Decreasing cost, new applications, strong investor interest and continued political support have contributed to this development, making PV the number one green technology in terms of capacity addition in Europe", said Ingmar Wilhelm, EPIA President. Figure 1.4 shows growth in PV cumulative total capacity from 2000 to 2010. This growth is attributed to the high cost of fossil fuels and the decrease in PV prices.

The global PV market in 2010: approximately 16 GW.
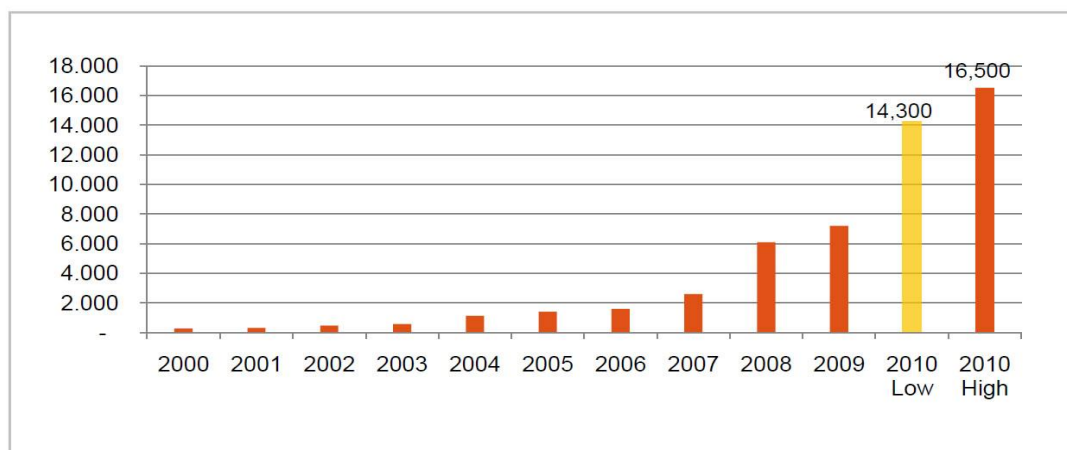
Figure 1.4 - Cumulative Installed PV Power (EPIA 2012)

1.2.2 Wind energy

Wind has always been an energy source used by several civilizations many years ago. The first use of wind power was to make possible the sailing of ships in the Nile River some 5000 years ago. Many civilizations used wind power for transportation and other applications. In the 1700s and 1800s, the Europeans used the wind energy to crush grains and pump water. Recently, there was small interest in using wind energy other than for battery charging for distant dwellings. These low-power systems were quickly replaced once the electricity grid became available. The sudden increases in the price of oil in 1973 stimulate a large number of government funded programs for research and development of wind turbines and other alternative energy technologies. In the United Kingdom's this led to the construction of a series of wind turbines from 100kW to 7.5MW (Rogowsky 2009). Figure 1.5, summarises the history of sizes of leading commercial wind turbines up to the present and illustrates a few concepts for the larges turbines of the near future.
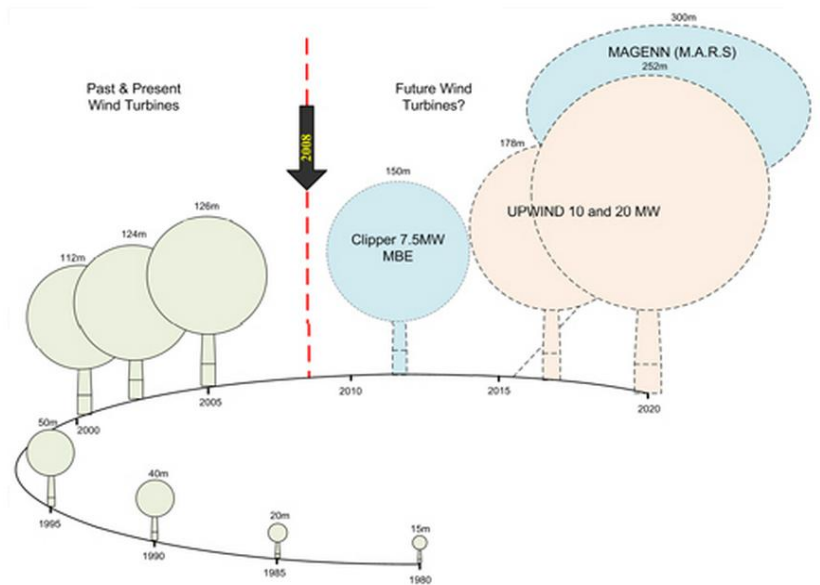
Figure 1.5 – Growth in size of commercial wind turbine designs (WindFacts 2011)

A wind turbine is a machine that converts the kinetic energy from the wind into mechanical energy; therefore the maximum energy delivered not only depends on the machine limits but also on wind speed. On the other hand, windmills convert the power of the wind into mechanical power. It is said that the first windmills on record were built by the Persians in approximately 900 AD (Manwell 2002). These windmills were used for any mechanical task such as water pumping, sawing wood and grinding grain.

In July 1887, the world's first electricity generating wind turbine, which was a battery charging machine was installed by a Scottish scientist James Blyth to light his holiday home in Marykirk Scotland (Price 2004) but it was not until 1951 that the first utility grid-connected wind turbine to operate in the UK was built by John Brown & Company in the Orkney Islands (Price 2004; Musgrove 1976). Today's wind turbines are manufactured in a wide range of vertical and horizontal axis types. The size of these turbines ranges from a few Watts to several Million Watts. Figure 1.6 shows the components of a horizontal axis modern wind turbine. In some cases the generator is

connected directly to the rotor, therefore no gearbox is used. The generator converts the mechanical power in the rotor to electrical power.
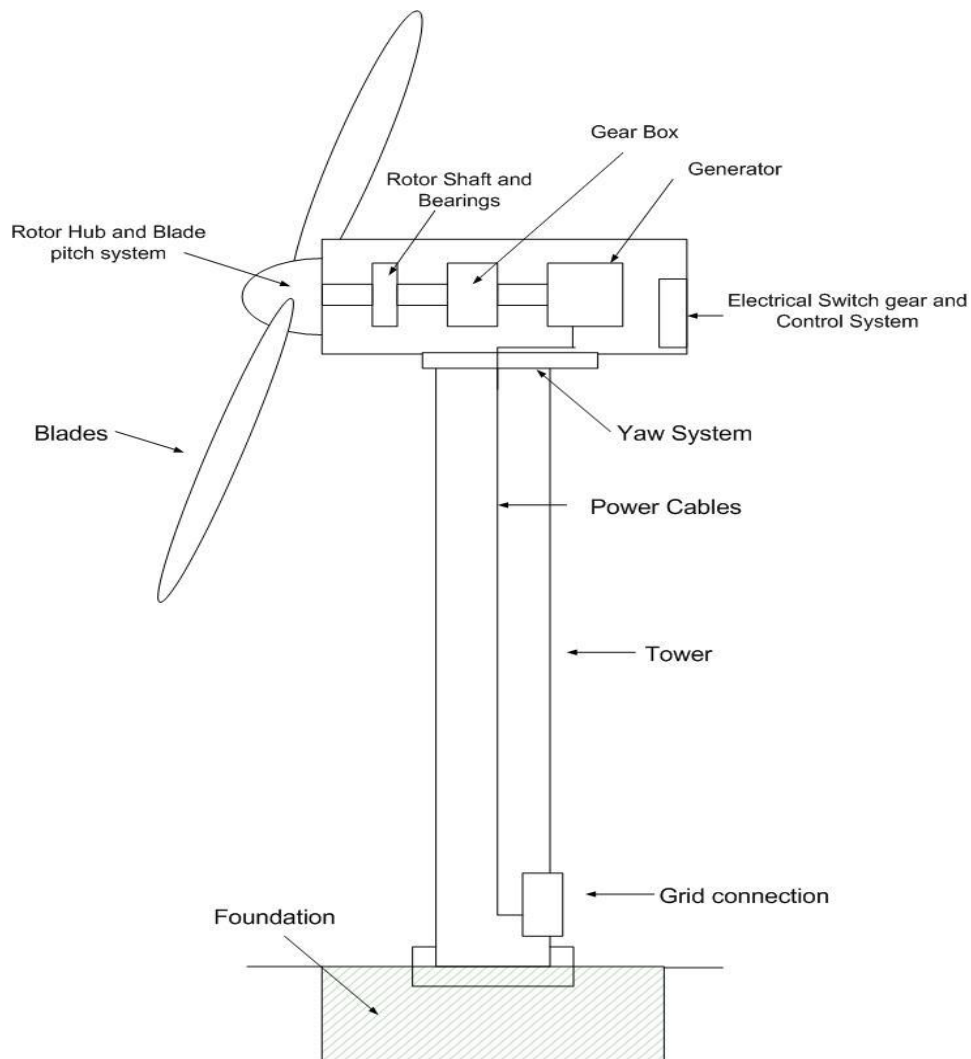
Figure 1.6 - Modern wind turbine components

1.3 Power electronics

1.3.1 Power electronics system

In electronic device most power electronics system divided into two stages:

- Power stage

- Control stage

The power stage is responsible to transfer an amount of power from the input to the output, and the control stage is used to control that amount of power. A block diagram of the power electronic system with *m* sources and *n* loads is given in Figure1.7
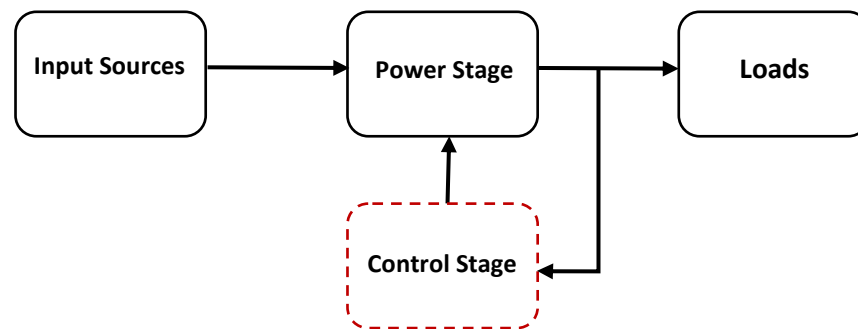
Figure 1.7 - Power electronic system diagram

Where the input sources (electrical inputs) are like current, voltage ... etc., and the output signals are like voltages, currents...etc.

The main function of a power electronic system is to forward the energy to the required load, and the power converter function is to convert the input to the required output energy using switching electronic devices.

In these days there are four conversion circuits that are used in the power electronics circuits:

a) Rectification (AC-DC)

b) Inversion (DC-AC)

c) Conversion (DC-DC)

d) AC-AC converter with same or different frequency.

Our focus in this work will be, on the inversion and conversion.

1.3.2 Power electronics industry

Usually the utility system transmits and generates power at fixed frequency such as 60 Hz or 50 Hz, while keeping the constant voltage at the consumer terminal. Nowadays people are using different electrical product that consumes energy from the AC or DC power supply and converts it to the required form, for example the product that is running on AC, will have a frequency that is similar, higher or smaller than the income frequency, for that there should be a power electronic interface between the utility system and the load, so the power can be controlled.

Most of the power electronic component consists of a converter using a semi-conductor switching device. And as we said before the converters can be classified as rectification (AC-DC), inversion (DC-AC), conversion (DC-DC) and AC-AC converter with same or different frequency. The purpose for using a semi-conductor switching device in the convertor is to increase the efficiency of conversion to the higher value.

1.3.3 Applications for power electronics

Nowadays power electronics is covering a wide range of industrial and commercial applications, including computers, telecommunication, aircraft, transportation, information processing and power utilities.

Additional to that, power electronics application can be found in telecommunication, utility systems, industrial, residential, commercial and transportation fields as shown in Table 1.1

Table 1.1 - Other application, for Power electronic

Telecommunication
• Battery chargers • Power supplies
Utility systems
• High voltage dc transmission (HVDC) • Supplemental energy sources (wind) • Energy storage system
Industrial
• Pumps •Fans •Machine tool (robots) •Lighting •Industrial laser
Transportation
•Battry charger for electric vehicles
Residential
•Ligithing •Electronics (personal computer, other entertainment equipments) •Air conditioning •Refrigeration and freezers
Commercial
•Lighiting •Computer and office equipments •Heating and air condition

1.4 Research aim and objectives

System control for energy flow and management is an essential part in developing any hybrid power system. However previous studies, as it will be explain in Chapter two, have used conventional approaches for controlling standalone hybrid power systems,

which have afterwards been proven it's instability in handling various changes in weather conditions.

Therefore, the ultimate aim of this research is to develop a control algorithm to be more robust with ability to handle various changes, by establishing new management criteria depending upon informational data and the environmental changes. Hence, the developed algorithm will be designed to optimise the power flow between the hybrid power system and energy storage elements in order to satisfy the load requirements based on artificial neural network (ANN) and fuzzy logic controllers. The ANN algorithm will be used for maximizing the generated power based on maximum power point tracker (MPPT) implementation. The advanced fuzzy logic controller will be developed to distribute the power among the hybrid system and to manage the charge and discharge current flow for performance optimization. The developed management system performance will be assessed using a hybrid system comprises PV panels, wind turbine, battery storage, and proton exchange membrane fuel cell (PEMFC).

To achieve the above mentioned aim, research objectives are outlined below:

a) Review hybrid power system operation principles and methods used for hybrid solar-wind system optimization, i.e. graphical construction method, genetic algorithms, iterative technique...etc.

b) Create a database comprises real weather parameters collected from central Manchester campus; i.e. irradiance, temperature, wind speed.

c) Develop a generalized PV model to be representative to all photovoltaic cell, module, and array.

d) Implement and analyse a MPPT controller model; to operate the PV at the maximum power point (MPP) using P&O algorithm and artificial neural network.

e) Validate and compare the developed model outcome with an empirical data collected from a real PV module

f) Develop a grid connected hybrid system models, with a feedback controller; to balance the average power delivered to the grid.

g) Implement and analyse a standalone solar-wind hybrid system model with energy storage system e.g. battery storage or ultra-capacitor bank.

h) Develop algorithm for optimizing the energy captured by the PV/wind turbine/energy storage hybrid power system using artificial intelligence and adaptive based algorithms.

i) Develop a fuel cell model for the standalone hybrid power system and combine it with the PV-wind turbine model developed in objective (g).

j) Improve the control algorithm in objective (h), to include the fuel cell model that developed in objective (i).

1.5 Simulation environment

In order to meet our goals in this research, we will use the following tools:

- MatLab which is a high-level language that enables the user to perform computationally intensive tasks in an easy-to-use environment where problems and solutions are expressed in familiar mathematical notation.

- SIMULINK which is a commercial tool for modelling, simulating and analyzing multi domain dynamic system.

1.6 Organisation of thesis

The remaining chapters are organized as follows: Chapter two concentrate on reviewing the current state of the local meteorological data generation, modelling, optimization, and control technologies for the hybrid systems and try to find what

further work is needed. Chapters three, four and five introduce the dynamic behaviour of the photovoltaic, wind turbine, and backup power systems (batteries and fuel cells) respectively, and discusses the output characteristics of each. Chapter six present the dynamic simulation models for the hybrid PV/wind turbine/PEM fuel cell/Li-Ion battery power system. The proposed control structure will be addressed in Chapter seven. Here, two different MPPT techniques will be presented (P&O and neural network). To demonstrate the effectiveness of the proposed strategy, simulation results are presented in Chapter eight. Finally, Chapter nine summarizes the work accomplished and proposed future research in this field of work.

Chapter 2

Literature Review

*This **chapter** presents a **review** of the **solar-wind hybrid power system**. The review process includes **meteorological data** generation, **modelling**, **optimization**, and system **control** for **energy flow** and **management**. At the **end** of the review process the **research question** is formulated and the **main purposes** of this **thesis** are established.*

2.1 Overview

The demand for new and environmentally friendly energy system is growing worldwide. Solar and wind energy systems are taking the biggest share from, this current trend (Erdem 2010). To increase the energy reliability, solar and wind energy are used as dual energy sources. However, a drawback, common to solar and wind options, is their unpredictable nature and dependence on weather and climatic changes, and the variations of solar and wind energy may not match with the time distribution of load demand. This shortcoming not only affects the system's energy performance, but also results in batteries being discarded too early. Therefore, a third energy system is needed to improve the energy supply reliability. Thus, the PEM fuel cell ideally fulfills the need for any start up power. When the solar-wind system energy output is insufficient, the fuel cell backups the supply system. However, fuel cell lifetime is less than 2000h for transportation and ~20,000h for stationary fuel cells (Wang 2011). In addition, battery charge-discharge cycle and battery bank energy efficiency gains importance. Therefore, managing flow of energy throughout the hybrid system is essential to increase the operation time of the membrane and to enable continuous energy flow.

This chapter will concentrate on reviewing the current state of the local meteorological data generation, modelling, optimization, and control technologies for the hybrid power systems and try to find what further work is needed.

2.2 Meteorological data collection for feasibility study

The availability and magnitude of solar and wind energy at a particular site are determine by the climatic conditions. For different locations, climatic conditions, including solar radiation, air temperature, and wind speed. For better utilization of the wind and solar energy resources, an analysis of the characteristics of solar radiation and wind conditions at a potential site should be made at the stage of inception.

The long-term system performance is one of the most important design criteria for stand-alone solar-wind hybrid power systems. Weather data containing hourly solar radiation, ambient temperature, and wind speed are required in the performance simulation of these systems. The global whether data could be obtained from local meteorological station and other sources like internet.

Until now, a lot of researches have been done on the analysis of solar and wind energy resources. Among these studies, Mahmoudi (Mahmoudi et al. 2008), analyzed hourly wind speed and solar radiation measurement to assess the feasibility of using hybrid (wind, solar) energy conversion system to meet the energy required to power a seawater greenhouse in the Arabian Gulf country of Oman. Reichling and Kulacki (2008), modelled a hybrid solar wind power plant in south western Minnesota for a two year period, using hourly solar irradiation and wind speed data. Tina (Tina et al. 2006), estimates the long term performance of a hybrid solar-wind power system for both stand-alone and grid linked applications. Dihrab and Sopian (2010), presented a hybrid solar-wind system as a renewable source of power generation for grid-connected application in three cities in Iraq. The proposed system was simulated using MatLab, in which the input parameters for the solver were the meteorological data for the selected area and sizes of PV and wind turbines. Shakya (Shakya et al. 2005), studied the feasibility of stand-alone photovoltaic-wind turbine hybrid

power system incorporating compressed hydrogen gas storage in Australia (Cooma). Cooma has an average annual solar and wind energy availability of 1784 and 932 kWh/m^2, respectively. Elhadidy and Shaahid (2000), analyzed hourly wind speed and solar radiation measurements from a meteorological monitoring station in Dhahran, to study the impact of key parameters such as PV array area, number of wind turbines, and battery storage capacity on the operation of hybrid energy conversion systems, while satisfying a specific annual load of 41,500 kWh. Parametric analysis indicates that with two 10 kW wind turbines together with three days of battery storage and photovoltaic deployment of 30 m^2, the diesel back-up system has to provide about 23% of the load demand. Behave (1999), described a techno-economic study to design a hybrid solar-wind domestic power generating system for a site on the western coast of India. Solar radiation data for Bombay which is very close to the site and for which such data was available were used, while monthly average wind speeds for Alibag were used. Results show that the optimum system would be able to supply 84.16% of the annual electrical energy requirement of the site.

2.3 Modelling of hybrid system components

The hybrid system consists of three power generation systems, photovoltaic arrays, a wind turbine and a fuel cell. The PV and wind turbine are used as the main power generation for the system and the fuel cell is assigned as a backup power generator for the continuous power supply. The control system of the hybrid power system uses the fuel cell as a backup power.

The design of hybrid power system is mainly dependent on the performance of individual components. In order to predict the system's performance, individual components should be modeled first and then their combination can be evaluated to meet the demand reliability.

Over recent years several modelling studies on hybrid renewable energy systems, have been conducted. Among them, Natsheh and Albarbar (2011), developed a solar power plant model which takes cell temperature and solar irradiance as its input parameters and outputs the power under different conditions. The model has been implemented using the MatLab/Simulink software package, and designed with a dialog box like those used in the Simulink block libraries. The proposed PV model has been verified through an experiment set-up to make sure the correctness and usability. Gow and Manning (1999), developed a general PV model which can be implemented on simulation platforms such as PSPICE or SABER and is designed to be of use to power electronics specialists. The model accepts irradiance and temperature as variable parameters and outputs the current–voltage (I–V) characteristic for a PV cell. Tsai (2010), implemented an insulation-oriented PV model using MatLab/Simulink software package. The proposed model takes ambient temperature as reference input and uses the solar insulation as a unique varying parameter. The cell temperature is then explicitly affected by the sunlight intensity.

Kerr and Cuevas (2003) presented a new technique, which can determine the current–voltage (I–V) characteristics of PV modules based on simultaneously measuring the open-circuit voltage as a function of a slowly varying light intensity. And they also have given a detailed theoretical analysis and interpretation of such quasi-steady-state V_{oc} measurements. Borowy and Salameh (1996), presented a simplified model with which the maximum power output could be calculated for one certain PV module once solar radiation on the PV module and ambient temperature were found. Nishioka (Nishioka et al. 2003) analyzed the temperature coefficient dependence of system performance in order to estimate the annual output of a PV system in an actual

operating environment. It was found that the annual output energy of the PV system increased about 1.0% by an improvement of 0.1%/^{o}C of the temperature coefficient.

Natsheh (Natsheh et al. 2011) developed a novel model of smart grid-connected PV/WT hybrid system. The mode comprises photovoltaic array, wind turbine, asynchronous (induction) generator, controller and converters. Solar irradiance, temperature and wind speed data was gathered from a grid connected, 28.8kW solar power system located in central Manchester. Onar (Onar et al. 2008), modeled a hybrid wind/FC/UC power system for a grid independent user with appropriate power flow controllers. The proposed system can be used for non-interconnected remote areas or isolated cogeneration power systems with non-ideal wind speed characteristics. Khan and Iqbal (2005), presented the model of a small wind-fuel cell hybrid energy system and analyzed life cycle of a wind-fuel cell integrated system. The system consists of a 400W wind turbine, a PEMFC, and a power converter. Kim (Kim et al. 2009), developed a grid-connected photovoltaic system model using PSCAD/EMTDC for electromagnetic transient analysis. The simulation model enabled extensive analysis of the control and dynamic performance of a PV system and its interaction behaviour with the power system, such as harmonics, and response to grid faults.

Tremblay (Tremblay et al. 2007), developed a generic battery model for the dynamic simulation of hybrid electric vehicles; they used only the battery state-of-charge (SOC) as a state variable in order to avoid the algebraic loop problem. El-Sharkh (El-Sharkh et al. 2004), presented a dynamic model for a 5 kW PEM fuel cell system to predict the output voltage and study the transient response of a PEM power plant to load changes. The proposed dynamic model includes the fuel cell model, the gas reformer model, and the power conditioning unit.

Chayawatto (Chayawatto et al. 2009), developed a mathematical model of a DC/AC full-bridge switching converter with current control for PV grid-connected system under islanding phenomena; this phenomena occur when the grid system is disconnected for any reason and the distributed generation still supplies to any section of local loads. Zhou (Zhou et al. 2007) presented a simulation model for PV array performance predictions for engineering applications based on the I-V curves of a PV module. Five parameters are introduced to account for the complex dependence of PV module performance upon solar radiation intensities and solar radiation intensities and PV module temperatures. The author claims that this simulation model is simple and especially useful for engineers to calculate the actual performance of the PV modules under operating conditions, with limited data provided by the PV module manufacturers.

2.4 Optimization sizing techniques for hybrid power system

2.4.1 Simulation and optimization software

Simulation software's are the most common tools for evaluating performance of the hybrid systems. By using computer simulation, the optimum configuration can be found by comparing the performance and energy production cost of different system configurations. Several software tools are available for designing of hybrid systems, such as HOMER, HYBRID$_2$, and HOGA.

The Hybrid Optimisation Model for Electric Renewables (HOMER) program has been developed by NREL (National Renewable Energy Laboratory, USA) to optimise hybrid systems. HOMER is a time-step simulator using hourly load and environmental data inputs for renewable energy system assessment. It has been used extensively in previous renewable energy system case studies (Khan & Iqbal 2005;

Zoulias & Lymberopoulos 2007) and in renewable energy system validation tests (Rodolfo & José´ 2005). This program uses the kinetic battery model. However, the program's limitation is that it does not enable the user to intuitively select the appropriate components for a system, as algorithms and calculations are not visible or accessible.

HYBRID$_2$ is hybrid system simulation software developed by the Renewable Energy Research Laboratory (RERL) of the University of Massachusetts. This program is very precise, as it can define time intervals from 10 min to 1 h.

However, NREL recommends optimizing the system with HOMER and then, once the optimum system is obtained, improving the design using HYBRID$_2$.

The Electric Engineering Department of the University of Zaragoza (Spain) developed HOGA which is a hybrid system optimization program. The optimization is carried out by means of genetic algorithms, and can be mono-objective or multi-objective. The simulation is carried out using 1-h intervals, during which all of the parameters remained constant.

2.4.2 Optimization scenarios based on different meteorological data

Some research use long period meteorological data (Koutroulis et al. 2006) or typical meteorological year data (Yang and Lu 2004) for the hybrid system optimizations. The time-series simulation method is the most commonly used renewable energy system optimization routine. Generally, most of the researchers used time-series meteorological station data for feasibility study and design of hybrid systems. The hybrid system's behaviour is calculated based on the time-series meteorological input data, which usually have a resolution of 1-h intervals. Notton (Notton et al. 1996) and Baring-Gould (Baring-Gould et al. 2002), use incremental time-scales of 1 min and 1h, respectively. Notton (Notton et al. 1996), also studied the effect of time step, input

and output power profile on the sizing result of stand-alone solar energy systems based on a simulation procedure. Other applications which also use time-series simulation method include Borowy and Salameh (1994), which developed an algorithm to optimize hybrid solar-wind system; the model proposed was based on a long-term hourly solar radiation and peak load demand data of the site chosen. However, the main disadvantages of the time-series simulation method are that:

- It requires significant computational effort.

- Meteorological data, especially wind data, may not be available for many locations.

Hence, to improve the performance of hybrid system optimizations, many studies have been conducted to decrease the simulation time and the number of variables used. Among them, Celik (2003) developed a predictive algorithm which requiring monthly average values of solar radiations and wind speed. This algorithm enabled the estimation of system performance using simple wind distribution parameters and thus eliminating the necessity for time-series hourly data.

2.4.3 Optimization techniques

Increase the number of optimization variables, will significantly increase the complexity of simulation, resulting in an increase in the time and effort required. Therefore it is very important for designers to find a feasible optimization technique to select the optimum system configurations quickly and accurately.

In this section, various optimization techniques for hybrid solar–wind system will be presented such as probabilistic approach, iterative technique, graphic construction methods, and artificial intelligence methods. Using feasible optimization method, optimum configurations which meet the load requirement can be obtained (Yang et al. 2008).

a) Probabilistic approach

Bucciarelli (1984), proposed a sizing method for treating storage energy variation as a random walk. The probability density for daily decrement or increment of storage level was approximated by a two-event probability distribution[1] (Bagul et al. 1996). Gordon (1987) and Bagul (Bagul et al. 1996) modified this method further by using three-event probabilistic approach to overcome the limitations of conventional two-event approach in matching the actual distribution of the energy generated by hybrid systems.

Tina (Tina et al. 2006) presents a probabilistic approach based on the convolution technique (Karaki et al. 1999) to assess the long-term performance of a hybrid solar-wind power system (HSWPS) for both stand-alone and grid-linked applications. The hybrid system performance is assessed by employing probabilistic models for both wind turbines and PV array. Finally, a numerical example application was included to illustrate the validity of the developed probabilistic model: the results are compared to those resulting from time- domain simulations.

Disadvantage of this probabilistic approach is that it cannot represent the dynamic changing performance of the hybrid system (Zhou et al. 2010).

b) Graphic construction method

Borowy and Salameh (1996), presented a graphical construction technique for figuring the optimum combination of PV array and battery for a stand-alone hybrid solar-wind system, based on using long-term data of solar radiation and wind speed. The load demand for the hybrid system was determined by identifying the load

---

[1] In probability theory, an event is a set of outcomes of an experiment (a subset of the sample space) to which a probability is assigned.

consumption of a typical house in Massachusetts. In this study they assumed that the total cost of the system is linearly related to both the number of PV modules and the number of batteries. The minimum cost will be at the point of tangency of the curve that represents the relationship between the number of batteries and the number of PV modules. Then the optimum sizing of the PV array and the battery bank can be achieved. Markvart (**1996**) presented another graphical technique to optimally design a hybrid solar–wind power generation system by considering the monthly-average solar and wind energy values.

The main disadvantage of this graphic construction method is that only two parameters can be included in the optimization process (Zhou et al. 2010).

c) Iterative technique

Kellogg (Kellogg et al. 1998), presented an iterative optimization method to select the PV module number and wind turbine size using an iterative procedure to make the difference between the demanded and generated power as close to zero as possible over a period of time. From this iterative procedure, several possible combinations of solar-wind generation capacities were obtained. The total annual cost for each configuration is then calculated and the combination with the lowest cost is selected to represent the optimum mixture.

Similarly, Yang (Yang et al. 2007) proposed a Hybrid Solar-Wind System Optimization (HSWSO) model, which utilizes the iterative technique to optimize the capacity sizes of different components of hybrid power generation systems. Three sizing parameters are considered in the simulation, i.e. the rated power of wind system, capacity of PV system, and capacity of the battery bank. The HSWSO model consists of three parts: the model of the hybrid system, the model of Loss of Power Supply Probability (LPSP) and the model of the Levelised Cost of Energy (LCE). For

the desired LPSP value, the optimum configuration can be identified finally by iteratively searching all the possible sets of configurations to achieve the lowest Levelised Cost of Energy.

The disadvantage of this technique is that it usually results in increased computational efforts and sub-optimal solutions (Zhou et al. 2010).

d) Artificial intelligence (AI) methods

AI is a term that in its broadest sense would mean the capability of a machine to imitate intelligent human behaviour (Negnevitsky 2004). Artificial Intelligence methods, such as genetic algorithms, fuzzy logic, and artificial neural networks, are selected because they have shown to be highly applicable to cases of non-linear systems, where the location of the global optimum is a difficult task. Yang (Yang et al. 2008), recommended an optimal sizing method to optimize the configurations of a hybrid solar-wind system employing battery banks. Based on a genetic algorithm, one optimal sizing method was developed to calculate the optimum system configuration that can achieve the customers required loss of power supply probability (LPSP) with a minimum annualized cost of system. The decision variables included in the optimization process are the PV module number, wind turbine number, battery number, PV module slope angle, and wind turbine installation height.

Koutroulis (Koutroulis et al. 2006) proposed a methodology for optimum design of a hybrid solar-wind system. The advantage of this methodology is to suggest the optimum number and type of units ensuring that the 20-year round total system cost is minimized by genetic algorithms subject to the constraint that the load energy requirements are completely covered, resulting in zero load rejection. Rodolfo and Jose´ (2005) developed the HOGA program (Hybrid Optimisation by Genetic

Algorithms), a program that uses a genetic algorithm to design a PV-Diesel system (sizing). The program is developed using C^{++} programming language.

Genetic algorithms are also widely used in the solution of power economic dispatch problems (Li 1998) and the design of large power distribution systems (Ramirez-Rosado & Bernal-Agustin 1998) because of their ability to handle complex problems with linear or non-linear cost functions both, accurately and efficiently. Based on genetic algorithms, Yang et al. designed a hybrid solar–wind power generation project. It was built to supply power for a telecommunication relay station on a remote island, Dalajia Island, along the south-east coast of China (Yang et al. 2008; Yang et al. 2009). The electric use for the normal operation of the telecommunication station includes 1300W GSM base station RBS2206 consumption (24V AC) and 200W for microwave communication (24V DC). According to the project requirement and technical considerations, continuous 1500W energy consumption is chosen as the demand load. In addition, based on the one year data of the project, Zhou (Zhou et al. 2008) studied the system behaviours and good performance observed.

Kalogirou (2004), proposed an optimization model of solar energy systems by using genetic algorithms and artificial neural networks. The system is modelled using a TRNSYS computer program and the climatic conditions of Cyprus. The artificial neural network is trained using the results of a small number of TRNSYS simulations, to learn the correlation of solar-collector area and storage-tank size on the auxiliary energy required by the system from which the life-cycle savings can be determined. Subsequently, a genetic algorithm is used to estimate the optimum configurations, for maximizing life-cycle savings. Al-Alawi (Al-Alawi et al. 2007), developed an optimization mode of a PV-diesel water power system by using artificial neural

networks. The integrated system consists of photovoltaic modules, diesel generator, battery bank for energy storage and a reverse osmosis desalination unit. The proposed artificial neural networking model is designed to predict the diesel generators ON/OFF status at any given specific time and outlines the optimum power needed from the diesel generator at that time.

2.5 System control for energy flow and management

One main problem for the hybrid system is related to the supervision and control of the energy distribution. The dynamic interaction between the load demand and the renewable energy sources can lead to, critical problems of stability and power quality, that are not very common in conventional power systems. Therefore, managing flow of energy throughout the proposed hybrid system is essential to ensure the continuous power supply for the load demand. In the literature, there are a few studies related to power management for a stand-alone hybrid power system (Dursun & Kilic 2012). Among them, Dursun and Kilic (2012), presented three different power management strategies of a stand-alone hybrid power system. The system consists of three power generation systems, photovoltaic (PV) panels, a wind turbine and a proton exchange membrane fuel cell (PEMFC). PV and wind turbine is the main supply for the system, and the fuel cell performs as a backup power source. The proposed power management strategies for the hybrid power system satisfy the load and battery bank SOC. Ahmed (Ahmed et al. 2011) proposed power management strategy studied power fluctuations on a hybrid power system. The hybrid system consists of photovoltaic, wind turbine and fuel cell. The fuel cell is used to suppress the fluctuations of the photovoltaic and wind turbine output power. Onar (Onar et al. 2006) proposed a power management strategy algorithm which dealt with a hybrid (wind turbine/fuel cell) power system containing an ultra capacitor bank. In this

algorithm, when the wind speed is sufficient, the wind turbine can meet the load demand. If the available power from the wind turbine cannot satisfy the load demand, the FC system can meet the excess power demand, while the UC can meet the load demand above the maximum power available from the FC system for short durations. Wang and Nehrir (2008), proposed a power management strategy for an AC-linked hybrid wind/PV/FC energy system. However, all of the early mentioned methods have used conventional approaches for controlling hybrid power systems, such as linear PI controller which has afterwards been proven it's instability in handling various changes in weather conditions (Zhou et al. 2010; Tofighi & Kalantar 2011).

In conventional approach, power electronics based DC-DC converters are used for maximum energy extract from solar energy resource and control the complete hybrid (Reddy & Agarwal 2007)**.** Onar **(**Onar et al. 2008), and Das (Das et al. 2005), designed a PI controller for the power electronics of PV/wind turbine/fuel cell hybrid power system. Tofighi and Kalantar (2011) modelled a power electronic interface between a DC hybrid power source with photovoltaic main source and Li-ion battery storage as the secondary power source based on the Euler Lagrange framework. The dump load consumes the excess power of the PV system whenever the generated power is greater than the load power, and the battery does not need to be charged. The control signals are achieved by passivity-based control. Elgendy (Elgendy et al. 2012), presents a comprehensive analysis evaluation, of the reference voltage perturbation with PI controller and direct duty ratio perturbation techniques, for implementing the P&O MPPT algorithm (see Section 7.3.1). Although the simplicity is the main feature of the direct duty ratio perturbation, they found that it has a slower transient response compared to the indirect method and worse performance at rapidly changing irradiance.

Beside the conventional approaches some advanced control techniques, such as genetic algorithms, fuzzy logic, and artificial neural networks (ANN) exist which can readily incorporate human intelligence in complicated control system based on human knowledge and experience.

Previous studies showed that using the artificial intelligence in the hybrid vehicle can control the FC system within a specified high-efficiency region. Hajizadeh and Golkar (**2007**) presented a control strategy for active power flow in a hybrid fuel cell/battery distributed generation system. The proposed method includes an advance supervisory controller in the first layer which captures all of the possible operation modes. In the second layer, an advance fuzzy logic controller has been developed to distribute the power among the fuel cell and battery system, to satisfy the load power requirement with respect to dynamic restrictions of these systems such as fuel cell temperature, battery state of charge, power demand, fuel cell power, and battery power. Finally in the third layer, there are local controllers to regulate the set points of each subsystems to reach the best performance. Kim (Kim et al. 2008), presented an optimal method to design the relative power capacity between the fuel cell and the battery for a fuel cell/battery hybrid mini-bus. The power distribution is controlled based on the fuzzy logic, and the optimal engine sizes are determined based on the simulator considering with the component models to calculate the efficiency of the fuel cell and battery. Li (Li et al. 2009), presented a fuzzy logic based power management strategy that secures the power balance in a hybrid FC vehicular power system. Fuel cell output power was determined according to the driving load requirement by using fuzzy dynamic decision making algorithm along with fuzzy self-organizing map network.

2.6 Summery

From the above mentioned research works it was noted that few publications were appearing in literature concerning optimising the energy captured by the hybrid power system (Dursun & Kilic 2012). However, all of the early mentioned methods have used conventional approaches (Elgendy et al. 2012; Dursun & Kilic 2012; Onar et al. 2008; Reddy & Agarwal 2007; Ahmed et al. 2011; Ipsakis et al. 2009) for controlling stand-alone hybrid power systems, which has afterwards been proven:

- Its instability in handling various changes in weather conditions (Zhou et al. 2010; Tofighi & Kalantar 2011), with tracking efficiency less than 70% (Esram & Chapman 2007);

- Its slow transient response to irradiance changes and high susceptibility to noise (Elgendy et al. 2012).

Consequently, this resulted in developing other approaches led to more robust algorithm; by establishing new management criteria depending upon informational data and the environmental changes. However the questions that should be considered here are, under various operating conditions can this algorithm:

❖ Increase the tracking response and consequently increase the tracking efficiency;

❖ Remove the power fluctuations caused by the variability of the renewable sources;

❖ Split the power between the power sources to sustain the efficiency of the system;

❖ Maintain the battery SOC at a reasonable level;

❖ Improve the generating performance of the PEMFC and prolong its life.

Previous studies showed that using the artificial intelligence can:

- Find the global optimum hybrid system configuration with relative computational simplicity and without any demerits like other approaches (Zhou et al. 2010): probabilistic, iterative, graphic construction...etc

- Control the FC in the hybrid vehicle system within a specified high-efficiency region (Kim et al. 2008; Li et al. 2009).

Therefore, this research work will focus on developing a novel control algorithm (Natsheh & Albarbar 2013) based on artificial intelligence for the photovoltaic/wind turbine/fuel cell/energy storage hybrid power system. The proposed method will introduces an on-line energy management by a hierarchical controller between four energy sources comprises PV panels, wind turbine, battery storage, and PEMFC. The intended study will start by looking into design and evaluation parameters of individual systems. Chapters three, four and five will introduce the dynamic behaviour of the photovoltaic, wind turbine, and backup power systems respectively. While, Chapter six will presents the dynamic simulation models of individual systems. The proposed control structure will be addressed in Chapter seven.

Chapter 3

Photovoltaic Energy Conversions

*This **chapter** outlines the **dynamic behaviour** of the **photovoltaic** (PV) system and discusses the **nonlinearity** of **PV** output **characteristics**.*

*First, it **summarizes** the **commercial solar cells** used in **PV module**. Second, it shows the **operational mechanism** for crystalline silicon solar cell. Third, it describes the **mathematical modelling** for solar cell, module and array. Finally, it emphasise how to **intensify** the **electricity generated** from the **solar panels**.*

3.1 Introduction to solar energy

The sun is the original source of almost all the energy used on earth. The earth receives a stock ring amount of energy from the sun, as much energy falls on the planet each hour is the total human's population uses in a whole years.

Solar Panels made from photovoltaic cells (or PV for short). Simply broken-down photo means light and voltaic related to the production of electricity. Photovoltaic technology enables the creation of electricity using light. PV cells have at least two layers of semiconductors: one that's positively charged, and one that's negatively charged. When the light shines on the semiconductor the electric field across the junction between these two layers causes electricity to flow. The greater the intensity of light the stronger the electricity flow will be.

Many sorts of PV panels are available for use. The PV tiles which replaced normal tiles are easy to install. Figure 3.1 shows the installation process. They can be installed onto a domestic house easily and they work very simply - any South facing roof is suitable.

The light that hits the panels is converted into clean electricity. This is a silent operation here because there are no moving parts. The electricity generated by the panels comes in the form of a direct current. By installing an inverter, it is converted into alternation current, so it's in sync with the mains electricity and can be used normally. The clean electricity is then fed into the mains by the fuse board. By using meters, the amount of unused electricity generated can be measured and recorded; any spare electricity can be sold back to the electricity supplier.

The amount of energy available from the sun differs depending on one's location. For example, Edinburgh receives 800kWh/m^2; London's share is 1000kWh/m^2; and Madrid gets 1500kWh/m^2 per year (NWS 2012). Although the UK is considered a

country with a wet and cloudy climate, 800kWh/m^2 is enough energy to power an energy efficient home. Only 10m^2 of PV is needed to provide enough electricity to power such a home entirely from solar energy. Therefore, solar photovoltaic provide a simple and practical way for powering buildings with clean energy.

Figure 3.1 - Solar Panel Roof Tiles (BGE 2012)

3.2 Photovoltaic cells and efficiencies

The performance of a solar cell is measured in terms of its efficiency in turning sunlight into electricity. Improving solar cell efficiencies while holding down the cost per cell remains one rather important goal of the PV industry.

PV cells are generally made either from crystalline silicon, thin film, or from other types of technology as shown below.

1) The Crystalline Silicon Technology (CST):

Crystalline silicon cells are made from thin slices cut from a single crystal of silicon (monocrystalline) or from a block of silicon crystals (polycrystalline). CST is the

most common technology representing about 90% of the market today. Its efficiency ranges between 14% and 22%.

Two main types of crystalline cells can be distinguished:

- Monocrystalline (Mono c-Si)

- Polycrystalline (or Multicrystalline) (multi c-Si)

2) Thin film technology:

Thin film modules are made by depositing extremely thin layers of photosensitive materials onto a low-cost backing such as stainless steel, glass or plastic. Thin Film manufacturing processes result in lower production costs compared to the more material-intensive crystalline technology. Such price advantage is counterbalanced by lower efficiency rates (7.3%-10.6%). However, this is an average value and not all Thin Film technologies have the same efficiency.

Four types of thin film modules are commercially available at the moment

- Amorphous Silicon (a-Si)

- Cadmium Telluride (CdTe)

- Copper Indium Selenide, Copper Indium Gallium diSelenide (CIS, CIGS)

- Multi Junction Cells (a-Si/μc-Si)

3) Other cell types:

Several other types of more recently developed photovoltaic technologies have been commercialised or are still at the research level. The main ones are:

- Concentrated photovoltaic: it is solar cells that are designed to operate with concentrated sunlight. They are built into concentrated collectors that use a lens to focus the sunlight onto the cells. The main idea is to use very little of the expensive semiconducting PV material while still collecting as much sunlight as possible.

- Flexible cells: based on a similar production process to thin film cells, when the active material is deposited in a thin plastic, the cell can be flexible. This opens the range of applications, especially for building integration (roofs-tiles) and end-consumer applications.

A Summary for the efficiency of the commercial solar cell is listed in Table 3.1.

Table 3.1 - Commercial Solar Cell Efficiency

Technology	First Generation: Crystalline Silicon		Second Generation: Thin Film				Third Generation: PV	
	Mono	Multi	a-Si	CdTe	CI(G)S	a-Si/µc-Si	CPV	DSSC/ OPV
Cell Efficiency	16-22%	14-18%	5.4-7.7%	9-12.5%	7.3-12.7%	7.5-9.8%	30-38%	2-4%

The cells efficiency decreases with increases in the temperature. Crystalline cells are more sensitive to heat than thin films cells. The output of a crystalline cell decreases approximately 0.5% with every increase of one degree Celsius in cell temperature. For this reason modules should be kept as cool as practically possible. For this reason, amorphous silicon cells may be preferred in very hot conditions because their output decreases by approximately 0.2% per degree Celsius increase.

3.2.1 Energy conversion operation by using crystalline silicon cell

In this work the PV panel used was made from crystalline silicon cells. Figure 3.2 shows the operation of the silicon solar cell. It can be seen that when light strikes the cell, a certain portion of the light's energy is absorbed within the semiconductor material. The energy knocks electrons loose, allowing electrons to flow freely. The

PV cells have one or more electric fields that act to force the electrons freed by light absorption to flow in a certain direction. The P-type silicon ("p" for positive) has free holes which are just the absence of electrons. The N-type silicon ("n" for negative) has free electrons.

P-n junction is created when a p-type semiconductor is joined to an n-type semiconductor. Diffusion current is produced due to the concentration differences of holes and free electrons between the n- and p- regions: electrons flow from the n-side and fill holes on the p-side. This creates a region that is almost devoid of free charge carriers (i.e. free electrons or holes) and is therefore called the depletion zone.
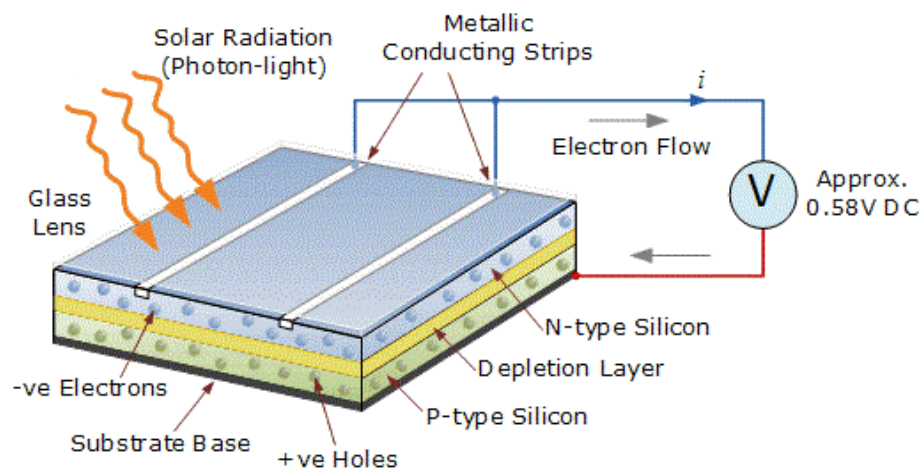
Figure 3.2 - Solar cell diagram (HTE 2012)

There is in the depleted zone a net positive charge on the n-side and a net negative charge on the p-side in the depleted zone. Such situation results in an electric field that opposes any further flow of electrons. The more electrons move from the n-to the p-side, the stronger the opposing field will be, and eventually equilibrium will be reached in which no further electrons are able to move against the electric field.

The equilibrium conditions are disturbed when light hits the solar cell and the so-called inner photo effect creates additional charge carriers that are free to move in the electric field of the depletion zone.

The holes move towards the p-region and the electrons towards the n-region, thus creating an external voltage at the cell. This external voltage in a solar cell is material dependent and does not depend on the cell's surface area.

3.3 The mathematical modeling of solar cell, module and array

As mention in the earlier sections, the solar cell is basically a p-n junction fabricated in a thin wafer or a layer of semiconductor. The electromagnetic radiation of solar energy can be directly converted into electricity through the photovoltaic effect. When exposed to sunlight, photons with energy greater than the band-gap energy of the semiconductor are absorbed and they create some electron-hole pairs proportional to the incident irradiation. Under the influence of the internal electric fields of the p-n junction, these carriers are swept apart and they create a photocurrent which is directly proportional to solar insulation. The PV system naturally exhibits a nonlinear I-V and P-V characteristics which vary according to the solar irradiance and cell temperature.

3.3.1 The solar cell

The common mathematical model for the solar cell has been studied over the past three decades (Phang et.al. 1984). The circuit of the solar cell model is shown in Figure 3.3. The model consists of a photocurrent, diode, parallel resistor (leakage current) and a series resistor.
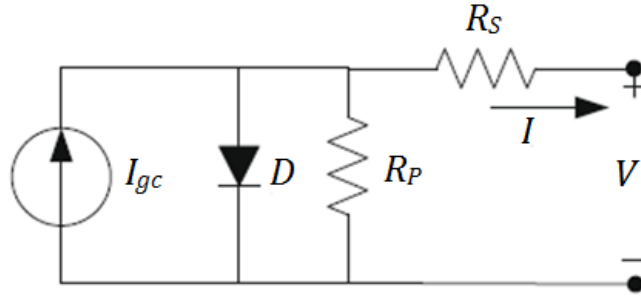
Figure 3.3 - General equivalent circuit of PV cell

The power output of a single diode solar cell is given by (Villalva et al. 2009).

$$P = IV \tag{3.1}$$

According to both the PV cell circuit shown in Figure 3.3 and Kirchhoff's circuit laws, the photovoltaic current can be presented as follows (Villalva et al. 2009):

$$I = I_{gc} - I_{ds}\left[\exp\left(\frac{q}{K_B F T_c}(V + I R_s)\right) - 1\right] - \frac{V + IR_s}{R_p} \tag{3.2}$$

Where I_{gc} is the light generated current; I_{ds} is the dark saturation current dependant on the cell temperature; q is the electric charge (1.6 x 10^{-19} C); K_B is the Boltzmann's constant (1.38 x 10^{-23} J/K); F is the cell idealizing factor; T_c is the cell's absolute temperature; R_s is the series resistance; and R_p is the parallel resistance. The photocurrent (I_{gc}) which mainly depends on the solar irradiation and cell temperature is described as (Villalva et al. 2009):

$$I_{gc} = \left[\mu_{sc}(T_c - T_r) + I_{sc}\right]G \tag{3.3}$$

Where μ_{sc} is the temperature coefficient of the cell's short circuit current; T_r is the cell's reference temperature; I_{sc} is the cell's short circuit current at a 25°C and 1kW/m^2; and G is the solar irradiation in kW/m^2. Furthermore, the cell's saturation current (I_{ds}) varies according to the cell temperature and can be described as (Villalva et al. 2009):

$$I_{ds} = I_{o\alpha} \left(\frac{T_c}{T_r} \right)^3 \exp\left(\frac{q v_g}{K_B F} \left(\frac{1}{T_r} - \frac{1}{T_c} \right) \right)$$ (3.4)

$$I_{o\alpha} = \frac{I_{sc}}{\exp\left(\dfrac{q v_{oc}}{K_B F T_c} \right) - 1}$$ (3.5)

Where $I_{o\alpha}$ is the cell's reverse saturation current at a solar radiation and reference temperature; v_g is the band-gap energy of the semiconductor used in the cell; and v_{oc} is the cells open circuit voltage. The cell ideal factor (F) is dependent on the cell technology as shown in Table 3.2.

Table 3.2 - Ideal factor (F) dependent on the PV technology

Cell Technology	Ideal factor (F)
Si-poly	1.3
Si-mono	1.2
a-Si-triple	5
a-Si:tandem	3.3
a-Si:H	1.8
CdTe	1.5
CIS	1.5
AsGa	1.3

3.3.2 PV module and array

The output power of the solar cell is said to reach approximately 2W at 0.5V. To increase the power, the cells are connected in series-parallel configuration on a module. For photovoltaic systems, the PV array is the group of several PV modules which are connected in series and parallel circuits to generate the required voltage and current. Figure 3.4 shows this configuration.
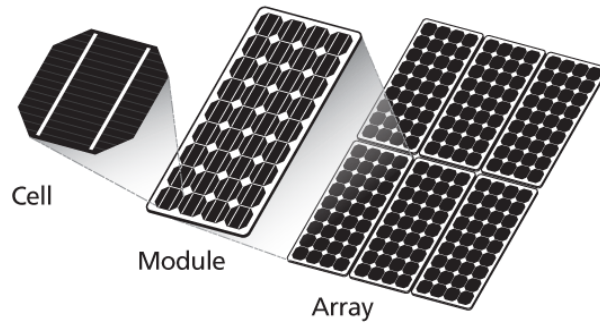
Figure 3.4 - PV cell, module, and array

The equivalent circuit for the solar module arranged in N_P parallel and N_S series branches is shown in Figure 3.5.
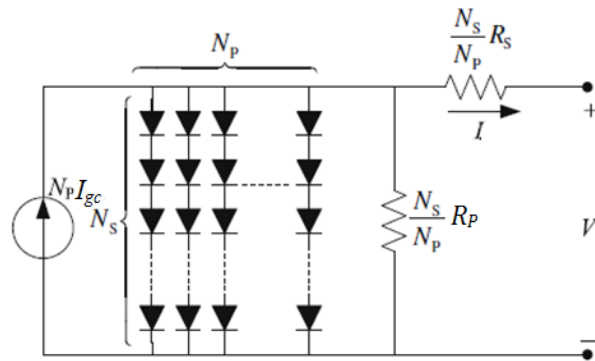
Figure 3.5- General equivalent circuit of PV module

The terminal equation for the current and voltage of the cell module comes out as follows (Kim & Youn 2005):

$$I_{PV} = N_P I_{gc} - N_P I_{ds} \left[\exp\left(\frac{q}{K_B F T_c} \left(\frac{V}{N_S} + I \frac{R_S}{N_P} \right) \right) - 1 \right] - \frac{N_P/N_S V + I R_S}{R_P} \qquad \textbf{(3.6)}$$

Where N_S is the number of cells in series; N_P is the number of cells in parallel.

3.4 PV panel sizing calculation

At this stage, we shall calculate the number of modules that are needed to supply a load of 4.6kW in the city of Manchester, UK. First, we need the solar resource at the site. For example, the daily average solar irradiance and temperature during the month of June 2010 in Manchester is 554W/m² and 35°C respectively. The irradiance and temperature data were gathered during the day light (8:00am - 19:00pm) from central Manchester. Assume for the example the Astronergy CHSM6610P PV module which produces 225W at 1kW/m² and 25ºC.

Using the formulas (3.2) to (3.6), we can compute the power generated by the photovoltaic module. The output characteristics for the PV module are shown in Figure 3.6 (a) and (b).
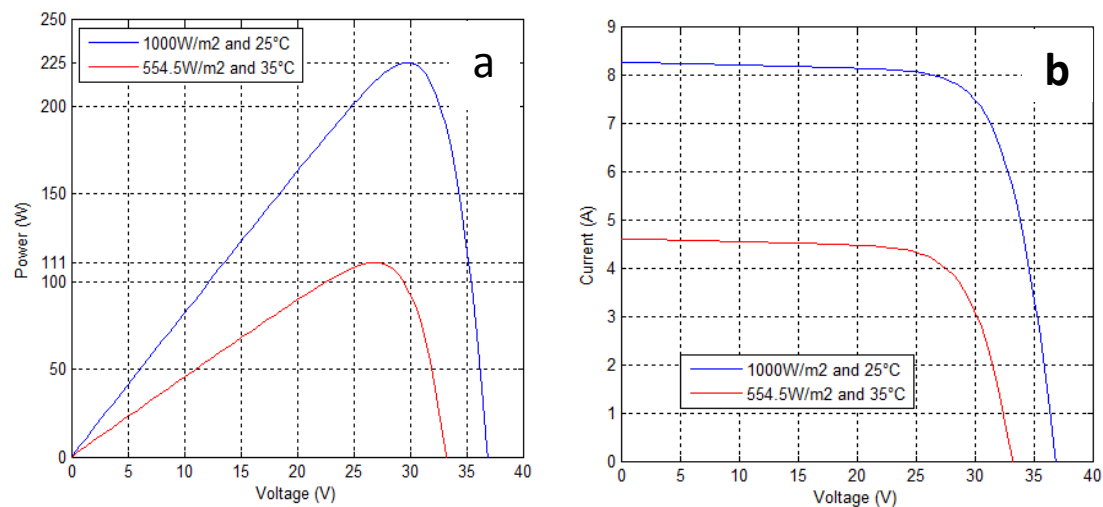
Figure 3.6 - (a) P-V Curve for the Astronergy PV module at 1000W/m² and 554.5W/m²
(b) I-V Curve for the Astronergy PV module at 1000W/m² and 554.5W/m²

Now if we try to calculate the number of solar module needed by the system, we take the load power of 4.6kW and divide it by the power generated from the solar module (4600W) / (111) = 41.4. The result means that we will need 42 Astronergy solar modules to generate enough power for a load of 4.6kW.

3.5 Photovoltaic manufactures

The photovoltaic modules are available in a range of sizes. Some are used in grid connected and others in standalone systems. Both types range from 80W to 300W. The performances of PV modules and arrays are generally rated according to their maximum DC power output (watts) under the Standard Test Conditions (STC). STCs are defined by the module (cell) operating temperature of 25ºC (77 F) and the incident solar irradiance level of 1000 W/m². Since these conditions are not always present, PV modules and arrays operate in the field with performance of 85 to 90 percent of the STC rating. Table 3.3 present the PV modules specifications used in this thesis. All the data was taken from the manufacture's data sheet.

Table 3.3 - PV modules specifications

Solar Module Parameter	Lorentz Mono-Crystalline	Sharp's NUS0E3E	Astronergy CHSM6610P
Maximum power (P_{MPP})	95W	180W	225W
Open circuit voltage (V_{oc})	20.6V	30V	36.88V
Voltage at MPP (V_{amp})	17.2V	23.7V	29.76V
Short circuit current (I_{sc})	6.2V	8.37A	8.27A
Current at MPP (I_{amp})	5.5V	7.6A	7.55A
Temp coefficient for P_{MPP}	-0.38 (%/ºC)	-0.485 (%/ºC)	-0.46 (%/ºC)
Temp coefficient for V_{oc}	-58.7 (mV/ºC)	-104 (mV/ºC)	-0.129 (V /ºC)
Temp coefficient for I_{sc}	5.3 (mA/ºC)	+0.053 (%/ºC)	+0.052 (%/ºC)
No. of cells (N_S)	32	48	60
Cell type	Monocrystalline	Monocrystalline	Polycrystalline

3.6 Summary

Photovoltaic module consists of solar cells which are generally made either from:

- Crystalline silicon;

- Thin films; or

- Other technologies such as CPV, OPV, and DSSC

Crystalline cells are the most common technology, and they are more sensitive to heat than thin film cells.

During daylight, the PV system naturally exhibits nonlinear output characteristics (I-V and P-V), which vary according to the sun radiation and cell temperature as mentioned in Section 3.3. However in the dark, the solar cell will remain inactive; yet it will work as a diode.

The amount of electrical power generated by a solar panel is directly related to the intensity of light energy. According to the Joint Research Centre (JRC) of European Commission, every horizontal square meter of the UK receives solar energy between 750 and 1,100 kWh each year. Some of this energy is received as direct sunlight and some as diffused sunlight.

There are many factors that may affect the performance of photovoltaic panels. Among those are the shading, the collector azimuth, and the collector slope. Therefore, the solar industry uses solar windows while installing PV panels to determine the direction and availability of sunlight for a specific building or location.

The next chapter presents the dynamic behaviour of the wind turbine conversion system and discusses the rotor power characteristics with respect to the wind speed and the rotor speed.

Chapter 4

Wind Power and Rotor Characteristics

*This **chapter** outlines the **dynamic behaviour** of the **wind turbine conversion system**.*

*First, it gives a glimpse for the **types, components, noise level, and manufactures** of*

*small wind turbine. Then, it provides explanations on how much **power can be***

*extracted from the wind**, and how the **wind turbine is modelled**.*

4.1 Introduction to wind energy

Wind energy is a source of renewable power which comes from the air currents flowing across the earth's surface. The wind turbines harvest such kinetic energy and convert it into usable power which can provide electricity for home, school, farm, or business applications on small (residential) or large (utility) scales.

The wind energy is one of the fastest growing sources of electricity and one of the fastest growing markets in the world today. Figure 4.1 shows a diagram for the growth of wind energy in the United Kingdom in particular.

In March 2012, the installed capacity of wind power in United Kingdom came out at 6,580MW, with 333 operational wind farms and 3,506 wind turbines (RES 2012). These growing trends can be attributed to the multi-dimensional benefits associated with wind energy:

- Sustainable energy: wind is a renewable energy resource; it is inexhaustible and requires no "fuel" other than the wind that blows across the earth.
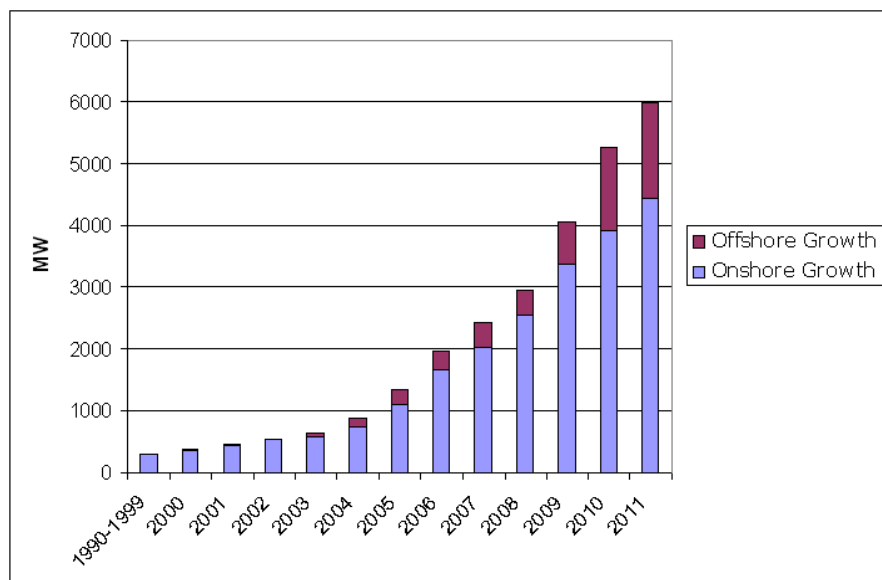
Figure 4.1 - UK installed wind power capacity 1990–2011 (operational)

- Green power: the electricity produced from the wind power is said to be "clean" because its production causes no pollution or greenhouse gas release. As both health and environmental concerns are now considered serious threats to human health and to the environment, clean energy sources are becoming a growing demand.

- Affordability: the wind power is very cost-competitive source of electricity. So wind turbines are manufactured and put in service around the world.

- Economic Development: in addition to being affordable, the wind power is a locally-produced source of electricity that enables communities to keep energy dollars and to invest them in their economy. Job creation (manufacturing, service, construction, and operation) and tax base increase are other economic advantages for countries which utilize wind energy.

4.2 The wind turbines

A wind turbine is a machine that converts the kinetic energy from the wind into mechanical energy. If the mechanical energy is then converted to electricity, the machine is called a wind generator (Gipe 2004).

In the wind turbine business there are basically two types of turbines to choose from:

- The horizontal axis wind turbines(HAWT); and

- The vertical axis wind turbines (VAWT).

The size of these modern wind turbines ranges from a few Watts (Small Wind Turbines) to several Mega Watts (Large Wind Turbines). HAWT dominate much of the wind industry. Horizontal axis basically means that the rotating axis of the wind turbine is horizontal or parallel with the ground. In big wind applications, HAWT are almost all users will ever see. However, in small wind and residential wind applications, VAWT have a good share of the market. The advantage of horizontal wind is that it could produce more electricity from a given amount of wind. So if you are trying to produce as much electricity as possible at all times, the horizontal axis is likely to be your choice. The disadvantage of horizontal axis, however, is that it is usually heavier than VAWT and it does not function well in turbulent winds.

As for VAWT, the rotational axis of the turbine stands vertical or perpendicular to the ground. So, VAWT are primarily used in small wind projects and in residential applications. There are two main advantages for using a vertical axis:

- The turbine generator and the gearbox can be placed lower to the ground thus making maintenance easier and construction costs lower ; and

- The turbine does not need to be pointed towards the wind to be effective which makes it ideal for installations where wind conditions are not consistent.

Despite these advantages, VAWTs suffer from serious drawbacks. Among those are:

- VAWTs have a very low starting torque.

- As the VAWT are mounted closer to the ground, less wind speed will be available, which means less electricity will be produced.

As a conclusion to the comparison between these two types of turbines, one could say that most of today's commercial machines are HAWT with three bladed rotors. While research and development activities on VAWT were intense during the end of the last century, VAWT could not evolve as a reliable alternative to the horizontal axis machines (Mathew 2006). Figure 4.2 shows VAWT and HAWT.
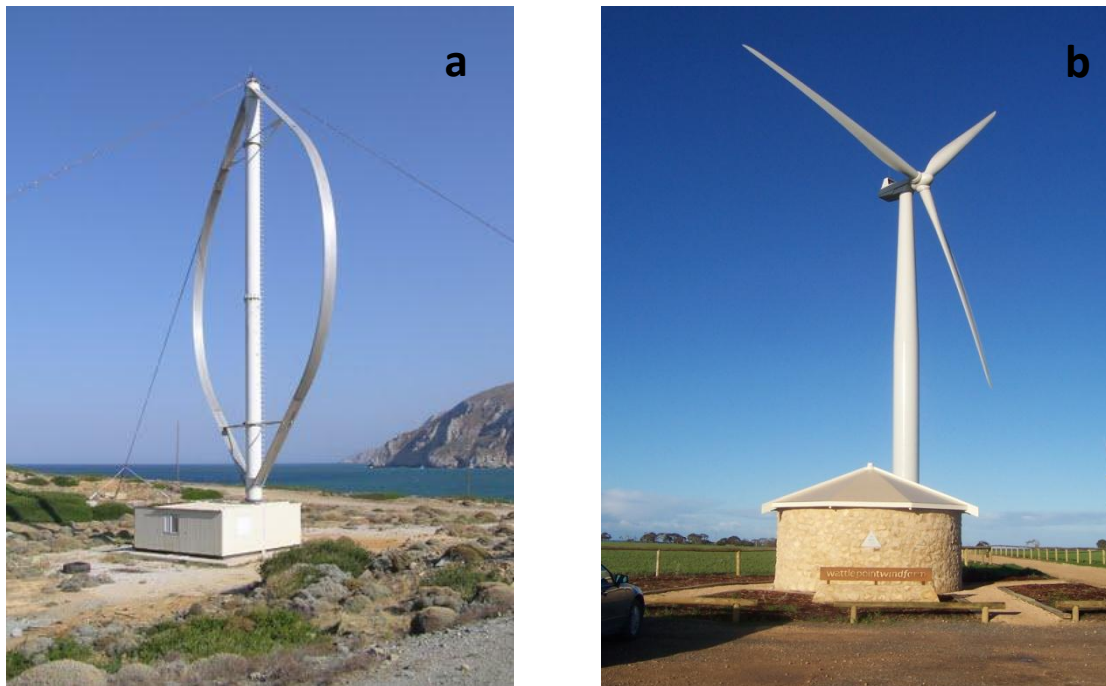
Figure 4.2 - (a) Vertical axis wind turbines (VAWT) **(b)** Horizontal axis wind turbines (HAWT)

4.3 The small wind turbines

Small wind turbines are wind turbines which have lower energy output than large commercial wind turbines. They are typically used for powering houses, farms and remote locations that usually consume less than 50kW of total capacity. Small units often have direct drive generators, direct current output, and a vane to point into the wind. For the purposes of this study, the turbines that will be used for optimization are the small horizontal axis with three blades.

4.3.1 The small wind turbines components

The basic components for small HAWT are shown in Figure 4.3 and they include:
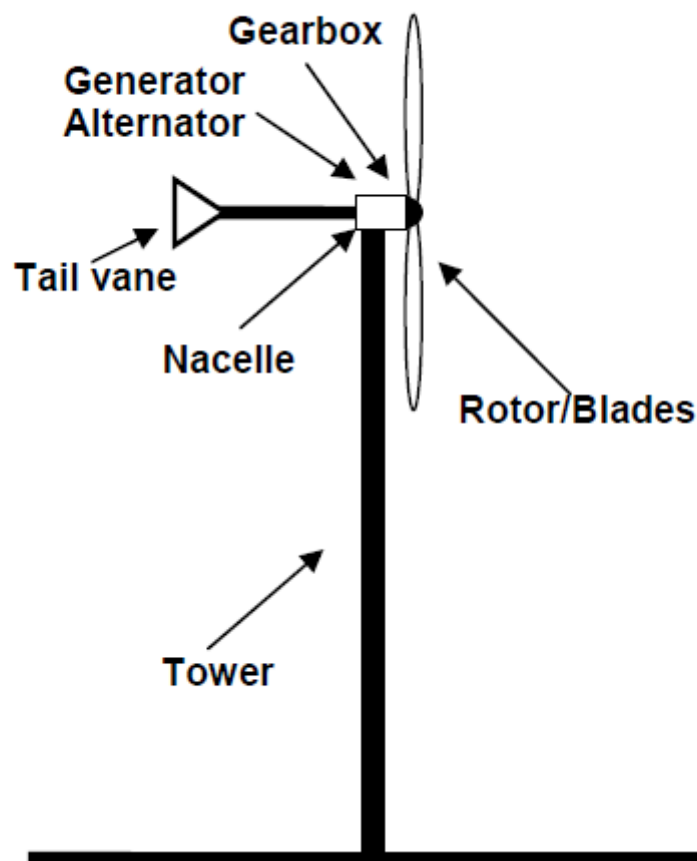
Figure 4.3 - Components of a small wind turbine

- Rotor/blades: the rotor drives the generator by harnessing the kinetic energy in the wind. The blades are usually made of fibreglass, metal, reinforced plastic or reinforced wood, and they are aerodynamically shaped to best capture the wind. The amount of energy a turbine can capture is proportional to the rotor sweep area.

- Generator/Alternator: the generator is the part that produces electricity from the kinetic energy captured by the rotor. A generator produces direct current power or, if in use, an alternator produces alternating current power, depending on the application for the turbine.

- Gearbox: most turbines above 10kW use a gearbox to match the rotor speed to the generator speed.

- Nacelle: the housing that protects the essential motorized parts of a turbine is called the Nacelle.

- Tail vane (Yaw system): most small wind turbines use a simple tail vane that directs the rotor into the wind.

- Control & protection system: the system is usually supplied as part of a small wind turbine package. Control systems vary from simple fuses, switches and battery charge regulators to computerized systems for control of yaw systems and brakes. The sophistication of the control and protection system varies depending on the application of the wind turbine.

- Tower: the tower provides the support of the small wind turbine. The wind speed increases at higher heights, which means that the higher the tower the greater the power. Several types of towers are in use. Among those are:
  - The Guyed tower is used for the wind turbines from 500W to 10kW with simple structure, low cost and easy installation; this type is

especially suitable for home use. However, the tower is permanently supported by guy wires, and it needs much land space.

o The Tilt Up tower is typically used on smaller turbines up to 5kW or so. The benefit of tilt up tower is that it can be raised and lowered for easy maintenance and repair as shown in Figure 4.4. Such good degree of flexibility will reduce the maintenance cost and protect the wind turbine in times of strong winds or typhoons. As a design limitation, it cannot be applied for large wind turbines from 10kW to 50kW.
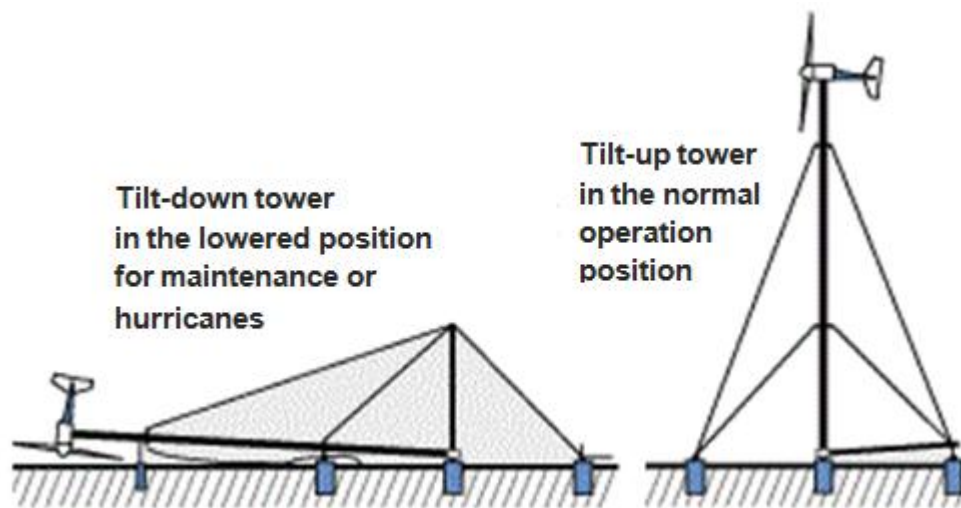
Figure 4.4 - Tilt up tower diagram (FWE 2012)

o The self-supporting towers do not have any guy wires. These towers tend to be the heaviest and most expensive, and they can be used for wind turbines from 1kW and above.

4.3.2 The noise of a small wind turbine

The noise of a small wind turbine varies depending on tower height and size of turbine. The manufacturer must specify the sound level in (dB) of the turbine at a given distance. At a distance of 250m, a typical wind turbine produces a sound pressure level of about 45dB (Gipe 1993). Figure 4.5 offers a comparison of dBs.
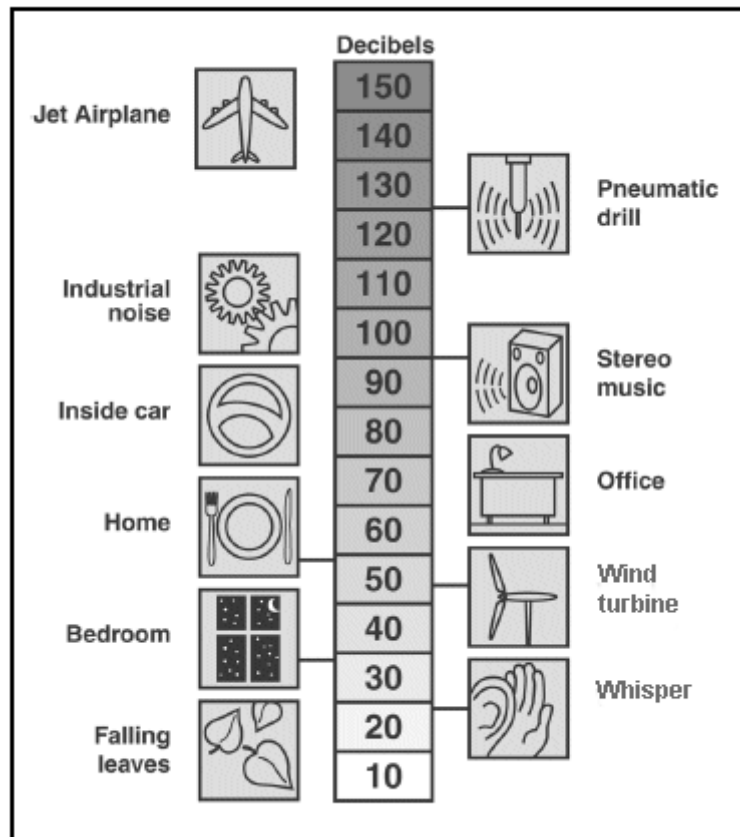
Figure 4.5 - Comparison of decibel levels from a wind turbine (Rivera 2008)

The figure shows how a sound level of 45dB is below the background noise level produced in a home or an office. Most small wind turbines make less noise than a residential air conditioner. Still, before instalment, one must check that the noise level of the small turbine does not violate local regulations.

4.3.3 The small wind turbines manufacturers

Today there are more than fifty manufacturers of small wind turbines worldwide, and they produce more than one hundred different models (Gipe 2004; Rivera 2008). Table 4.1 presents examples of small wind turbines available in the market today. These turbines are the ones mostly used in Europe and United States for small wind power applications.

Table 4.1 - Small wind turbines

Product	Rotor Diameter (m)	Rotor Area (m²)	Weight	Voltage (V)
SouthWest (Air X)	1.14	1.02	13	12, 24, 48 Vdc
SouthWest (Whisper 100)	2.1	3.46	47	12, 24, 48 Vdc
SouthWest (Skystream 3.7)	3.72	10.87	154	120/240 AC
Bergey (BWC XL.1)	2.5	4.91	75	24, 48Vdc
Bornay (Inclin 250)	1.4	1.54	93	12, 24, 48, 220 Vdc
Bornay (Inclin 600)	2	3.14	93	12, 24, 48, 220 Vdc
Bornay (Inclin 1500)	2.7	5.73	93	12, 24, 48, 220 Vdc
Bornay (Inclin 3000)	3.7	10.75	276	12, 24, 48, 220 Vdc
Bornay (Inclin 6000)	3.7	10.75	342	12, 24, 48, 220 Vdc
Abundant Renewable Energy (ARE442)	7.2	40.72	1350	48Vdc
Kestrel Wind (600)	1.6	2	44	12, 24, 48, 110, 200Vdc
Kestrel Wind (800)	2.3	4.15	66.1	12, 24, 48, 110, 200 Vdc
Kestrel Wind (1000)	3	7.07	88	12, 24, 48, 110, 200 Vdc
Kestrel Wind (3000)	4	12.5	397	48, 110, 250Vdc

4.4 The mathematical modelling

The wind turbine converts the kinetic energy from the wind into mechanical energy and then delivers it via a mechanical drive unit to the rotor of an electric generator.

4.4.1 The power extraction from the wind

The kinetic energy of a mass in motions is (Hugo 2007; Serway & Vuille 2011):

$$E = \frac{1}{2}mv^2 \tag{4.1}$$

The power in the wind P_w is given by the rate of change of energy (Hugo 2007):

$$P_w = \frac{dE}{dt} = \frac{1}{2}v^2\frac{dm}{dt} \tag{4.2}$$

Where P_w is the power output in (W), v is the wind speed (m/s), and $\frac{dm}{dt}$ is the mass flow rate per second.

Also it was found that (Hugo 2007):

$$\frac{dm}{dt} = \rho A_s \frac{dx}{dt} \tag{4.3}$$

Where

$$\frac{dx}{dt} = v \tag{4.4}$$

We get:

$$\frac{dm}{dt} = \rho A_s v \tag{4.5}$$

Where ρ is the air density in (kg/m^3), A_s is the swept area of blades (m²), and $\frac{dx}{dt}$ is the distance change rate per second.

Hence, from Equation (4.2) and (4.5), the power in the wind can be defined as:

$$P_w = \frac{1}{2}\rho A_s v^3 \qquad \textbf{(4.6)}$$

As shown in Equation (4.6), the power in the wind (P_w) is a function of the air density (ρ), the swept area (A_s), and the wind speed (v). Increasing these factors will increase the power available from wind.

- **The air density**

The air density (ρ) changes slightly with air temperature and elevation. Cold air in the winter is denser than warm air in the summer. However at higher elevation the air is less dense than at lower elevation. The density of the air can be calculated using the ideal gas law as follows:

$$\rho = \frac{p}{R_{gas}A_T} \qquad \textbf{(4.7)}$$

Where ρ is the air density (kg/m^3), p is the absolute pressure (N/m^2), R_{gas} is the gas constant, and A_T is the absolute temperature.

- **The swept area**

The swept area refers to the area of the circle created by the blades as they sweep through the air; it is shown in Figure 4.6.

The swept area of the turbine can be calculated from the length of the turbine blades using the equation for the area of a circle:

$$A_s = \frac{\pi}{4}D_r^2 \qquad \textbf{(4.8)}$$

Where D_r is the rotor diameter in meters.
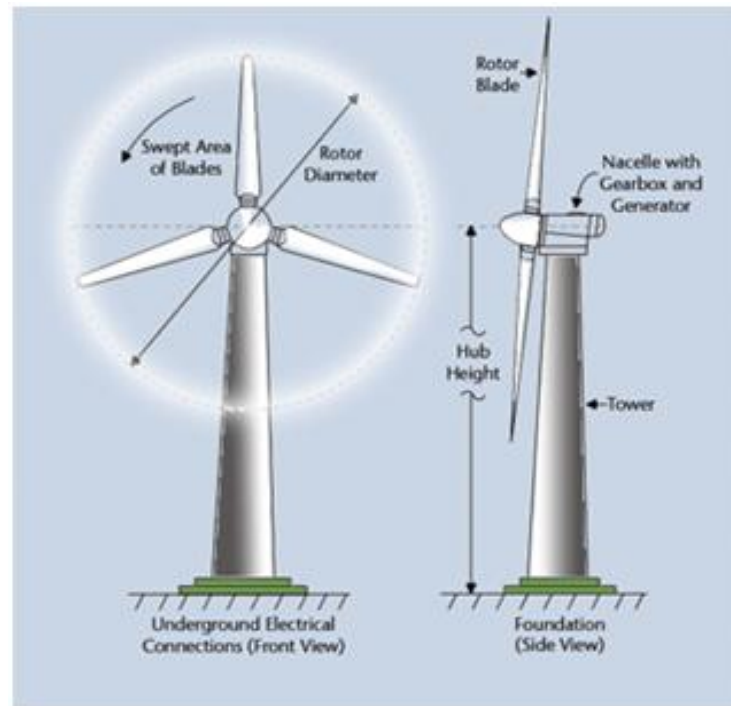
Figure 4.6 - Swept area of blades (WTSA 2012)

4.4.2 The rotor power characteristics

In 1919, a German physicist Albert Betz discovered that no wind turbine can convert more than 16/27 (59.3%) of the kinetic energy of the wind into mechanical energy turning a rotor. The theoretical maximum power efficiency of any design of wind turbine is 0.59 (Betz factor) for an ideal, frictionless flow converter. In real cases, the wind turbine will always have a smaller maximum power coefficient than the Betz factor; this is due to many losses caused by the rotor design and construction (number of blades, weight, etc.).

The power coefficient and the efficiency of a wind turbine system are different. The efficiency of a wind turbine includes the loss in the mechanical transmission, electrical generation, converter loss, etc., whereas the power coefficient is the efficiency of converting the power in the wind into mechanical energy in the rotor shaft. Figure 4.7 shows a diagram with the losses of a wind turbine system.
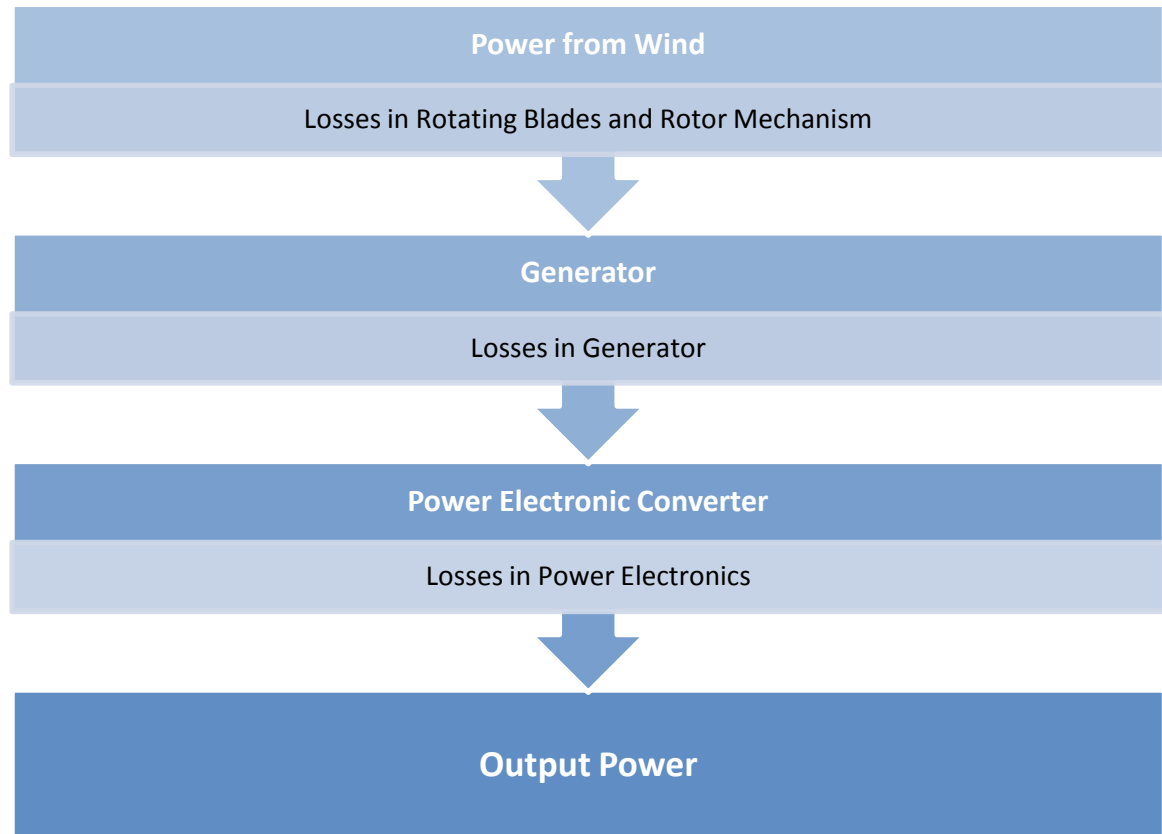
Figure 4.7 - Power flow and losses of wind turbines

Using the power coefficient the mechanical power on the rotor can be calculated as function of wind speed (Muljadi 2001):

$$P_m = c_p \frac{1}{2} \rho A_s v^3 \qquad (4.9)$$

Where P_m is the mechanical power on the rotor (W), c_p is the rotor power coefficient, ρ is the air density (kg/m^3), A_s is the swept area (m^2), and v is the wind speed (m/s). The power coefficient is usually given as a function of the tip speed ratio λ and the blade pitch angle β. In this thesis, the following power coefficient analytical function was used to model the wind turbine as demonstrated in (Lubosny 2003):

$$C_p(\lambda, \beta) = c_1 \left(\frac{c_2}{\lambda_i} - c_3 \beta - c_4 \right) e^{\left(-c_5 / \lambda_i \right)} + c_6 \lambda \qquad (4.10)$$

Where constants c_1 to c_6 are parameters that depend on the wind turbine rotor and

blade design, λ is the tip speed ratio of the rotor blade, β is the blade pitch angle (degree), and λ_i is a parameter given in (4.9).

$$\frac{1}{\lambda_i} = \frac{1}{\lambda + 0.08\beta} - \frac{0.035}{\beta^3 + 1}$$

(4.11)

The C_p-λ characteristics, for different values of the pitch angle β, are shown in Figure 4.8. The maximum value of C_p ($C_{p\text{-}max}$ = 0.48) is achieved for $\beta = 0^\circ$ and for $\lambda = 8.1$. This particular value of λ is defined as the nominal value (λ_{nom}).
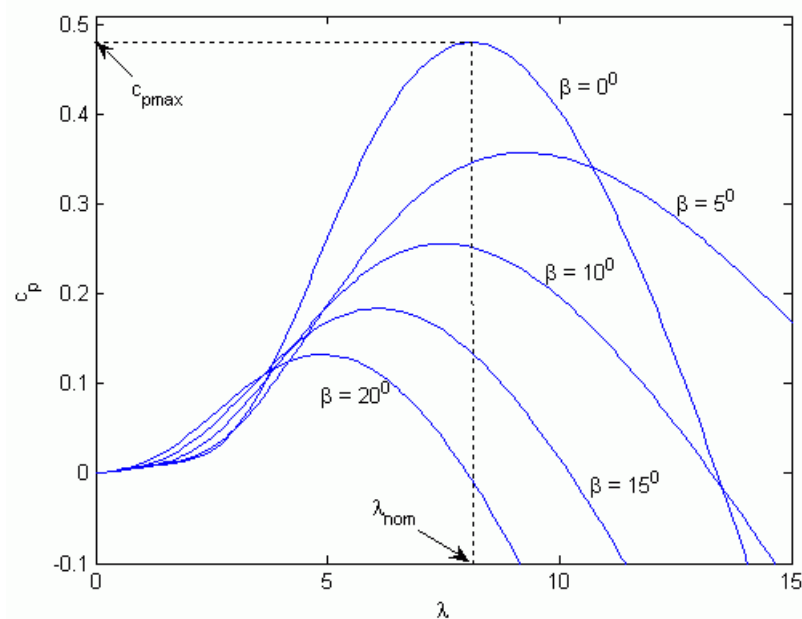
Figure 4.8 - Cp-λ characteristics of wind turbines for different values of pitch angle

4.4.3 The permanent magnet DC generator

The Permanent Magnet DC (PMDC) machine is used in a wide variety of applications due to its low price, high starting torque and easy control. Compared to other DC machine drives, the PMDC eliminates the need for separate field excitation and attendant electrical losses in the field windings (BEC 2012).

When an electric machine is used as a generator, a prime mover is needed to drive the generator. In wind energy applications, the wind turbine is the prime mover of the generator. The equivalent circuit of the PMDC machine is shown in Figure 4.9.
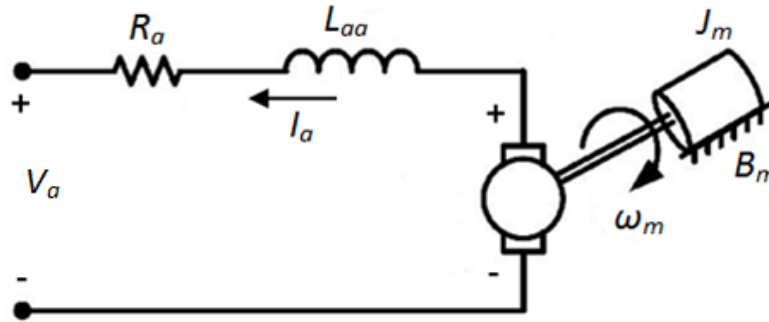
Figure 4.9 - Equivalent circuit of a PMDC machine operated as generator

According to both the PMDC machine circuit shown in Figure 4.9 and Kirchhoff's voltage law, the electrical side of the PMDC generator can be presented as follows (Sharaf et al. 2007):

$$V_a = K_m \omega_m - I_a R_a - L_{aa} \frac{dI_a}{dt} \tag{4.12}$$

Where V_a is the generator output voltage (V), K_m is the torque constant (N.m/A), ω_m is the motor speed (rad/s), I_a is the armature current (A), R_a is the armature resistance (Ω), and L_{aa} is the armature inductance (H).

On the mechanical side, the electromagnetic torque (T_e) developed by the DC machine is proportional to the armature current I_a, as shown below (Sharaf et al. 2007): **(4.13)**

$$T_e = K_m I_a$$

The applied torque produces an angular velocity ω_m according to the inertia J_m and the friction B_m of the machine and load. The relations are described by (Sharaf et al. 2007) as follows:

$$J_m \frac{d\omega_m}{dt} = T_e - T_L - B_m \, \omega_m \tag{4.14}$$

Where J_m is the total inertia (Kg.m^2), T_L is the load torque (N.m), T_e is the electromagnetic torque (N.m), and B_m is the viscous friction coefficient (N.m.s).

4.5 Summary

Modern wind turbines safely and efficiently turn wind into useable energy. They can rotate about either a horizontal or a vertical axis. More they come with different sizes. In this work small wind turbines are selected, since they are typically used for powering houses, farms and remote locations that usually consume less than 50kW of total capacity. They often have direct drive generators (permanent magnet), direct current output (see Table 4.1), and makes less noise than a residential air conditioner.

The output power of wind turbine depends on the wind speed and the generator speed. A wind turbine can only extract part of the power from the wind, which is limited by the Betz limit (maximum 59%). This fraction is described by the power coefficient of the turbine (see Equation (4.16)), which is a function of the blade pitch angle and the tip speed ratio.

The power extracted by the turbine increases as the wind speed increases. Therefore for safety consideration, a control system is needed to limit the generator output power to its nominal value for high wind speeds (see Section 6.1.2).

The next chapter present the dynamic behaviours of the lithium-ion battery and the proton exchange membrane fuel cell.

Chapter 5

Backup Power Systems: Batteries & Fuel Cells

*This chapter introduces and explains the **dynamic behaviour** and **characteristics** of **Lithium-Ion** (Li-Ion) **battery** and **proton exchange membrane fuel cell** (PEMFC). Hence, it shows the **advantages** of Li-Ion battery and PEMFC over other types of rechargeable batteries and fuel cells. Then, it describes the **operational mechanism** and the **mathematical modelling** for each.*

5.1 Introduction

The growth of photovoltaic and wind power generation systems has exceeded the most optimistic estimation, as shown in Figure 5.1 (Jacobson & Delucchi 2009; Jacobson & Delucchi 2010). And according to a 2011-projection by the international energy agency, solar power generators may produce most of the world's electricity by 2060 (Sills 2011).
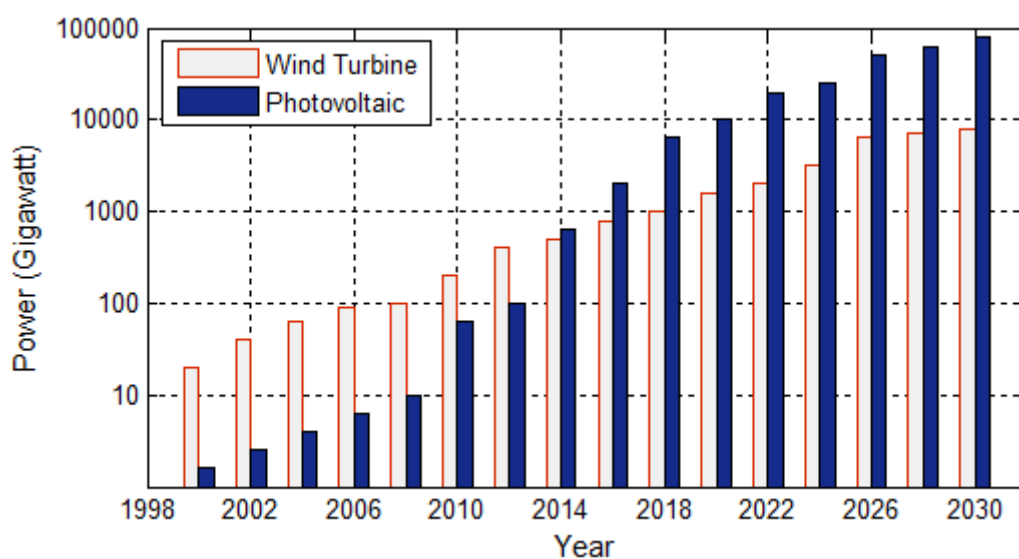
Figure 5.1 - Projected growth of wind power and photovoltaic's, based on history through 2011

However, the natural variations in solar radiation, temperature, and wind speed cause power fluctuations in solar PV and wind turbine systems.

To alleviate this problem and to meet sustained load demands during varying natural conditions, backup power sources are needed to be integrated with the solar-wind hybrid power system. Thus, fuel cells with reversible energy storage[2] ideally fulfil the need for any start up power.

---

[2] Reversible energy storage is accomplished by devices that store energy to perform useful operation at a later time; such as batteries.

Backup Power Systems

5.2 Batteries

A battery is a device that converts chemical energy directly to electrical energy. It contains one or more cells. Each cell consists of three main parts: a positive electrode (terminal), a negative electrode, and a liquid or solid separating them called the electrolyte. When a battery is connected to an electric circuit, a chemical reaction takes place in the electrolyte causing ions (in this case, atom with a positive electrical charge) to flow through it one way. With electrons (particles with a negative charge) flowing through the outer circuit in the other direction. This movement of electric charge makes an electric current flow through the cell and through the circuit it is connected to (Dell & Rand 2001).

Different types of batteries are produced for different applications. They can be used for storing solar power for satellites in space to powering heart pacemakers fitted inside people's chests.

5.2.1 Types of batteries

There are two types of batteries:

- Primary batteries (disposable batteries): which are designed to be used once and discarded.

- Secondary batteries (rechargeable batteries): which are designed to be recharged and used multiple times.

Most of the batteries used today with hybrid power system are from the rechargeable type (Rivera 2008). There are several kinds of rechargeable batteries. Among them, as shown in Table 5.1: NiCd (Nickel Cadmium), NiMH (Nickel Metal Hydride), Lead-Acid, and Lithium-Ion (Li-Ion).

Table 5.1 - Common rechargeable battery types

Parameters	NiCd	NiMH	Lead-Acid	Lithium-Ion
Nominal cell voltage (V)	1.2	1.2	2.1	3.6
Energy density (Wh/kg)	40-60	30-80	30-40	150-250
Specific power (W/kg)	150	250-1000	180	1800
Charge/discharge efficiency (%)	70%-90%	66%	70%-92%	99%$^{+}$
Self-discharge rate in (%/month)	20%	30%	3%-4%	5%-10%
Cycle durability[3] (#)	1500	500-1000	500-800	1200-10000

As shown in Table 5.1, Lithium-Ion battery has many advantages than other rechargeable batteries, such as (BU 2012):

- High energy density: it is typically twice that of the standard Nickel Cadmium.

- High cell voltage with 3.6 volts.

- Low battery maintenance: an advantage that most other chemistries cannot claim.

- Relatively low self-discharge: self-discharge is less than half that of Nickel-based batteries.

- High charge/discharge efficiency: more than 99%.

- High cycle durability: it can last for many hundreds or even thousands of charge/discharge cycles.

---

[3] The total number of cycles a battery is capable of producing before it fails.

Backup Power Systems

These characteristics have made the Li-Ion battery the fastest growing and most promising battery system for renewable energy applications (VT 2012; Richmond 2012). Therefore, Li-Ion battery is the rechargeable battery that will be investigated in this work.

5.2.2 The charge/discharge mechanism in Li-Ion battery

As with most batteries they have an outer case made of metal. This metal case holds a long spiral comprising three thin sheets pressed together:

- A Positive electrode (cathode)

- A Negative electrode (anode)

- A separator

The separator is a very thin sheet of micro-perforated plastic, which separates the positive and negative electrodes while allowing ions to pass through.

The positive electrode is made of Lithium Cobalt Oxide, or $LiCoO_2$. The negative electrode is made of Carbon. It can be seen from Figure 5.2, that during discharge, Lithium (Li^+) ions carry the current from the negative to the positive electrode, through the electrolyte and separator diaphragm.
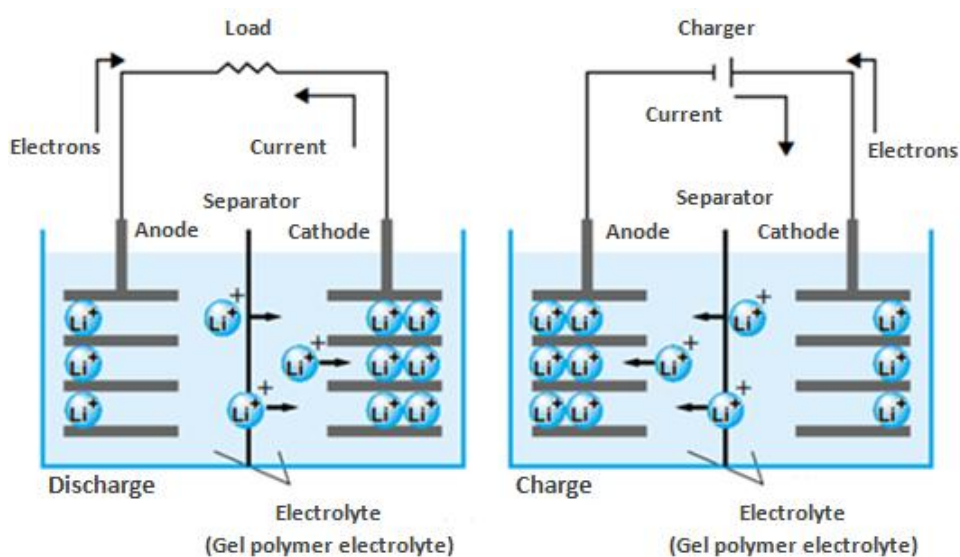
Figure 5.2 - Charge and discharge mechanism of Li-Ion rechargeable batteries (HSW 2012)

Backup Power Systems

During charging, an external electrical power source applies an over-voltage than that produced by the battery, forcing the current to pass in the reverse direction. The lithium ions then migrate from the positive to the negative electrode, where they become embedded in the porous electrode material in a process known as intercalation.

5.2.3 The mathematical modelling of Li-Ion battery

In the literature, several studies have been reported regarding to Li-Ion battery (Zhang & Lee 2011). In this work, the Li-Ion battery is modelled using a controlled voltage source in series with a constant resistance, as shown in Figure 5.3.
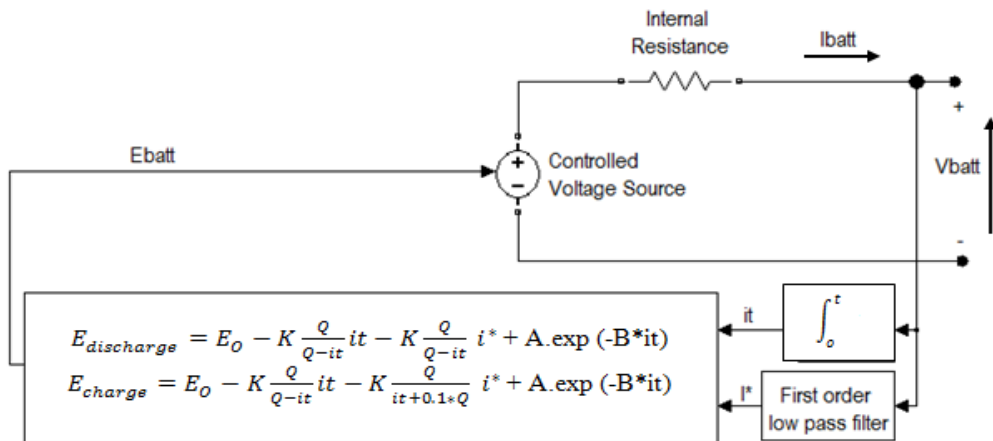
Figure 5.3 - Battery model equivalent circuit

- **Discharge model:**

The discharge battery model used is based on the Shepherd model (Shepherd 1965) but, it can represent accurately the voltage dynamics when the current varies and takes into account the open circuit voltage (OCV) as a function of state-of-charge (SOC). The OCV varies non-linearly with the SOC. Therefore, a term concerning the polarisation voltage has been added $\left(K\dfrac{Q}{Q-it}it \right)$ to better represent the OCV behaviour.

The battery voltage (V_{batt}) obtained can be described as (Tremblay & Dessaint 2009):

$$V_{batt} = E_o - K \frac{Q}{Q - it} \, it - R \, i - K \frac{Q}{Q - it} i^* + A \exp(-B \, it) \qquad \textbf{(5.1)}$$

Where E_o is the battery constant voltage[4] (V), K is the polarization constant (Ah^{-1}), Q is the maximum battery capacity (Ah), it ($\int i \, dt$) is the actual battery charge (Ah), R is the internal resistance (Ω), i is the battery current (A), i^* is the low frequency current dynamics[5] (A), A is the exponential zone amplitude (voltage drop during the exponential zone) (V), and B is the exponential zone time constant inverse (Ah)$^{-1}$.

- **Charge model:**

The battery charge behaviour, especially the end of the charge characteristic, is different and depends on the battery type. In Li-Ion battery the voltage will increase rapidly when the battery reach the full charge, as shown in Figure 5.4. This phenomenon can be modeled by the polarisation resistance term $\left(K \frac{Q}{it} \right)$. The polarisation resistance increases until the battery is almost fully charged ($it = 0$). Above this point, the polarisation resistance increases suddenly.

Theoretically, when $it = 0$ (fully charged), the polarisation resistance is infinite. This is not exactly the case in practice. Actually, experimental results have shown that the contribution of the polarisation resistance is shifted by about 10% of the capacity of the battery (Tremblay & Dessaint 2009). Hence the polarization resistance of the charge model can be described as:

$$\text{Pol. Resistance} = K \frac{Q}{it + 0.1Q} \qquad \textbf{(5.2)}$$

---

[4] It's the battery voltage when there is no flowing current.

[5] The filtered current (i^*) has been added to solve the algebraic loop problem due to the simulation of electrical systems in Simulink.
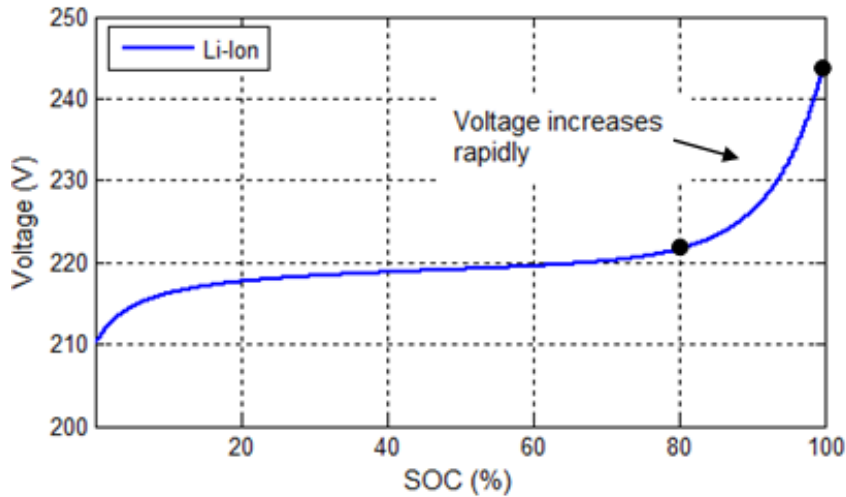
Figure 5.4 - Typical charge characteristic

Similar to the discharge model, the exponential voltage for the Li-Ion battery is the $A \exp(-B\, it)$ term. Hence, the battery voltage obtained can be described as (Tremblay & Dessaint 2009):

$$V_{batt} = E_o - K\frac{Q}{Q - it}\, it - Ri - K\frac{Q}{it + 0.1Q}i^* + A \exp(-B\, it) \qquad \textbf{(5.3)}$$

The main feature of this battery model is that the parameters can easily be deduced from a manufacturer's discharge curve. Figure 5.5 shows a typical discharge characteristic for Li-Ion battery. As shown, the first section represents the exponential voltage drop when the battery is charged. Depending on the battery type, this area is more or less wide. The second section represents the charge that can be extracted from the battery until the voltage drops below the battery nominal voltage. Finally, the third section represents the total discharge of the battery when the voltage drops rapidly.
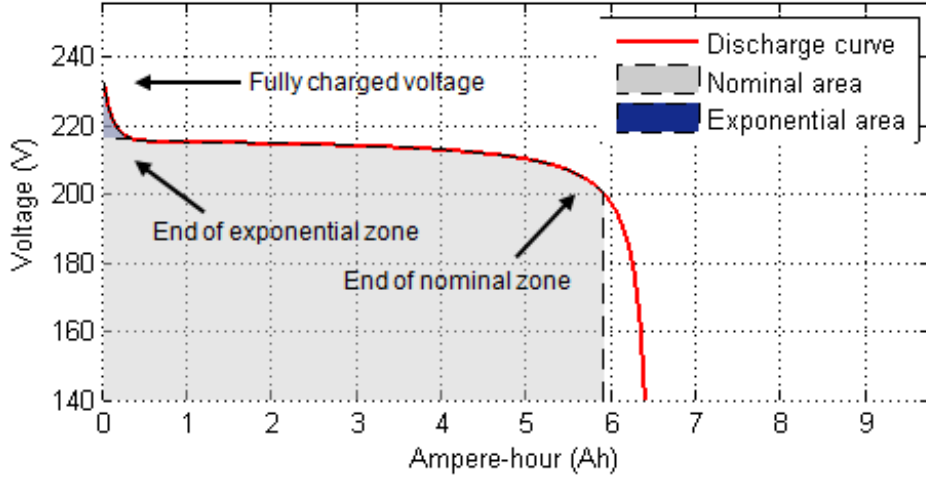
Figure 5.5 - Nominal current discharge characteristic

The three necessary points used to extract the model parameters are: the fully charged voltage, the end of the nominal zone and the end of the exponential zone. With these three points, it is possible to solve, using Equation (5.1), the following set of Equations (5.4), (5.5) and (5.6). For the fully charged voltage (V_{full}), the extracted charge is 0 ($it = 0$) and the filtered current (i^*) is 0 because the current step has just started:

$$V_{full} = E_o - (R * i) + A \qquad (5.4)$$

For the end of the exponential zone, the factor B can be approximated to $\left(\dfrac{3}{Q_{exp}}\right)$ since the energy of the exponential term is almost 0 after 3 time constants (Tremblay & Dessaint 2009).

In steady state the filtered current is equal to (i). Hence, the exponential zone voltage (V_{exp}) can be described as:

$$V_{exp} = E_o - K \frac{Q}{Q - Q_{exp}} (Q_{exp} + i) - Ri + A \exp(-\frac{3}{Q_{exp}} Q_{exp}) \qquad (5.5)$$

And the nominal zone voltage (V_{nom}) can be given by:

$$V_{nom} = E_o - K \frac{Q}{Q - Q_{nom}} (Q_{nom} + i) - Ri + A \exp(-\frac{3}{Q_{exp}} Q_{nom}) \qquad (5.6)$$

Backup Power Systems

5.2.4 Battery storage bank sizing

Calculating the number of batteries needed for a solar-wind hybrid power system mainly depends on the days of autonomy desired. Days of autonomy are the number of days a battery bank will supply a given load without being recharged by a wind turbine, PV array or another source. For critical loads 5 days of autonomy are recommended. If the load being supplied is not critical then 2 to 3 autonomy day are commonly used. A critical load is a load that must be used all the time (Rivera 2008). Another important factor is the maximum depth of discharge of the battery. The depth of discharge refers to how much capacity will be used from the battery. Most systems are designed for regular discharge values between 40 to 80 percent (Rivera 2008).

Hence, and according to (Sandia 1995), the required battery bank capacity (B_{C-R}) for a hybrid renewable energy system can be calculated as follow:

$$B_{C-R} = \frac{I_C \, N_D}{M_{DOD}} \tag{5.7}$$

Where I_C is the Amp-hour consumed by the load in a day (Ah/day), N_D is the number of autonomy days, and M_{DOD} is the maximum depth of discharge.

The number of batteries to be connected in parallel (N_{B-P}) to reach the Amp hours required by the system can be calculated as follow (Rivera 2008):

$$N_{B-P} = \frac{B_{C-R}}{B_C} \tag{5.8}$$

Where B_C is the capacity of the selected battery (Ah).

While, the number of batteries to be connected in series (N_{B-S}) to reach the voltage required by the system can be calculated as follow (Rivera 2008):

$$N_{B-S} = \frac{S_V}{B_V} \tag{5.9}$$

Where S_V is the DC system voltage (V), and B_V is the battery voltage (V).

Backup Power Systems

Now let's size a battery bank needed to supply 4800Wh per day to a DC electric load.

Assume that:

- The DC voltage of the battery bank is 24V.

- The number of autonomy days is 2 days.

- The maximum depth of discharge is 44.44%.

- The selected rechargeable battery is (12V-450Ah) Li-Ion

Then, by using the Equations from (5.7) to (5.9) we can calculate the batteries required by this system as follow:

$$B_{C-R} = \frac{I_C N_D}{M_{DOD}} = \frac{200 \times 2}{0.4444} = 900 Ah$$

$$number\ of\ battery\ in\ parallel = \frac{B_{C-R}}{B_C} = \frac{900}{450} = 2$$

$$number\ of\ battery\ in\ series = \frac{S_V}{B_V} = \frac{24}{12} = 2$$

$$total\ number = N_{B-P}\ N_{B-S} = 2 \times 2 = 4$$

Figure 5.6 shows the example battery bank wired connection.
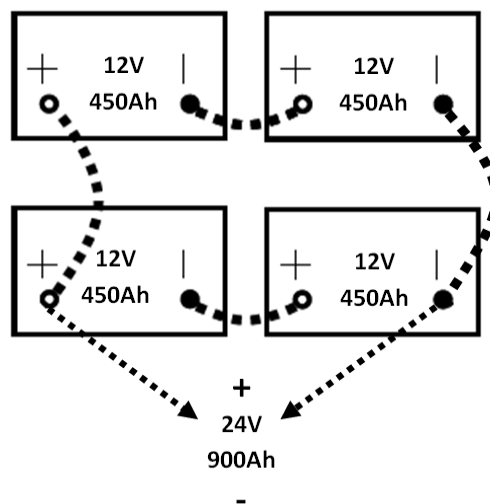
Figure 5.6- Series-parallel battery bank example configuration

Backup Power Systems

5.3 Fuel cells

A fuel cell is an electrochemical device which combines a fuel and oxygen to deliver power. Hydrogen is the most common fuel, but hydrocarbons such as natural gas and alcohols like methanol are sometimes used.

Like a battery, individual cells can be combined together to form a stack that deliver power which is needed for the given application. Unlike a battery, which is closed, a fuel cell is open on at least one side, the air side being invariably open.

A fuel cell essentially consists of two electrodes (cathode and anode) separated by an electrolyte, which carries electrically charged particles from one electrode to the other. Usually the type of electrolyte is used to differentiate between different types of fuel cells (EERE 2012).

5.3.1 Types of fuel cells

Fuel cells are classified according to the electrolyte they employ. This classification determines the fuel required, the operating temperature range, the kind of catalysts required, and other factors. These characteristics, in turn, affect the applications for which these cells are most suitable. As shown in Table 5.2, there are several types of fuel cells currently under development, each with its own advantages, limitations, and potential applications (EERE 2012). They can be divided into high temperature fuel cell systems (Molten Carbonate Fuel Cell, Solid Oxide Fuel Cell) and low temperature systems (Proton Exchange Membrane Fuel Cell, Direct Methanol Fuel Cell, Alkaline Fuel Cell).

Table 5.2 - Comparison of fuel cell types

Fuel Cell Name	Electrolyte	Operating Temperature	Electrical Efficiency
Alkaline Fuel Cell (AFC)	Potassium hydroxide (KOH) solution	Room temperature to 90°C	60-70%
Proton Exchange Membrane Fuel Cell (PEMFC)	Proton exchange membrane	Room temperature to 80°C	40-60%
Direct Methanol Fuel Cell (DMFC)	Proton exchange membrane	Room temperature to 130°C	20-30%
Phosphoric Acid Fuel Cell (PAFC)	Phosphoric acid	160-220°C	55%
Molten Carbonate Fuel Cell (MCFC)	Molten mixture of alkali metal carbonates	620-660°C	65%
Solid Oxide Fuel Cell (SOFC)	Oxide ion conducting ceramic	800-1000°C	60-65%

Due to the low operating temperature (room temperature to 80°C), high efficiency, and fast start up, PEM fuel cells are the best candidate for residential application (El-Sharkh et al. 2004).

5.3.2 The proton exchange membrane fuel cell mechanism

In a PEM fuel cell two electrodes are separated by a proton-conducting polymer membrane. As shown in Figure 5.7, hydrogen gas is supplied to one electrode (anode) and oxygen gas to the other (cathode). At the anode, a platinum catalyst causes the hydrogen to split into electrons and hydrogen ions. The polymer electrolyte membrane allows only the positively charged ions to pass through it to the cathode. While the negatively charged electrons travel along an external circuit to the cathode.

Backup Power Systems

At the cathode, the hydrogen ions and the electrons combine with oxygen to form water (which flows out of the cell).
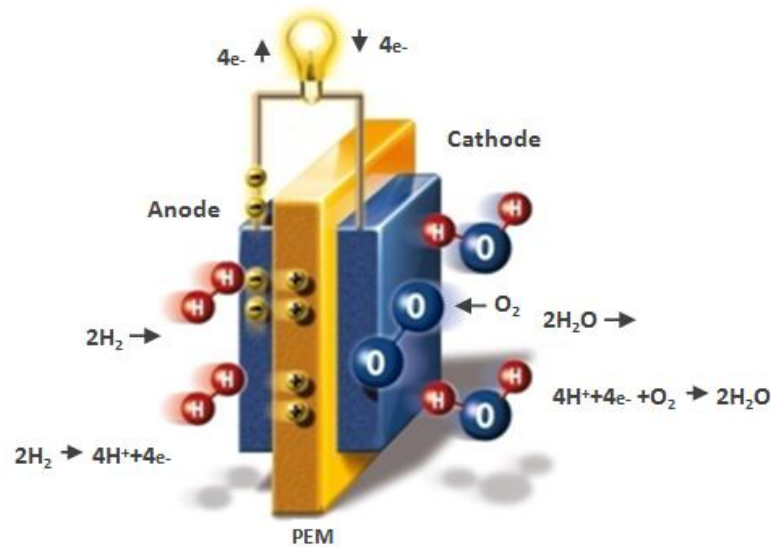
Figure 5.7- Proton exchange membrane fuel cell (HTE 2012)

5.3.3 The proton exchange membrane fuel cell stack

In order to achieve the required output voltage several individual fuel cells must be combined to a unit called a fuel cell stack. These adjacent cells are connected by a separator plate (with horizontal and vertical grooves), which has a number of tasks:

- Facilitate gas transport to and away from the cells.

- Seal off adjacent cells and prevent fuel and oxidant leakage.

- Provide the electrical connections between the cells.

- Dissipate the heat produced in the cells.

Figure 5.8 shows a diagram for a PEMFC stack containing three individual fuel cells. So simply by varying the number of individual cells, stack can be designed for any desirable output voltage.

Backup Power Systems
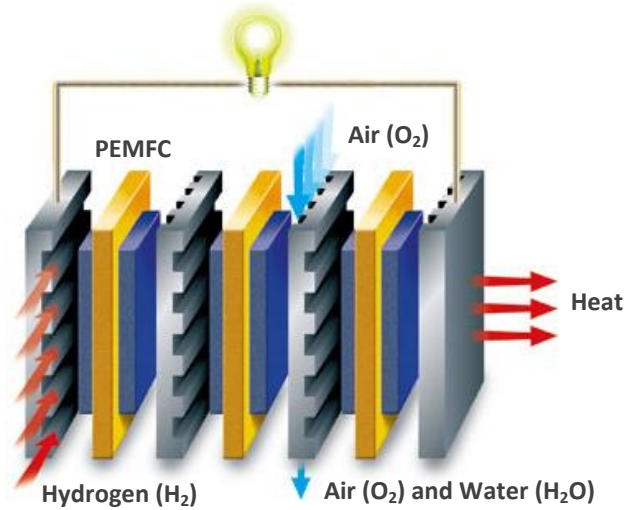
Figure 5.8 - Proton exchange membrane fuel cell stack (HTE 2012)

5.3.4 The mathematical modeling of PEMFC

The modified PEMFC model[6] used in this study is based on the dynamic PEMFC

stack model developed and validated in (Souleman et al. 2009). The model combines

the features of chemical and electrical models, and fuel cell parameters are obtained

from manufacturer's datasheets. Figure 5.9 shows the fuel cell stack as a controlled

voltage source in series with a constant resistance.

$$E_{oc} - NA \ln\left(\frac{I_{fc}}{I_o}\right) \times \left(s\frac{T_d}{3}+1\right)^{-1}$$
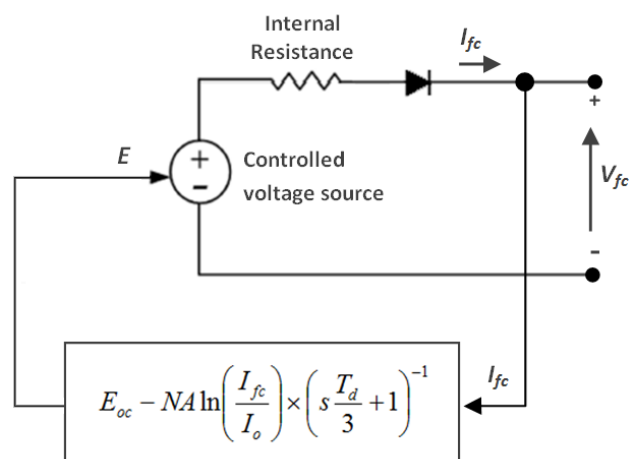
Figure 5.9 - Detailed fuel cell stack model

---

[6] To improve the generating performance of the PEMFC and prolong its life, stack temperature is
controlled by a fuzzy logic temperature controller (see Section 7.5).

Backup Power Systems

The fuel cell stack voltage (V_{fc}) is described as (Souleman et al. 2009):

$$V_{fc} = \left(E_{oc} - NA \ln\left(\frac{I_{fc}}{I_o}\right) \times \frac{1}{s\frac{T_d}{3} + 1} \right) - R_{ohm} I_{fc} \qquad \textbf{(5.10)}$$

Where E_{oc} is the open circuit voltage (V), N is the number of cells, A is the Tafel slope (V), I_o is the exchange current (A), I_{fc} is the fuel cell current (A), T_d is the response time (sec), and R_{ohm} is the internal resistance (Ω). Equation (5.10) is derived from (Larminie & Dicks 2003) and represents the stack voltage considering only the activation losses (losses due to the slowness of chemical reactions at electrode's surfaces). In (Larminie & Dicks 2003), these losses are modelled electrically by a parallel RC branch. Therefore, in a sudden change in stack current, the fuel cell voltage will exhibit a delay which is approximately 3 times the time constant ($\tau = RC$) prior to equilibrium. This phenomenon is represented in Equation (5.10) by delaying the activation losses with a first order transfer function ($\frac{1}{s\frac{T_d}{3} + 1}$) with T_d being the stack settling time. E_{OC}, A, and i_0, are determined as follows (Souleman et al. 2009):

$$E_{OC} = K_C E_N \qquad \textbf{(5.11)}$$

$$A = \frac{R_u T}{z \alpha F_c} \qquad \textbf{(5.12)}$$

$$I_o = \frac{z K_B F_c \left(P_{H_2} + P_{O_2}\right)}{R_u h} e^{-\frac{\Delta G}{R_u T}} \qquad \textbf{(5.13)}$$

Where E_N is the Nernst voltage (V), K_C is the voltage constant at nominal condition of operation, z is the number of moving electrons, F_c is the Faraday's constant (96485 A.s/mol), P_{H2} is the partial pressure of hydrogen inside the stack (atm), P_{O2} is the partial pressure of oxygen inside the stack (atm), ΔG is the activation energy

Backup Power Systems

barrier (J), T is the temperature of operation (K), R_u is Universal gas constant (8.3145 J/ (mol.K)), h is the Planck's constant (6.626×10^{-34} J.s), and α is the charge transfer coefficient. The partial pressures, rates of conversion (utilizations), and Nernst voltage are determined as follows (Souleman et al. 2009):

$$P_{H_2} = \left(1 - U_{fH_2}\right) x^{\%} P_{fuel} \tag{5.14}$$

$$P_{O_2} = \left(1 - U_{fO_2}\right) y^{\%} P_{air} \tag{5.15}$$

$$U_{fH_2} = \frac{60000\, R_u\, T\, N\, i_{fc}}{z\, F_c\, P_{fuel}\, V_{fuel}\, x^{\%}} \tag{5.16}$$

$$U_{fO_2} = \frac{60000\, R_u\, T\, N\, i_{fc}}{2z\, F_c\, P_{air}\, V_{air}\, y^{\%}} \tag{5.17}$$

$$E_N = 1.229 + (T - 298)\frac{-44.43}{zF} + \frac{R_u T}{zF} \ln\left(P_{H2} P_{O2}^{0.5}\right) \tag{5.18}$$

Where x is the percentage of hydrogen in the fuel (%), P_{fuel} is the absolute supply pressure of fuel (atm), y is the percentage of oxygen in the oxidant (%), P_{air} is the absolute supply pressure of air (atm), V_{fuel} is the fuel flow rate (l/m), and V_{air} is the air flow rate (l/m).

Knowing the Nernst voltage and the partial pressures of gases, the new values of the open circuit voltage and the exchange current can therefore be calculated using Equations (5.11) and (5.13) respectively.

Fuel cell manufacturers provide specifications (usually given at nominal condition of operation) of their stacks which include the peak power, polarization curve, number of cell, operating temperature, efficiency, inlet pressures, etc. These data are used to obtain the models parameters. For the proposed model, in addition to (E_{oc}, i_0, $N A$ and R_{ohm}), three more parameters (α, ΔG, K_c) are to be determined. Therefore, in addition

to the four points $((0, E_{OC})$, $(1, V_1)$, (I_{nom}, V_{nom}), and $(I_{max}, V_{min}))$ on the polarization curve (Figure 5.10), the following variables are needed:

- Nominal stack efficiency in %

- Number of cells in series

- Nominal operating temperature in °C

- Absolute supply pressures in atm

- Nominal air flow rate in liter/min

- Nominal composition of fuel and air in %
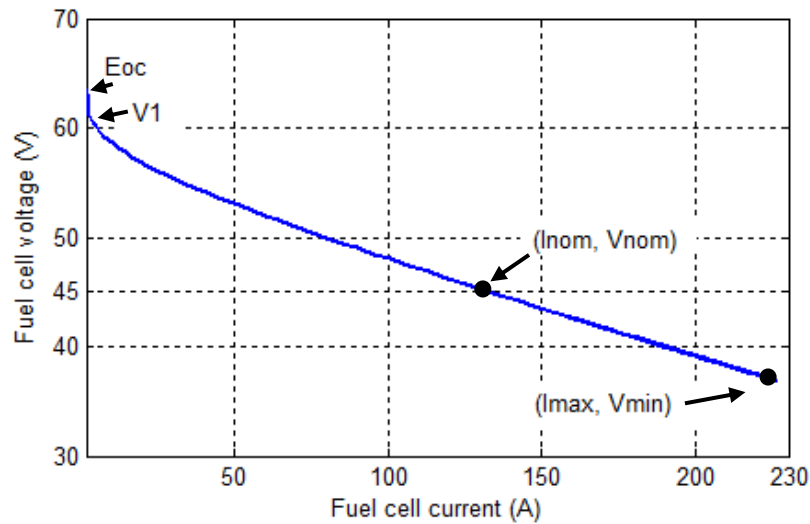
Figure 5.10 - Typical polarization curve

At nominal conditions of operation, $(N A, R_{ohm}, $ and $I_o)$ parameters can be determined as follows:

$$N A = \frac{(V_1 - V_{nom})(I_{max} - 1) - (V_1 - V_{min})(I_{nom} - 1)}{\ln(I_{nom})(I_{max} - 1) - \ln(I_{max})(I_{nom} - 1)} \tag{5.19}$$

$$R_{ohm} = \frac{V_1 - V_{nom} - NA\ln(I_{nom})}{I_{nom} - 1} \tag{5.20}$$

$$I_o = \exp\left(\frac{V_1 - E_{OC} + R_{ohm}}{NA}\right) \tag{5.21}$$

Backup Power Systems

With *Eoc*, i_0 and *N A* known and assuming that the stack operates at constant rates of conversion or utilizations at nominal condition. *α*, *ΔG*, and K_C can be determined as follows:

$$\alpha = \frac{NR_u T_{nom}}{zFNA} \tag{5.22}$$

$$\Delta G = -R_u T_{nom} \ln\left(\frac{I_o}{K_1}\right) \tag{5.23}$$

$$K_1 = \frac{2FK_B\left(P_{H2nm} + P_{O2nom}\right)}{hR_u} \tag{5.24}$$

$$K_C = \frac{E_{OC}}{E_{N(nom)}} \tag{5.25}$$

$$E_{N(nom)} = E_N \ where \left(U_{fO_2} = U_{fO_2(nom)} \ and \ U_{fH_2} = U_{fH_2(nom)}\right) \tag{5.26}$$

And the nominal rates of conversion of gases are calculated as follows:

$$U_{fH_2nom} = \frac{\eta_{nom}\Delta h^o\left(H_2O(gas)\right)N}{z F_c V_{nom}} \tag{5.27}$$

$$U_{fO_2nom} = \frac{60000 R_u T_{nom} N I_{nom}}{2z F_c P_{air(nom)} V_{air(nom)} y_{nom}^{\%}} \tag{5.28}$$

Where η_{nom} is the nominal LHV efficiency of the fuel cell stack (%), $\Delta h^o(H_2O(gas))$ is equal to 41.83×10^3 J/mol, V_{nom} is nominal voltage (V), I_{nom} is nominal current (A), $V_{air(nom)}$ is the nominal air flow rate (l/min), $P_{air(nom)}$ is the nominal absolute air supply pressure (pa), and T_{nom} is the nominal operating temperature (°C). From these rates of conversion, the nominal partial pressures of gases can be derived as follows:

$$P_{H_2\,nom} = \left(1 - Uf_{H2nom}\right)x_{nom}^{\%} P_{fuel(nom)} \tag{5.29}$$

$$P_{O_2\,nom} = \left(1 - U_{fO_2nom}\right)y_{nom}^{\%} P_{air(nom)} \tag{5.30}$$

Backup Power Systems

In case that the polarizations carve is not provided by the fuel cell manufacturers, then at steady state and according to Equations (5.10) and (5.11), V_1, V_{nom}, and V_{min} can be calculated as follows:

$$V_1 = E_{oc} - NA\ln(I_o) - R_{ohm} \tag{5.31}$$

$$V_{nom} = E_{oc} - NA\ln\left(\frac{I_{nom}}{I_o}\right) - R_{ohm}I_{nom} \tag{5.32}$$

$$V_{min} = E_{oc} - NA\ln\left(\frac{I_{max}}{I_o}\right) - R_{ohm}I_{max} \tag{5.33}$$

5.4 Summery

Geographic and seasonal climatic conditions affect the solar-wind energy output. Therefore, a fuel cell/battery power system is used to improve the energy supply reliability. Due to the low operating temperature, high efficiency, and fast start up, PEM fuel cells are the best candidate for residential application. While for batteries Li-Ion is the best candidate due to the high density, low maintenance, high cycle durability, and high efficiency.

The mathematical models for Li-Ion battery and PEMFC are presented in Sections 5.2.3 and 5.3.4, respectively. As illustrated, each model requires only few variables from manufacturer's datasheets. For Li-Ion battery, the three necessary points used to extract the model parameters are: the fully charged voltage, the end of the nominal zone and the end of the exponential zone. While for PEMFC, in addition to the polarization curve (Figure 5.10), the following variables are needed: nominal

stack efficiency, number of cells, nominal operating temperature, absolute supply pressures, nominal air flow rate, and nominal composition of fuel and air.

The next chapter will addressed the implementation and design for the proposed hybrid system model using MatLab/Simulink.

Chapter 6

Hybrid Power System: Modelling & Simulation

*In power applications and system design, **modelling and simulation** are essential to*

***optimize control** and **enhance system operations**. In this chapter, the **dynamic**

***simulation model** is described for a **hybrid power system** comprises **PV panels, wind**

***turbine, fuel cells, battery bank, converters and controllers.** The **main controller**, as*

*will be presented in **Chapter seven**, will developed to **ensure the continuous power**

***supply** for the **load demand**.*

6.1 Numerical simulation and experimental validation

The following subsections present the implementation of the PV/wind turbine/ PEMFC/Li-Ion battery system model. Modelling and simulation are implemented using MatLab/ Simulink and SimPowerSystem software packages. The block diagram of the developed hybrid power system is shown in Figure 6.1.
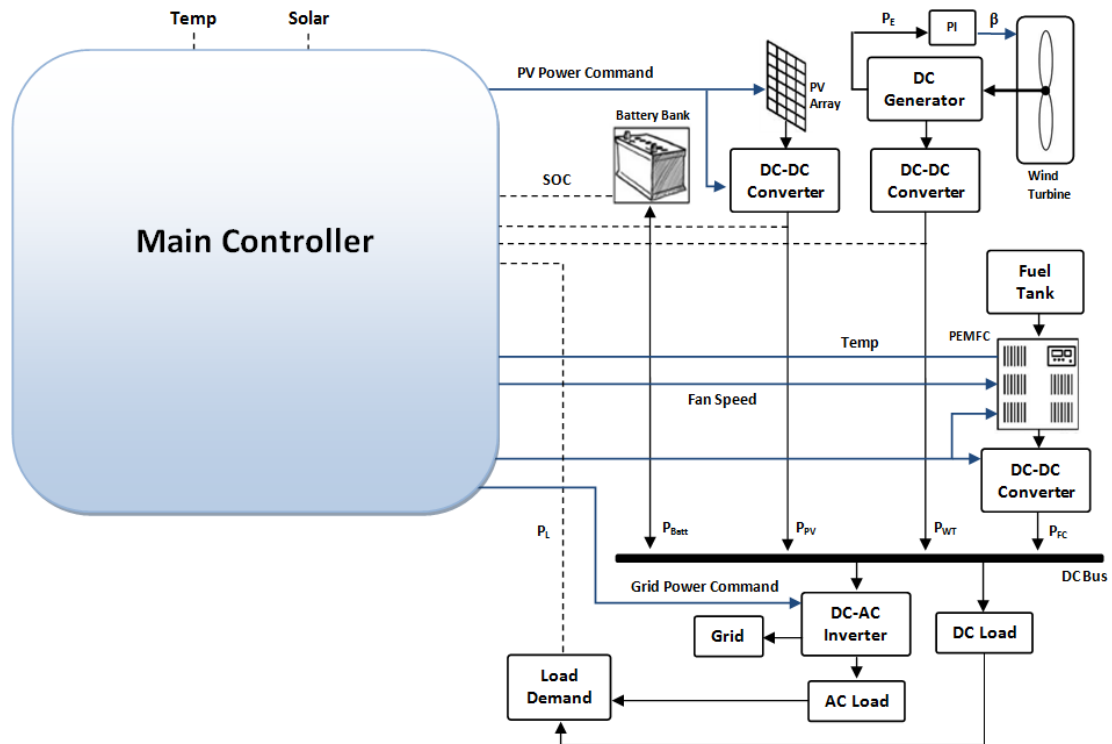
Figure 6.1 - Block diagram of the developed hybrid power system

6.1.1 The photovoltaic model

A model of PV panel with moderate complexity which includes the series resistance, the saturation current of the diode, and the temperature independence of the photocurrent source is considered based on the Shockley diode equation (see Section 3.3). The PV model is built and implemented using Simulink to verify the nonlinear I–V and P–V output characteristics. The block diagram of the proposed

model[7] is implemented and shown in Figure 6.2. The symbol f(u) in the Function block library shown in Figure 6.2 is a built-in function notation in Simulink. Each function uses a notation with a meaningful lettering to make it readable and maintainable; e.g. reverse saturation current function stands for the implementation of Equation (3.5).
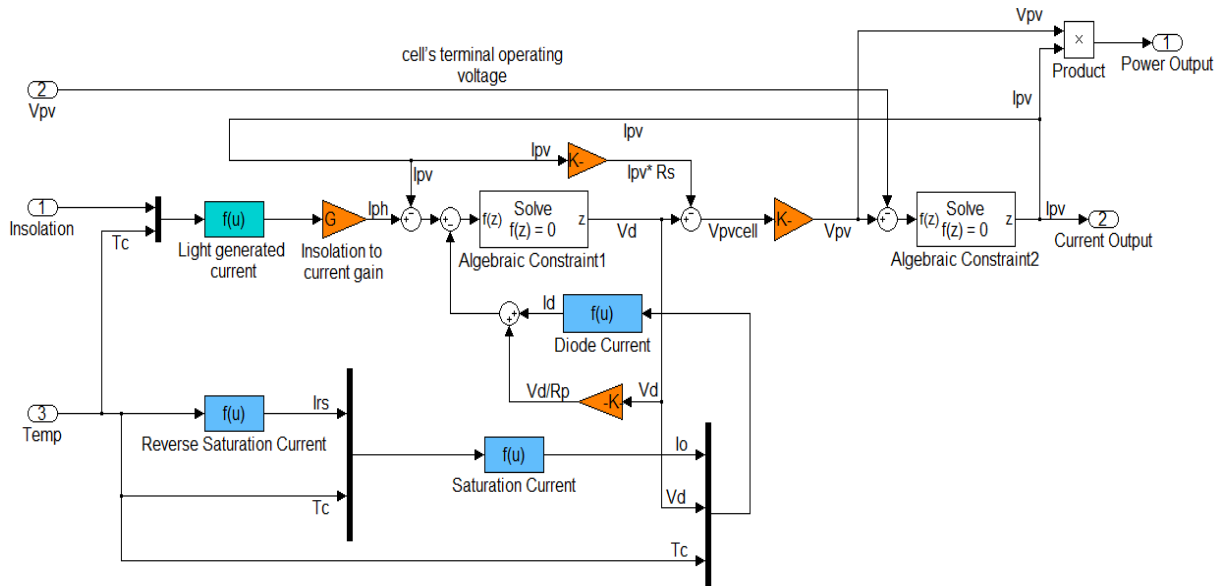
Figure 6.2 - Subsystem implementation of the PV model

The PV model parameters are usually extracted from the manufactures data sheet, an extract of which can be seen in Table 3.3 (Section 3.5). The parameters required (PV panel) are the open circuit voltage, short circuit current, maximum power current, and maximum power voltage.

Therefore, the proposed model is designed to have a dialog box as shown in Figure 6.3, in which the parameters of PV module can be configured in the same way for the Simulink block libraries.

---

[7] The develop model is suitable with all PV cell, module and array; in order to analyze the MPPT.
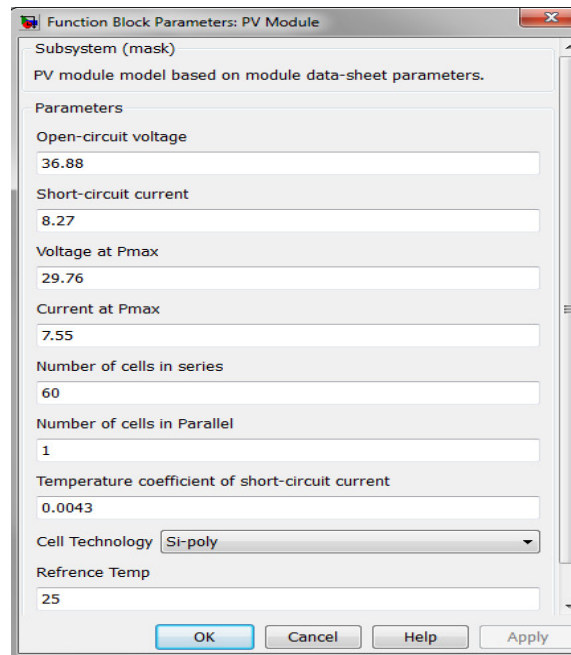
Figure 6.3 - Dialog box of the PV model

The inputs for the proposed PV model are solar irradiation, cell temperature and PV manufacturing data sheet information. In this chapter, Astronergy CHSM6610P-225 PV module is taken as an example. The proposed PV model was simulated using MatLab/Simulink, as shown in Figure 6.4.
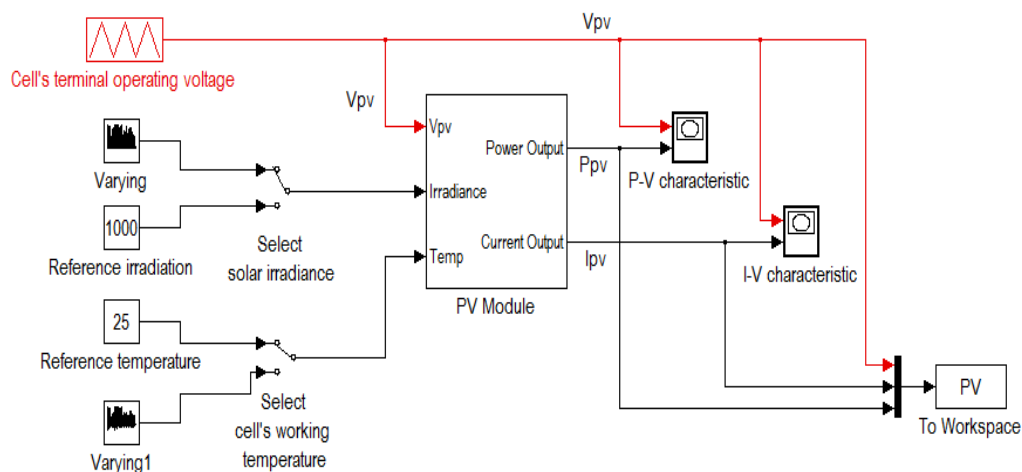
Figure 6.4 - Implementation of the PV model

Both P-V and I-V output characteristics of generalized PV model for Astronergy PV module are shown in Figure 6.5. The nonlinear nature of PV module is apparent as

shown in the figures, i.e., the output power and current of PV module depend on the solar irradiance and cell temperature, and the cell terminal operating voltage as well. It was found from Figure 6.5(a) and 6.5(b) that, with increased solar irradiance, there is an increase in both the maximum power output and the short circuit current. On the other hand, we observed from Figure 6.5(c) and 6.5(d) that with an increase in the cell temperature, the maximum power output decreases whilst the short circuit current increases.
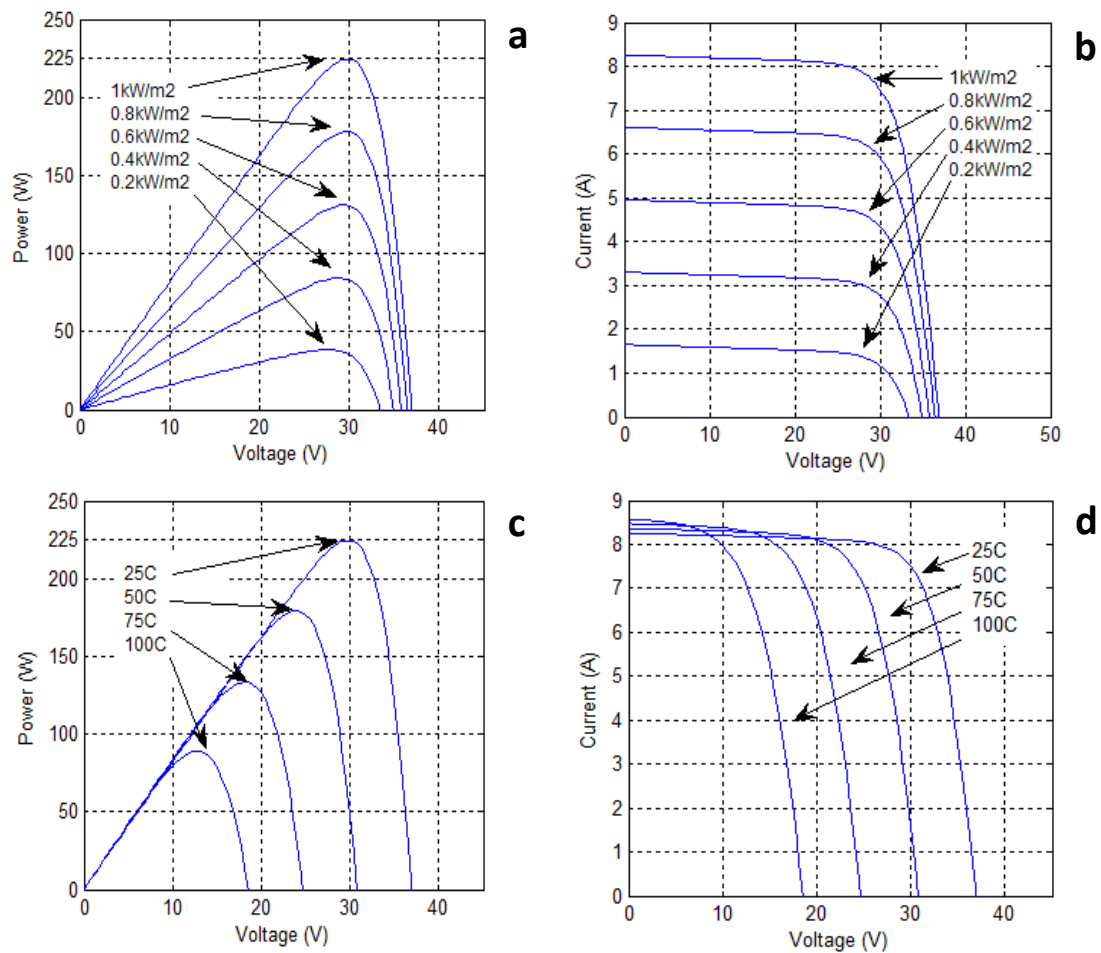
Figure 6.5 - I-V and P-V output characteristics **(a-b)** with different G **(c-d)** with different T_c

The developed model was validated through a series of experiments as show in Figure 6.6.

The experimental rig consists of one Astronergy CHSM6610P-225 solar panel, adjustable load resistance, and some measurement instrumentation.

Figure 6.6 - The experimental test rig

The PV module was placed at an inclination angle of 45°. A series of measurements were then conducted using the set up on a warm sunny day in August ($850W/m^{2}$). Measurements were taken under different load setting, as shown in Table 6.1.

Observation of temperature, solar irradiance, working voltage and output current of PV module were taken and recorded each time the load was changed. It was found that both simulated and measured results for the output power of PV module are in good agreement as shown in Figure 6.7. The difference is less than 1.35W and the standard deviation is 0.39W. This proves the correctness of the proposed model.

Table 6.1 - Experiment results for the Astronergy CHSM6610P-225 solar panel

Load (Ω)	Voltage (V)	Current (A)	Power (W)
0.1	0.83	7.084	5.88
0.2	1.53	7.02	10.74
0.3	2.22	7.04	15.62
0.4	2.91	6.96	20.25
0.5	3.56	6.97	24.8
0.6	4.27	6.94	29.63
0.7	4.92	6.89	33.9
0.8	5.6	6.889	38.58
0.9	6.3	6.94	43.72
1	7	6.96	48.72
2	13.7	6.95	95.21
3	20.7	6.9	142.83
4	25.41	6.3	160.08
5	27.57	5.5	151.63
6	28.5	4.84	138
7	29.4	4	118.1
9	30.1	3.2	96.25
12	30.58	2.6	79.3
20	31.23	1.6	49.84
40	31.72	0.8	25.37
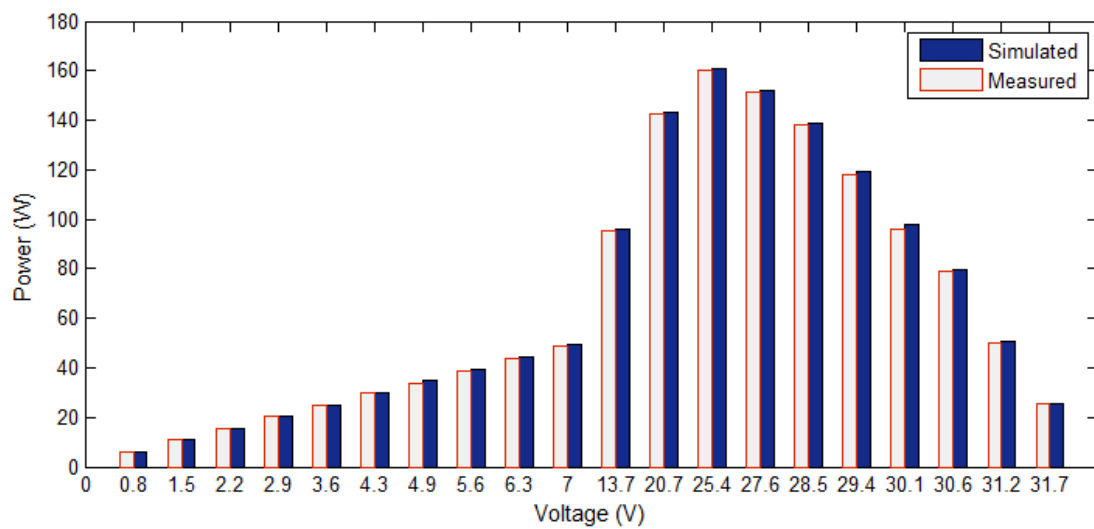
Figure 6.7 - Results comparison for the simulation and experimental approaches during a sunny day on August (850W/m^2, 44°C)

6.1.2 The wind turbine model

The amount of power that a wind turbine can extract from the wind depends on the turbine design. Factors such as the wind speed and the rotor diameter affect the amount of power that a turbine can extract from the wind. The wind turbine was modelled using the mathematical equations shown in Section 4.4. Figure 6.8 shows the wind turbine model which adopted for this study (Siegfried 1998). As illustrated, there are three inputs and one output. The three inputs are the generator speed, the pitch angle,[8] and the wind speed. The output is the torque applied to the generator shaft.
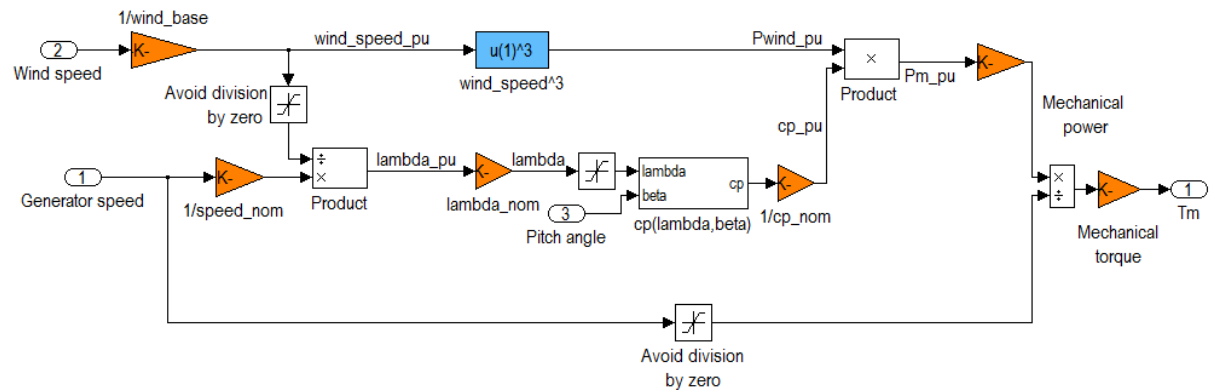
Figure 6.8 –Subsystem implementation of the wind turbine

The built-in SimPowerSystem block model of a DC machine is used as a power generator driven by the wind turbine (MathWorks 2012). As shown in Figure 6.9, the rotor shaft is driven by the wind turbine which produces the mechanical torque according to the generator and wind speed values. Model parameters are entered via the dialog boxes, as shown in Figure 6.10.

---

[8] The pitch angle is controlled in order to limit the generator output power to its nominal value for high wind speeds.
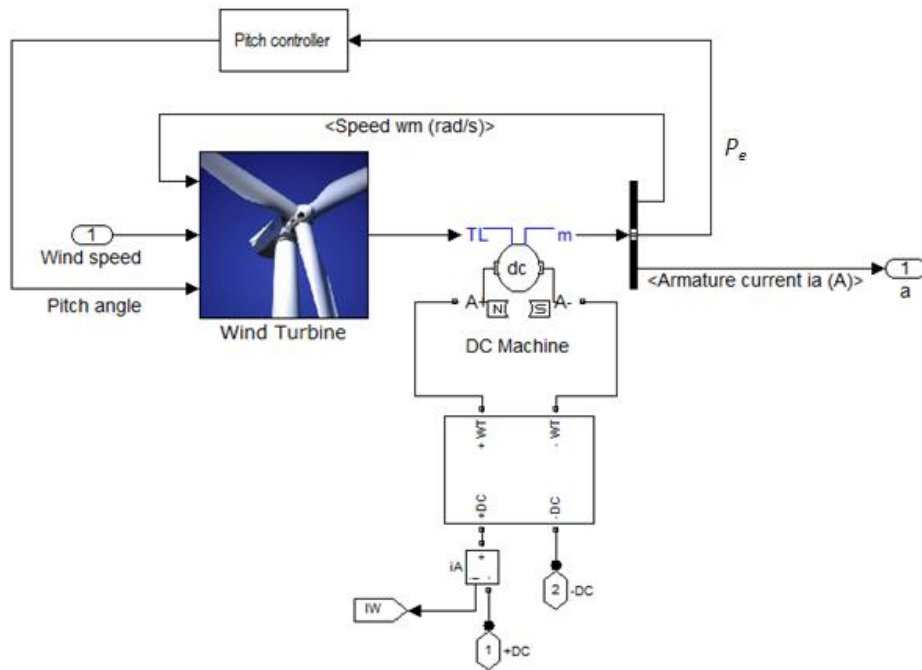
Figure 6.9 – Implementation of the wind turbine DC generator model
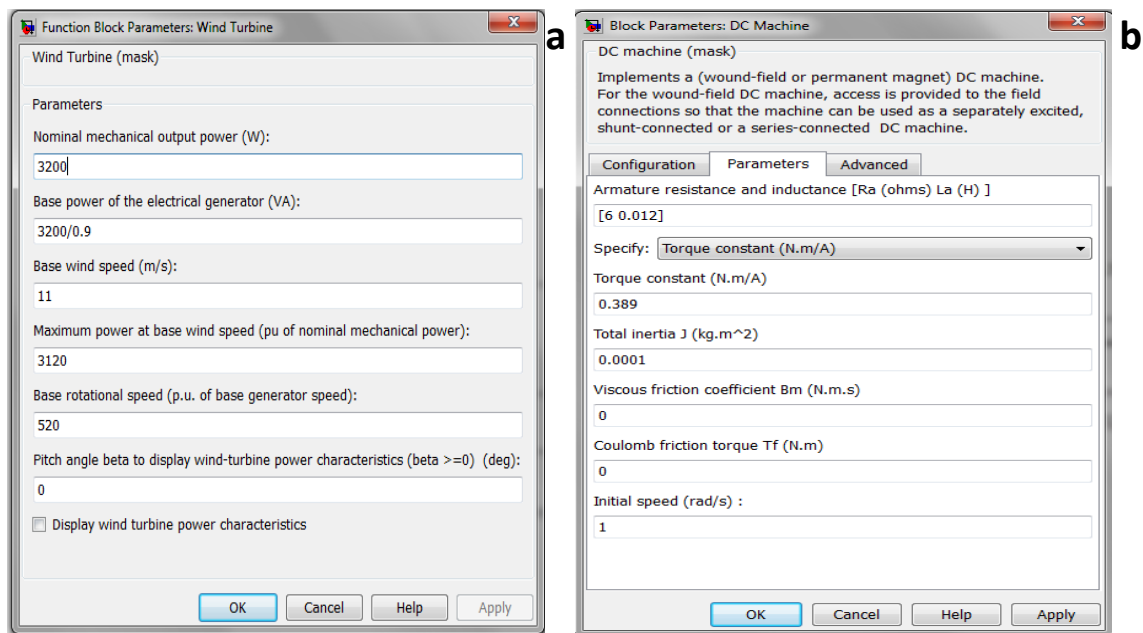
Figure 6.10 - (a) Dialog box of the WT model **(b)** Dialog box of the DC generator model

A Proportional-Integral (PI) controller[9] is used to control the blade pitch angle in order to limit the electric output power to the nominal mechanical power. The control system is illustrated in the figure below.

---

[9] The pitch angle change a little (Hwas & Katebi 2012), therefore PI controller has been selected.
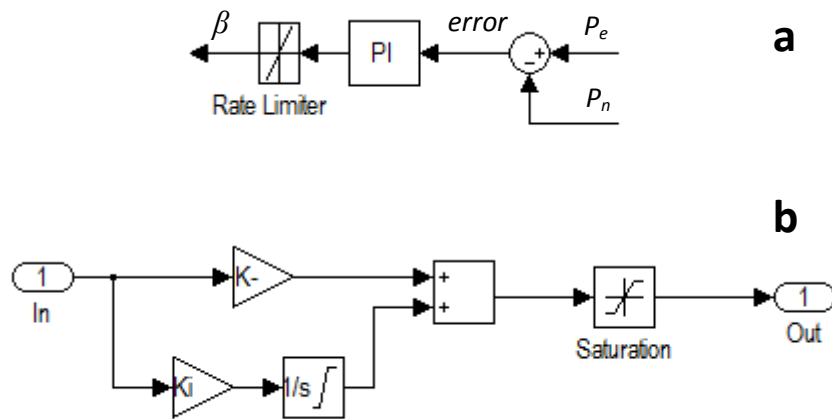
Figure 6.11 – (a) Pitch control **(b)** Subsystem implementation of the PI controller

Hence, the PI controller and desired pitch angle (β) can be expressed as follows:

$$\beta = K_P (p_e - p_n) + K_i \int (p_e - p_n) dt \tag{6.1}$$

Where K_p is the proportional gain, K_i is the integral gain, p_e is the electric output power, and p_n is the nominal mechanical power. The PI controller will keeps the pitch angle constant at zero degree when the measured electric output power is under its nominal value. When it increases above its nominal value the PI controller will increases the pitch angle to bring back the measured power to its nominal value. As shown in Figure 6.12, the control system successfully maintains the generator output power to its nominal value for high wind speeds.
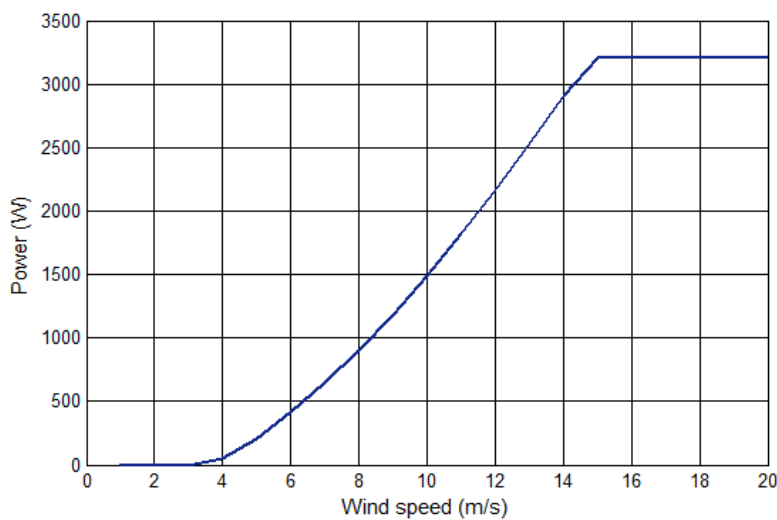
Figure 6.12 - wind turbine characteristics

6.1.3 The Li-Ion battery model

The model of the Li-Ion battery is implemented in MatLab/Simulink based on the mathematical equations shown in Section 5.2.3. It is implemented using several standard Simulink blocks as well as some of the SimPowerSystem blocks as shown in Figure 6.13. The output of this model is a vector containing three signals: state-of-charge (SOC), battery current and battery voltage.
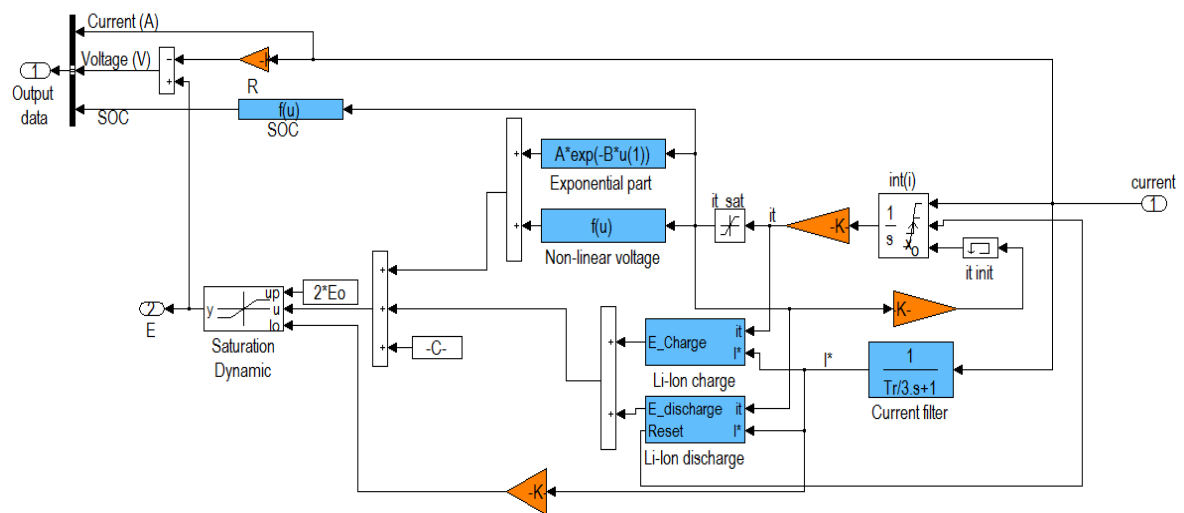
Figure 6.13 - Subsystem implementation of the Li-Ion battery model

The main feature of this battery model (see Section 5.2.3) is that the parameters can easily be deduced from a manufacturer's discharge curve. Model parameters are entered via the dialog box as shown in Figure 6.14.

In previous work (Tremblay & Dessaint 2009), the dynamic behaviour of the battery model has been validated with respect to current variation and the battery SOC. Figure 6.15 shows the dynamic discharge and charge of a 2.3Ah, 3.3V Li-Ion battery.
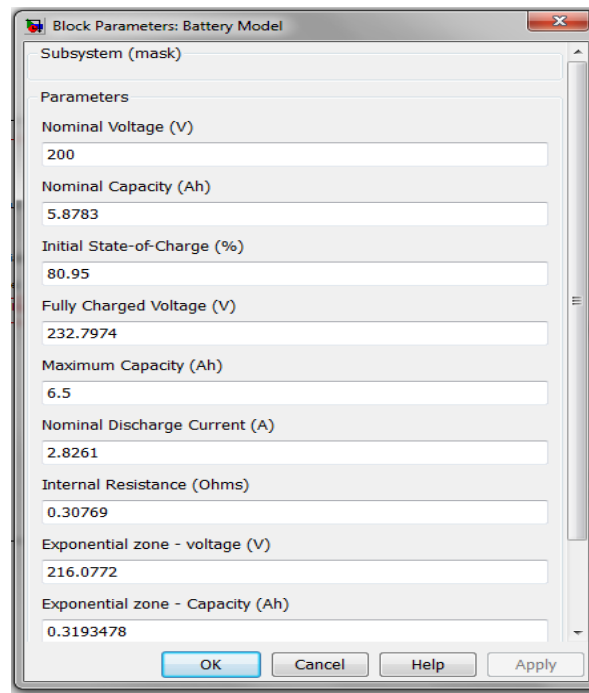
Figure 6.14 - Dialog box of the Li-Ion battery model
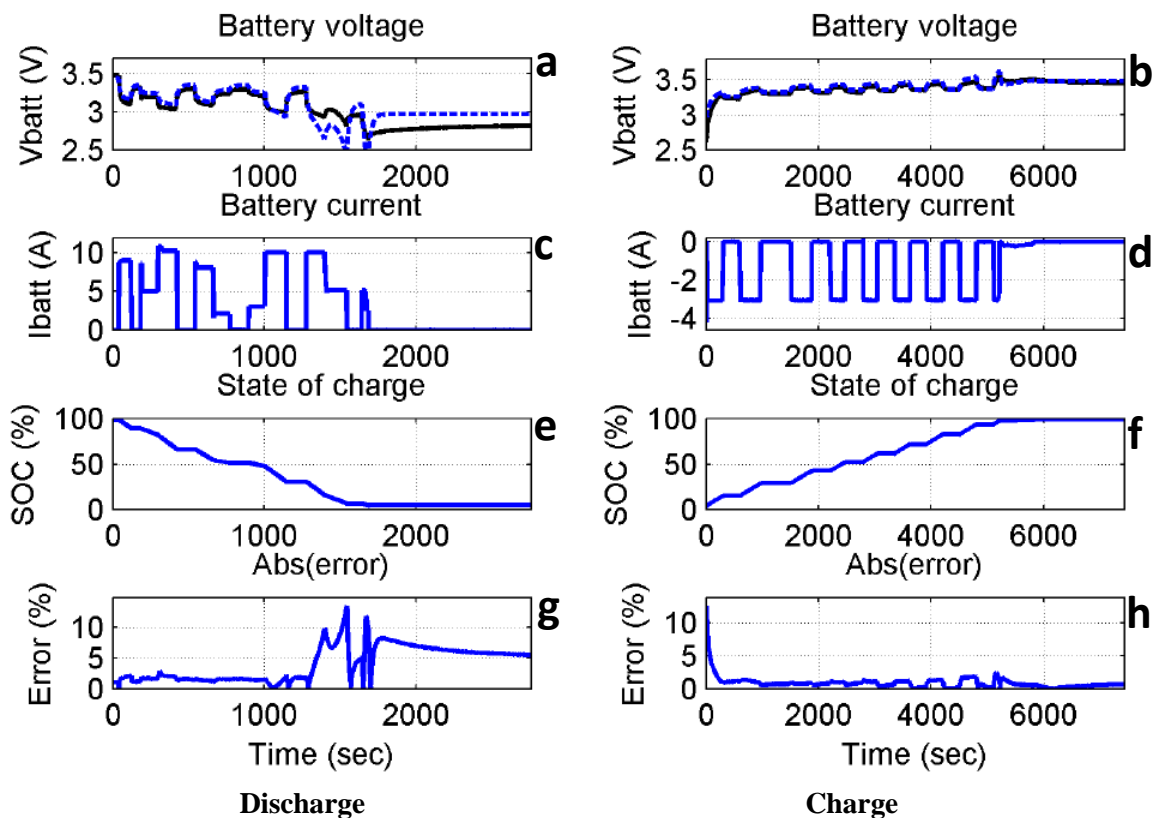
Figure 6.15 – Dynamic discharge and charge of a 2.3Ah, 3.3V Li-Ion battery

(a, b) simulated and experimental battery voltage **(c, d)** battery current variation

(e, f) estimated battery SOC **(g, h)** absolute error between the real and simulated voltage

It can be noted when the SOC between 20%-100%, the error between the real voltage (black solid line) and the simulated voltage (blue dotted line) is within 5%. When the SOC decreases below 20%, the error of the simulation model is around 10%. However, this is acceptable since the desired SOC limits[10] are between 40% - 80%.

6.1.4 The PEMFC stack model

The dynamic PEMFC model[11] described in Section 5.3.4 is built and implemented using MatLab/Simulink. The modified fuel cell model[12] combines the features of chemical (Qiuli et al. 2006) and electrical models (Runtz & Lyster 2005). Hence, it's suitable for electrical simulation programs and can represent the effect of operating parameters on the stack. The model is implemented as shown in Figure 6.16.
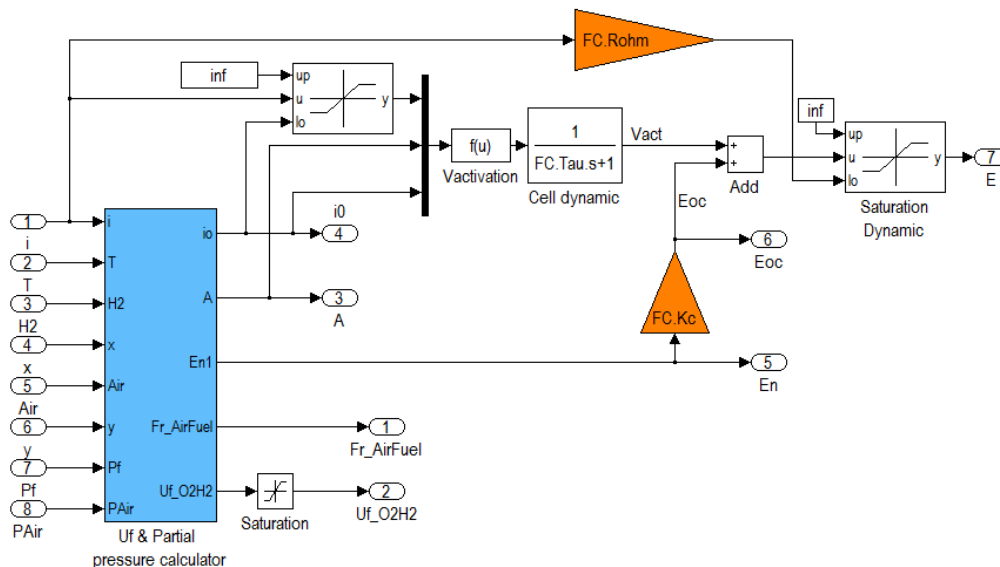
Figure 6.16 - Subsystem implementation of the PEMFC stack model

Fuel cell manufacturers provide specifications of their stacks which include the peak power, polarization curve, number of cell, etc. These data, as shown in Section 5.3.4,

---

[10] The proposed management system maintains the SOC at a reasonable level 40-80% (see Section 7.4).

[11] The model requires only few variables from manufacturer datasheets (see Section 5.3.4)

[12] The PEMFC stack model is modified to include a fuzzy logic temperature controller (see Section 7.5)

are used to obtain the models parameters. Model parameters are entered via the dialog box as shown in Figure 6.17.
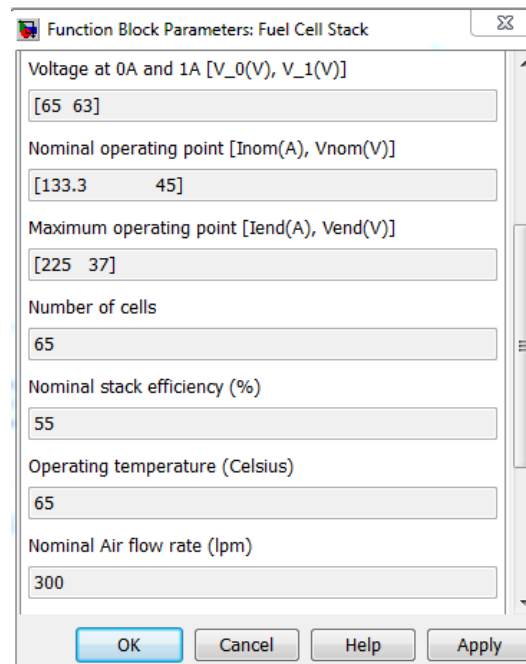
Figure 6.17 - Dialog box of the PEMFC model

There are several methods which can be used to validate the model. The suggested validation approach consists of comparing directly the obtained polarization curve using the model with those of the manufacturers. Figure 6.18 shows the result for the 6kW-45V, PEMFC stack (the NedStack PS6[13]). The dotted line shows the simulated curve whereas the solid line is the real curve (experimented curve) from datasheet. As describe in Section 5.3.4, the variables are extracted from the datasheet[1] as follow:

- Voltage at 0 A and 1 A = (65, 63)
- Maximum operating point (I_{max}, V_{min}) = (225, 37)
- Nominal operating point (I_{nom}, V_{nom}) = (133.3, 45)
- Nominal stack efficiency = 55%
- Operating temperature = 65°C
- Number of cells in series = 65

---

[13] The datasheet can be found at http://www.fuelcellmarkets.com/content/images/articles/ps6.pdf.

- Nominal air flow rate = 297 l/min
- Nominal composition of fuel and air = (99.99, 21)
- Nominal supply pressure (H_2, Air) = (1.5, 1)
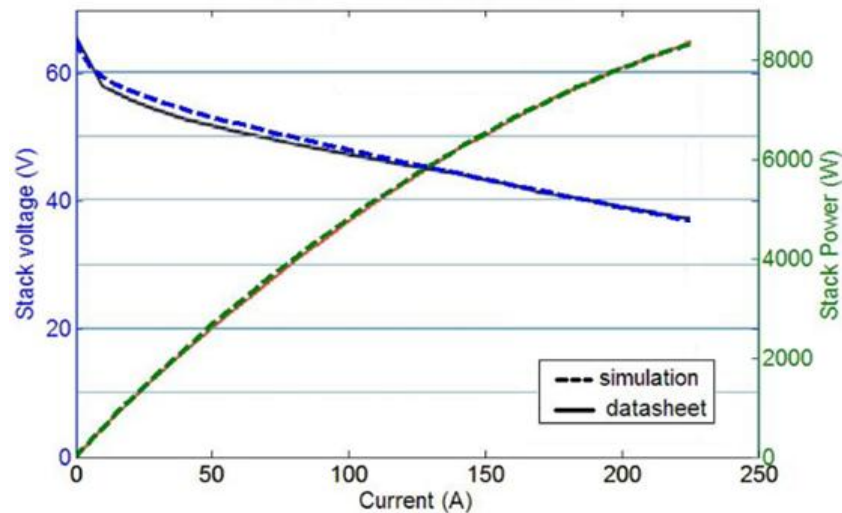
Figure 6.18 - Simulations and datasheet results

It is observed that the real curve matches exactly the simulated one, which shows that the obtained parameters of this model can represent the fuel cells correctly[14].

6.2 The power conditioners models

Power electronics refers to control and conversion of electrical power by semiconductor devices, wherein these devices operate as switches. It has applications that extend over the entire field of electrical power systems (see Section 1.3.3), with a power range from a few Watts to several Megawatts.

The main task of power electronics is to control and convert electrical power from one form to another. The four main forms of conversion are: AC-to-AC rectification, DC-to-AC conversion, DC-to-DC conversion, and AC-to-AC conversion

In the following discussion, we will explain the basic characteristics of DC/DC converter, and DC/AC inverter.

---

[14] The level of accuracy of the model depends on the precision of data provided by the user.

6.2.1 The DC/DC converters

To connect a photovoltaic, wind turbine or PEM fuel cell to an external power system (e.g. DC load), it is necessary to boost their voltage or to increase their number. Therefore, a DC averaged switched model converter is needed to regulate the output voltage before being supplied to other electronic devices.

There are many DC-to-DC converters including the step-down (buck) converter, the step-up (boost) converter, the buck-boost converter and many others. The following will evaluate the step-up (boost) converter which is shown in Figure 6.19.
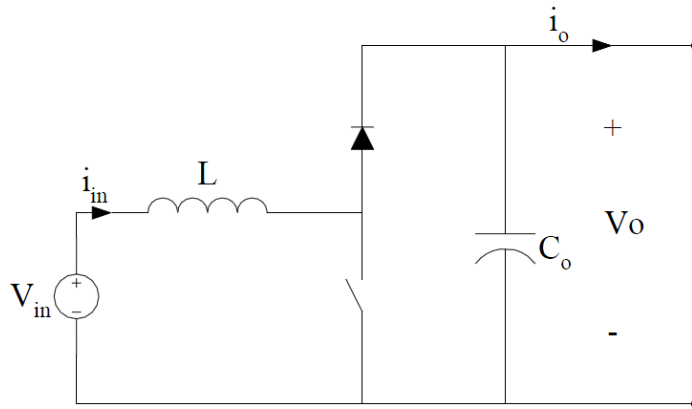
Figure 6.19 - Step-up boost converter

Boost converter is a class of switching mode power supply (SMPS), it contains at least one energy storage element, and at least two semiconductor devices (MOSFET and a diode).

Semiconductor devices (MOSFET and diode) operate as an ideal power switch; OFF when the switch current is very close to zero, and ON when the voltage across is relatively small. By applying net volt-seconds to inductor over one switching period (T_s), the boost converter output voltage can be calculated as follows:

$$\int_0^{T_s} V_L(t)dt = V_{in}(DT_s) + (V_{in} - V_o)(1-D)T_s \qquad \textbf{(6.2)}$$

Where V_L is the inductor voltage, V_{in} is the input voltage, V_o is the output voltage, T_s is the switching period and D is the switch duty cycle ($0 \leq D \leq 1$).

Equal to zero and collect term:

$$V_{in}(D+1-D) - V_o(1-D) = 0 \qquad \text{(6.3)}$$

Therefore, the voltage conversion ratio for the boost is:

$$R(D) = \frac{V_o}{V_{in}} = \frac{1}{(1-D)} \qquad \text{(6.4)}$$

Consequently, from the above equations, a DC switch model converter is built and implemented using MatLab/Simulink. The proposed model is implemented as shown in Figure 6.20.
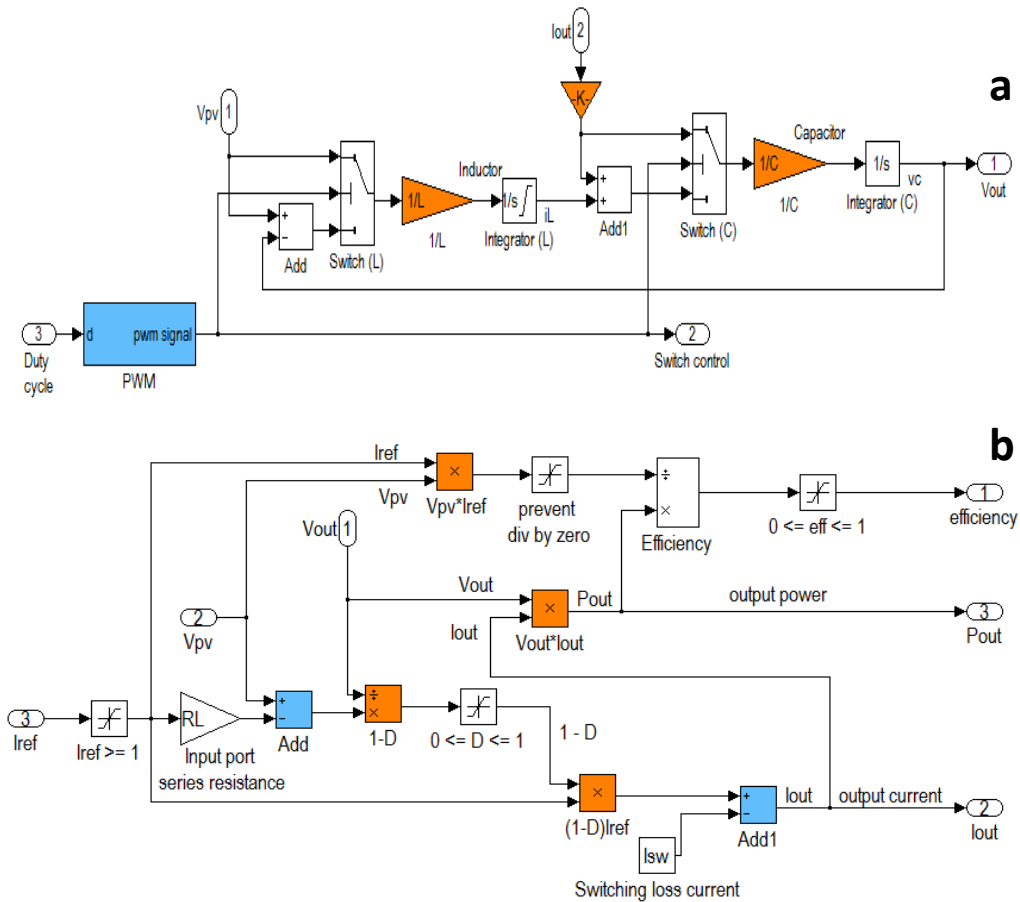
Figure 6.20 - Subsystem implementation of the DC/DC converter model with[15] **(a)** Duty cycle control **(b)** Input current reference (Natsheh & Albarbar 2011).

---

[15] Choices for the boost DC/DC control variable (Erickson 2000):
- Duty cycle D
- Input current reference I_{ref}
- Input voltage reference V_{ref}

As mention in Section 1.3, in power electronics the control stage is used to control that amount of power needed (more information can be found in Chapter 7).

6.2.2 The DC/AC inverters

A DC/AC switching inverter is developed, as shown in Figure 6.21.
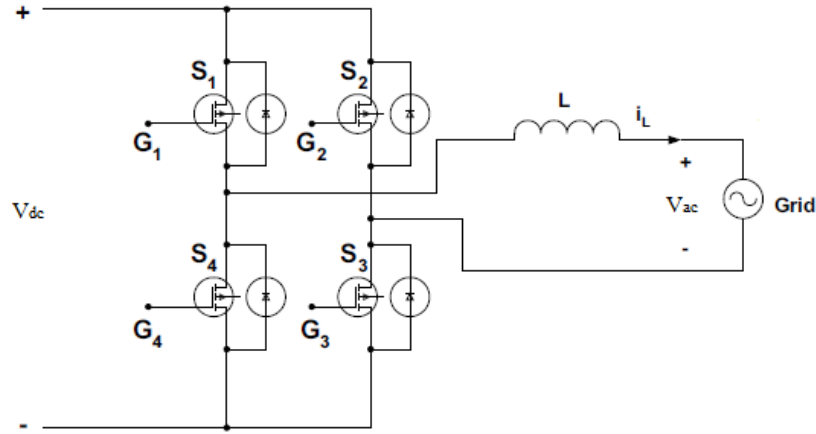
Figure 6.21 - DC/AC switching inverter

The basic operation of the DC/AC switching inverter is to generate AC waveform from the DC signal, by operating each pair of switches S_1-S_3 and S_2-S_4 alternately with their duty cycle for each switching period.

By applying net volt-seconds to the inductor over one switching period, the AC output voltage can be calculated as follow:

$$V_L = \frac{1}{T_s}\int_0^{T_s} V_L(t)\,dt = D(V_{dc} - V_{ac}) + (1-D)(-V_{dc} - V_{ac}) \tag{6.5}$$

Where V_{ac} is the AC voltage and V_{dc} is the DC voltage. Equal to zero and collect term:

$$(2D-1)V_{dc} - V_{ac} = 0 \tag{6.6}$$

Therefore, the voltage conversion ratio for the inverter is:

$$R(D) = \frac{V_{ac}}{V_{dc}} = 2D - 1 \tag{6.7}$$

With a voltage conversion ratio equal to (2*D*-1), an AC averaged switch model inverter is built and implemented using MatLab/Simulink (Natsheh & Albarbar 2012), to convert the direct current into alternating current, at a switching frequency greater

than the AC line frequency (50Hz - 60Hz). Losses are included due to output-port series resistance and input-port switching loss current. The proposed model is implemented as shown in Figure 6.22.
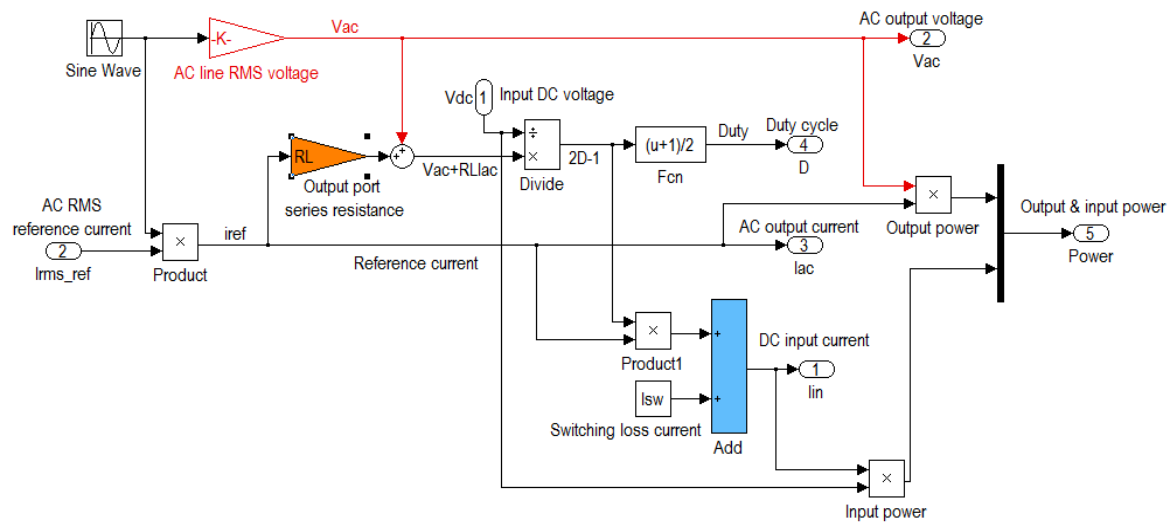
Figure 6.22 - Subsystem implementation of the DC/AC inverter model

6.3 Summery

The availability of hybrid system model is important for its theoretical study, as it can be used to study its behaviour. In this chapter the dynamic simulation model is described for a PV, wind turbine, PEMFC, and Li-Ion battery. Modelling and simulation are implemented using MatLab/Simulink and SimPowerSystem software packages.

▪ For PV panel: a generalized model has been developed and verified using Sharp's NUS0E3E PV panel datasheet. More, the developed model was validated through a series of experiments. It was found that both simulated and measured results for the output power of PV module are in good agreement. The standard deviation is 0.39W.

▪ For wind turbine: a PI controller has been implemented to control the blade pitch angle. Simulation result shows that the control system successfully maintains the generator output power to its nominal value for high wind speeds.

- For battery bank: the dynamic behaviour of a Li-Ion battery model has been validated with respect to current variation and the battery SOC. It was noted that when the SOC between 20%-100%, the error between the real voltage and the simulated voltage is less than 5%.

- For fuel cells: the developed model has been validated by comparing directly the obtained polarization curve using the model with those of the manufacturers It was observed that the real curve matches exactly the simulated one. The level of model accuracy depends on the precision of data provided by the user.

The next chapter addresses the implementation of the proposed control structure.

Chapter 7

Hybrid Systems Energy Controller Based on Artificial Intelligence

*This **chapter** presents a **novel** adaptive **scheme** for **energy management** in **stand-alone hybrid** power systems. The proposed **management system** is designed to **manage** the **power flow** between the **hybrid power** system and **energy storage** elements in order to **satisfy** the **load** requirements based on **artificial neural network** (ANN) and **fuzzy logic** controllers. The developed **management system performance**, as illustrated in **Chapter 6**, was assessed using a hybrid system comprises **PV** panels, **wind turbine** (WT), **battery** storage, and **proton exchange membrane fuel cell** (PEMFC).*

7.1 Introduction

Hybrid power systems with fuel cells and batteries have the great potential to improve the operation efficiency and dynamic response. However, the price of PEMFC is high and its membrane lifetime is short (less than 2000 h for transportation and ~ 20,000 h for stationary) (Wang et al. 2011). In addition, the dynamic interaction between the load demand and the renewable energy source can lead to, critical problems of stability and power quality, that are not very common in conventional power systems. Therefore, managing flow of energy throughout the proposed hybrid system is essential to ensure the continuous power supply for the load demand.

This chapter will present an optimized adaptive management strategy for power flows in stand-alone hybrid power systems. The method offers an on-line energy management by a hierarchical controller between four energy sources comprises photovoltaic panels, wind turbine, battery storage, and proton exchange membrane fuel cell. The proposed method includes a MPPT controller in the first layer, to achieve the maximum power point (MPP) for different types of PV panels; two different techniques will be presented (P&O and neural network). In the second layer, an advance fuzzy logic controller will be developed to distribute the power among the hybrid system and to manage the charge and discharge current flow for performance optimisation. Finally in the third layer, smart controllers are developed to maintain the stability of the PEMFC temperature and to regulate the fuel cell/battery set points to reach best performance. Figure 7.1 shows the proposed control structure for the hybrid generation system.

Each layer will be explained in detail later in this chapter, but before that an overview of Artificial Intelligence will be provided.
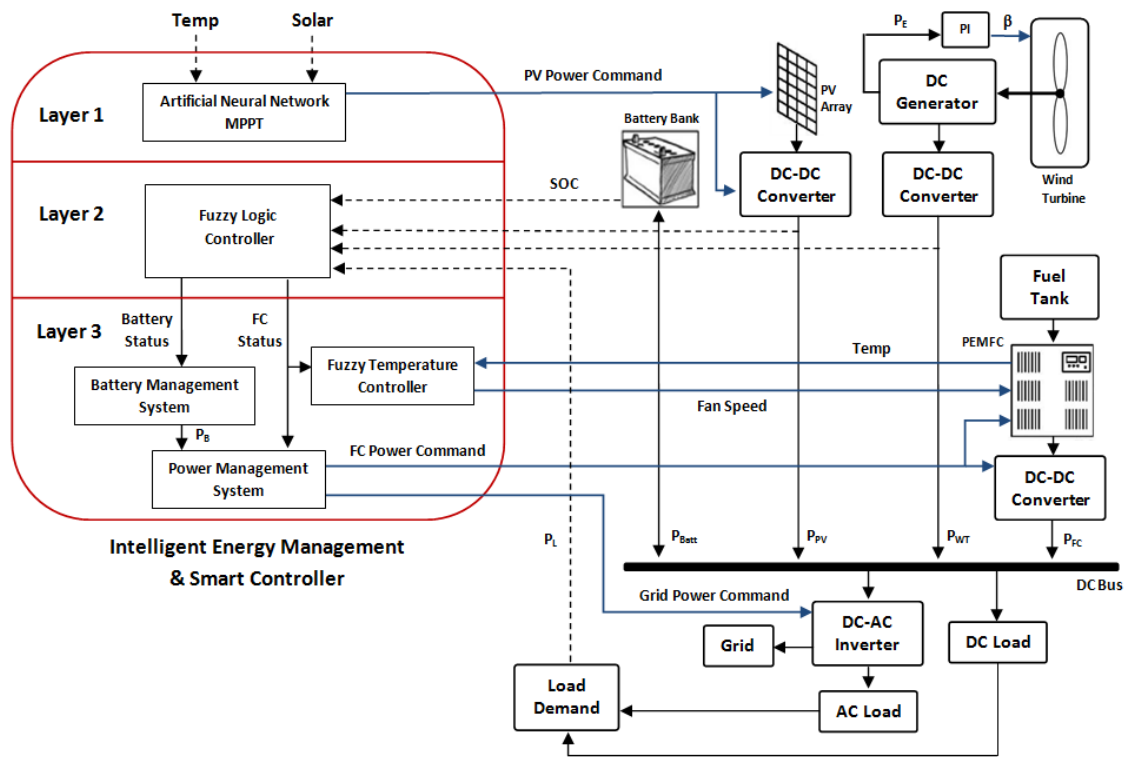
Figure 7.1 - Block diagram of the proposed system

7.2 Artificial intelligence: overview

7.2.1 Artificial neural networks

Artificial neural network has a form of multiprocessor computing system. It consists of a number of very simple and highly interconnected processors, called neurons, which are analogous to the biological neurons in the brain. The basic model of a single neuron is shown in Figure 7.2.
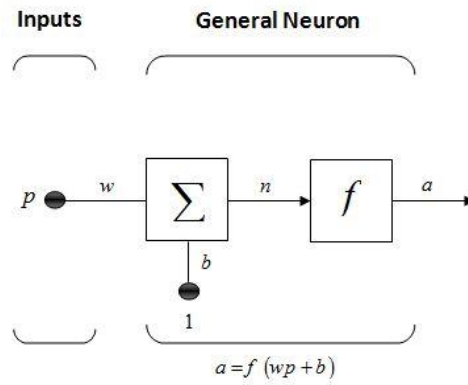
Figure 7.2 - Architecture of a single artificial neuron

Figure 7.2 shows a single artificial neuron with an input vector p , a connection weight vector w, a bias b , an activation function f and an output a . The output (a) of this neuron is defined as follows (Haykin 1998):

$$a = f(\mathbf{p} \cdot \mathbf{w} - b) = f\left(\sum_{n=1}^{N} p_n \cdot w_n - b\right), \forall \mathbf{p} = \begin{pmatrix} p_1 \\ \cdot \\ \cdot \\ \cdot \\ p_N \end{pmatrix}, \forall \mathbf{w} = \begin{pmatrix} w_1 \\ \cdot \\ \cdot \\ \cdot \\ w_N \end{pmatrix} \qquad (7.1)$$

The effect of the bias b on the activation function f is a shift to the left or the right, depending on whether it is positive or negative. The activation function f can be taken from a set of activation functions (as piecewise-linear function, hard limit function, sigmoid function). Some of the most popular activation functions are shown in Figure 7.3.
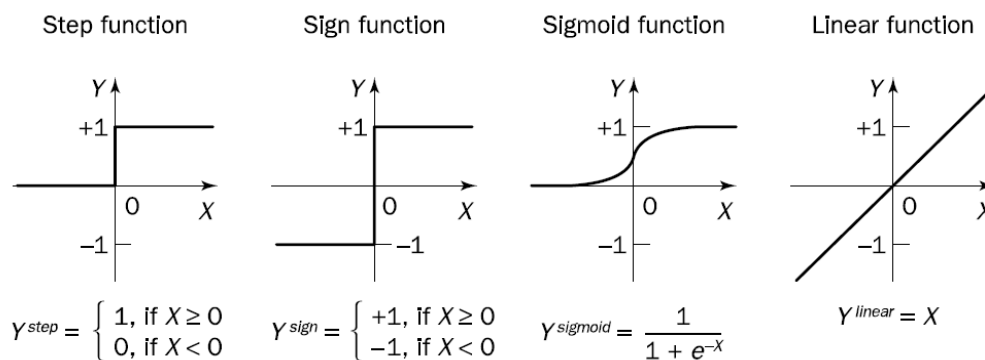
Figure 7.3 - Popular activation functions used in ANN

Using this basic model of a neuron as shown in Figure 7.2, different ANN architectures have evolved, among them feed-forward neural network.

Feed-forward ANNs allow signals to travel in one way only; from inputs to outputs. They are extensively used in nonlinear system modelling (Hagan & Bemuth 1996).

The earliest kind of neural network is a single layer perceptron network which consists of a single layer of output nodes; the inputs are fed directly to the outputs via a series of weights. In this way it can be considered the simplest kind of feed-forward network.

The next popular feed-forward model, as shown in Figure 7.4, is the multi-layer perceptron. It is a feed forward neural network model that maps sets of input data onto a set of outputs. It has more than two layers. The layers are fully connected. So that, every neuron in each layer is connected to every other neuron in the adjacent forward layer.
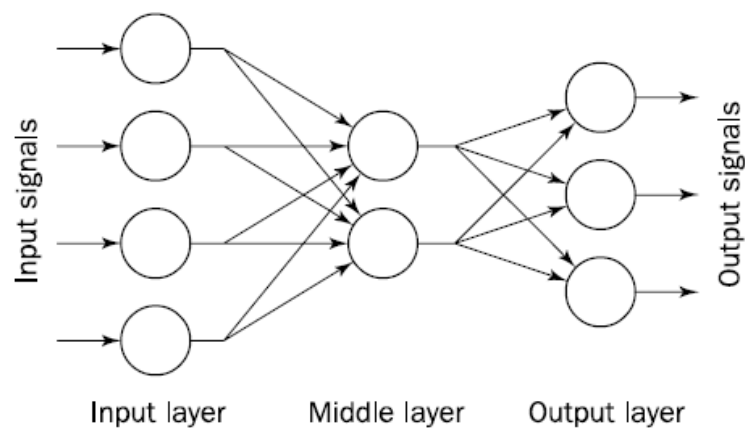
Figure 7.4 - Architecture of a multilayer perceptron

A neuron determines its output in a way similar to Rosenblatt's perceptron (Negnevitsky 2004).

First, it computes the net weighted input:

$$X = \sum_{i=1}^{n} x_i w_i - \theta \qquad (7.2)$$

Where n is the number of inputs and Θ is the threshold applied to the neuron.

Next, this input value is passed through the activation function[16].

Multi-layer networks use a variety of learning techniques, the most popular being back-propagation. In back-propagation, the learning law has two phases. First, a training input pattern is presented to the network input layer. The network then propagates the input pattern from layer to layer until the output pattern is generated by the output layer. If this pattern is different from the desired output, an error is calculated and then propagated backwards through the network from the output layer to the input layer. The weights are modified as the error is propagated. In this study, Levenberg Marquardt algorithm will be used in weights training. More information will be provided in Section 7.3.2.

7.2.2 Fuzzy expert system

Fuzzy logic is a type of logic that recognizes more than simple true and false values. It reflects how people think. It attempts to model our sense of words, our decision making and our common sense.

Fuzzy logic is determined as a set of mathematical principles for knowledge representation based on degrees of membership rather than on crisp membership of classical binary logic (Zadeh 1965).

In 1973, Lotfi Zadeh succeeded in outlined a new approach to analysis of complex systems (Zadeh 1973). He suggested capturing human knowledge in fuzzy rules. A fuzzy rule can be defined as a conditional statement in the form:

IF x is A
THEN y is B

---

[16]Multilayer network learns much faster when the sigmoidal activation function is represented by a hyperbolic tangent (Caudill 1991; Guyon 1991).

$$Y^{\tan h} = \frac{2}{1+e^{-2x}} - 1 \qquad \textbf{(7.3)}$$

Where x and y are linguistic variables, A and B are linguistic values determined by fuzzy sets on the universe of discourses X and Y, respectively.

In general, a fuzzy expert system incorporates not one but several rules that describe expert knowledge. The output of each rule is a fuzzy set, but usually we need to obtain a single number representing the expert system output.

To obtain a single crisp solution for the output variable, a fuzzy expert system first aggregates all output fuzzy sets into a single output fuzzy set, and then defuzzifies the resulting fuzzy set into a single number.

Although there are several defuzzification methods (Cox 1999), the most popular one is the centroid technique. It finds the point where a vertical line would slice the aggregate set into two equal masses. Mathematically this centre of gravity can be expressed as (Negnevitsky 2004):

$$COG = \frac{\sum_{x=a}^{b} \mu_A(x) x}{\sum_{x=a}^{b} \mu_A(x)} \qquad \textbf{(7.4)}$$

Where x is an element of the universe X, A is a fuzzy set of the universe X, and $\mu_A(x)$ is the membership function of set A.

In 1975, Mamdani built one of the first fuzzy systems to control a steam engine and boiler combination (Mamdani & Assilian 1975). He applied a set of fuzzy rules supplied by experienced human operators.

In general, the Mamdani-style fuzzy inference[17] process is performed in four steps: fuzzification of the input variables, rule evaluation, aggregation of the rule outputs, and finally defuzzification.

---

[17] Fuzzy inference can be defined as a process of mapping from a given input to an output, using the theory of fuzzy sets.

To shorten the time of fuzzy inference single spike, singleton, is used as the membership function of the rule consequent (Sugeno 1985). A singleton, or more precisely a fuzzy singleton, is a fuzzy set with a membership function that is unity at a single particular point on the universe of discourse and zero everywhere else.

Sugeno-style fuzzy inference is similar to the Mamdani method. Sugeno changed only a rule consequent. Instead of a fuzzy set, he used a mathematical function of the input variable. The format of the Sugeno-style fuzzy rule is:

IF x is A AND y is B

THEN z is $f(x, y)$

Where x, y and z are linguistic variables, A and B are fuzzy sets on universe of discourses X and Y, respectively, and $f(x, y)$ is a mathematical function.

The most commonly used **zero-order Sugeno fuzzy model** applies fuzzy rules in the following form:

IF x is A AND y is B

THEN z is k

Where k is a constant.

In this case, the output of each fuzzy rule is constant. In other words, all consequent membership functions are represented by singleton spikes.

The result (crisp output) is then obtained by finding the weighted average of these singletons.

It was found (Negnevitsky 2004) that Mamdani method is widely accepted for capturing expert knowledge. It allows us to describe the expertise in more intuitive, more human-like manner. However, for systems with many parameters Mamdani-type fuzzy inference entails a substantial computational burden. On the other hand, the Sugeno method is computationally effective and works well with optimization and

adaptive techniques, which makes it very attractive in control problems, particularly for dynamic nonlinear systems. Therefore in this work, system with many parameters (Section 7.4) Sugeno method has been used, whereas for system with few parameters (Section 7.5) Mamdani method has been used.

7.3 MPPT PV control systems

The output characteristics of the PV model with different solar irradiance and cell temperature are nonlinear. Furthermore, the solar irradiation is unpredictable, which makes the MPP of the PV module change continuously, as shown in Figure 7.5.
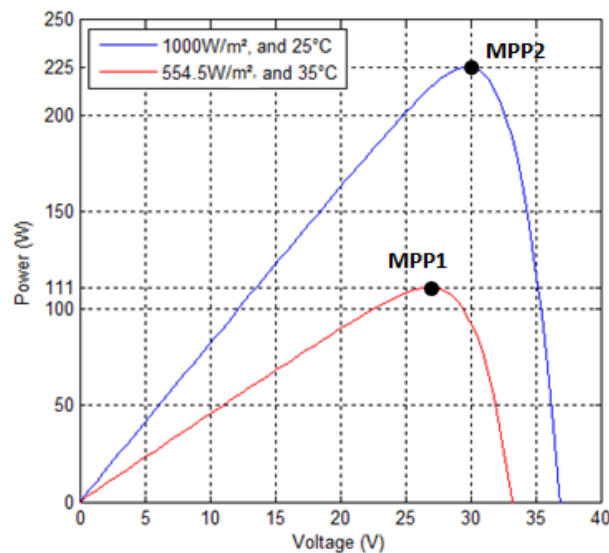
Figure 7.5 - MPP of a PV module under different conditions

Hence tracking the maximum power point (MPP) of a photovoltaic array is an essential part of a PV system. As such, many maximum power point tracking (MPPT) techniques have been developed and implemented (Esram & Chapman 2007). Among these techniques, hill-climbing MPPT such as perturb and observe (P&O), which is a simple algorithm that does not require previous knowledge of the PV module characteristics and is easy to implement with analogue and digital circuits.

In the literature there are two methods for implementing P&O algorithm: direct method (duty ratio perturbation) and indirect method (reference voltage/current perturbation).

In the direct methods, the MPP is searched by continuously perturbing the duty cycle of the DC-DC converter. Although the simplicity is the main feature of this method, it has a slower transient response compared to the indirect method and worse performance at rapidly changing irradiance (Elgendy et al. 2012).

In this section, intelligent control technique using artificial neural network is associated to an MPPT controller in order to increase the tracking response and consequently increase the tracking efficiency. Afterward, in chapter 8, to evaluate the performance of the proposed PV control system, a comparison between the indirect P&O algorithm and the proposed MPPT controller system is carried out, under different operating conditions.

7.3.1 Perturb and observe method

The problem considered by MPPT techniques is to automatically find the optimum voltage (V_{MPP}) or current (I_{MPP}) at which a PV array should operate, under a given solar irradiance and temperature.

Perturb and observe method is the most commonly used technique because of its simplicity and ease of implementation (Natsheh & Albarbar 2011). It requires two inputs: measurement of the current (I_{pv}) and measurement of the voltage (V_{pv}) (see Figure 7.6).
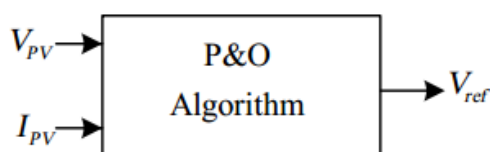
Figure 7.6 - P&O block diagram

The P&O algorithm operates by periodically perturbing (incrementing or decrementing) the PV array terminal voltage or current, and comparing the PV output power with the previous one. If it is positive the control system moves the PV array operating point in the same direction; otherwise, it is moved in the opposite direction. In the next perturbation cycle the algorithm continues in the same way. Figure 7.7 shows the flow chart of P&O algorithm.
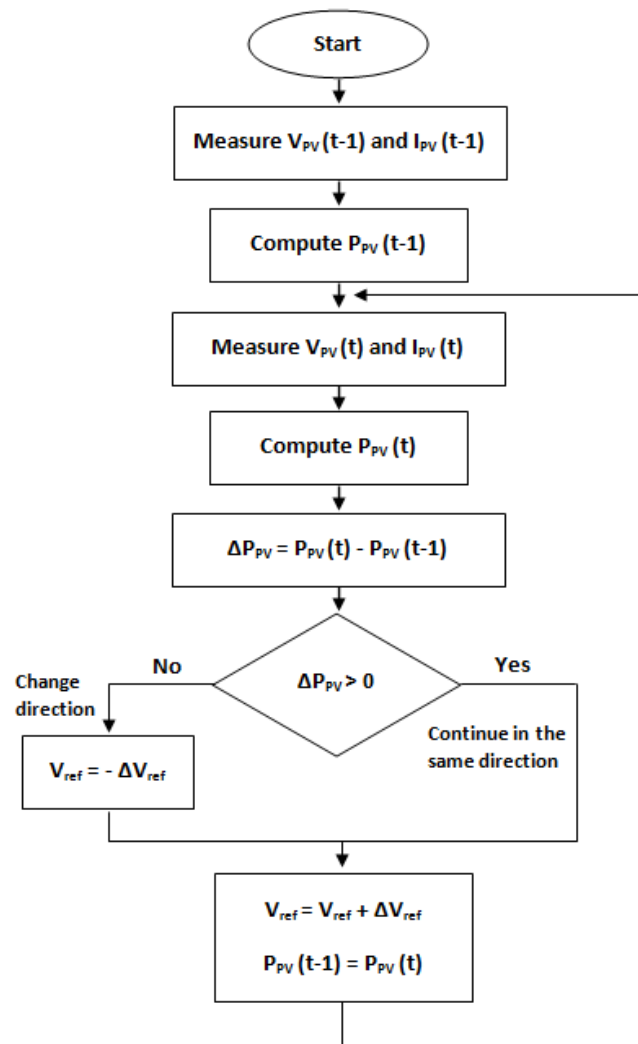
Figure 7.7 - P&O algorithm flow chart

The main problem of this method can be seen when solar radiation rapidly change. As illustrated in Figure 7.8, starting from an operating point **A**, if atmospheric conditions stay approximately constant, the voltage perturbation (ΔV) will bring the operating

point to **B** and the perturbation will be reversed due to a decrease in power. On the other hand, if the irradiance increases and shifts the power curve from P_1 to P_2 within one sampling period, the operating point will move from **A** to **C** (this represents an increase in the power and the perturbation is kept the same). Consequently, the operating point diverges from the MPP and will keep diverging if the irradiance steadily increases.
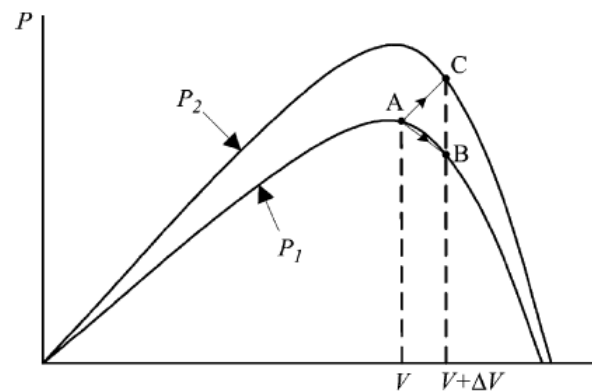
Figure 7.8 – Divergence of P&O from MPP (Wasynczuk, 1983)

Furthermore, P&O technique may cause many oscillations around the MPP, and this slows down the response of the system (see Section 8.1). Hence, to remove power fluctuates and to keep the load voltage stable, different controller has been used along with the P&O. Among these controllers: feedback controller (Natsheh & Albarbar 2011), linear PI (Elgendy et al. 2012), and non-linear passivity-based controller (PBC) (Tofighi & Kalantar 2011).

7.3.2 Artificial neural network method

A neural network is an artificial representation of the human body that tries to simulate its learning process. In other words, ANN is an adaptive system that changes its structure based on internal or external information that flows through the network. The aim of using ANN here is to optimize the response of the MPPT, in order to increase the tracking efficiency. Figure 7.9 shows the structure of the proposed PV control system.
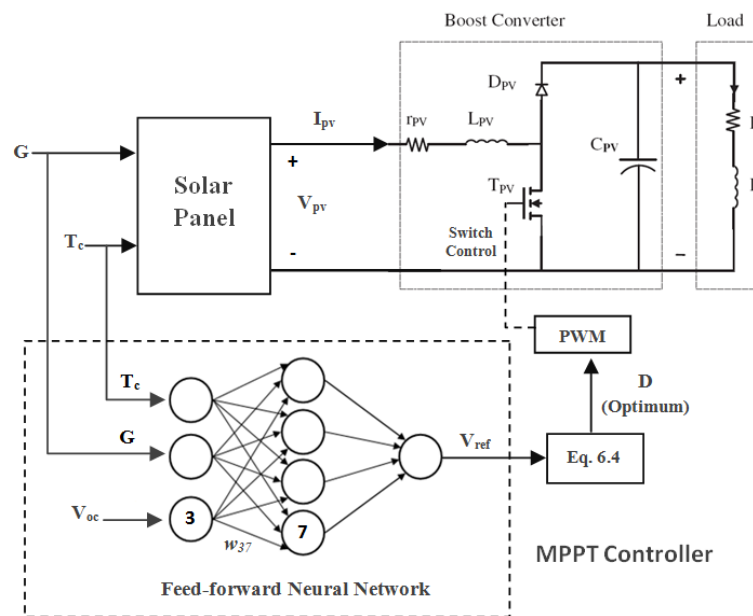
Figure 7.9 - The proposed PV control system

As shown the neural network control (NNC) is used to estimate the PV array operating voltage (V_{ref}) which corresponds to P_{max} at any given solar radiation and cell temperature. It consists of three layers. The input layer is composed of three nodes in inputs that are; the solar radiation (G), cell temperature (T_c) and the cell's open circuit voltage (V_{oc}) at a 25^oC and $1kW/m^2$. The hidden layer composed of four nodes whose function of activation is hyperbolic tangent sigmoid transfer function[18]. The output

---

[18] It's a neural transfer function which calculates the layer's output from its net input.

layer is composed of one node that is the optimum operating voltage (V_{ref}) whose function of activation is of linear type.

The links between the nodes are all weighted. The link between nodes 3 and 7 is labelled as having a weight of w_{37} in Figure 7.9. Once the NN model architecture is defined, data are collected and fed to the model. The network is then trained to recognize the relationships between the input and output parameters. The proposed NN controller uses the Levenberg Marquardt training algorithm. In this algorithm the interlayer connection weight and the processing element's thresholds are first initialized to small random values. The network is then presented with a set of training patterns. Each set is composed of three inputs (solar irradiance, temperature, cells open circuit voltage), and one output. The output or rather the targeted output (ideal V_{ref}) is generated from an applied MatLab code which analyzes the output P-V characteristics of the validated PV model.

Prior to conducting the network training operation using the LM algorithm, a training set of 2000 cases were obtained from four different PV panels, namely: Lorentz mono-crystalline, Sharp's-NUS0E3E, BP-485J, and Astronergy-CHSM6610P. The cell's open circuit voltage (V_{oc}) is used as a reference variable to select from among the four PV panels. This training data set covers the different solar radiation and temperature conditions that could possibly take place. Typical examples of the training patterns used as part of the training set are shown in Table 7.1.

Table 7.1 - Typical examples of the training set.

Input 1 Solar radiation (W/m²)	Input 2 Cell temperature (°C)	Input 3 Open-circuit voltage at (25°C, 1kW/m²)	Output Optimum operating voltage (V)
700	30	30	22.705
650	25	30	23.615
1000	50	30	19.065
400	20	20.6	17.245
850	35	20.6	15.88
150	10	20.6	16.335
650	30	36.88	28.165
450	20	36.88	29.985
900	40	36.88	26.345

The training patterns were presented repeatedly to the neural network model and the adjustment was performed after each iteration whenever the network's output is different from the desired output. The increment of weights ΔW can be obtained as follows:

$$\Delta \mathbf{W} = \left(\mathbf{J} \, \mathbf{J}^t + \mu \, \mathbf{I} \right)^{-1} \times \mathbf{J}^t \mathbf{e} \qquad (7.5)$$

Where

$$\mathbf{J} = \begin{bmatrix} \dfrac{\partial F(x_1, \mathbf{w})}{\partial w_1} & \cdots & \dfrac{\partial F(x_1, \mathbf{w})}{\partial w_W} \\ \vdots & \ddots & \vdots \\ \dfrac{\partial F(x_N, \mathbf{w})}{\partial w_1} & \cdots & \dfrac{\partial F(x_N, \mathbf{w})}{\partial w_W} \end{bmatrix} \qquad (7.6)$$

Where J is the Jacobian matrix, μ is the learning rate, e is the error vector containing the output errors for each input vector used on training the network, I is the identity matrix, $F(x_i, w)$ is the network function evaluated for the ith input vector of the

training set using the weight vector w and w_j is the jth element of the weight vector w of the network. The Jacobian is approximated by using the chain rule of calculus and the first derivatives of the activation functions. This process continues until the mean square error (MSE) converged and is measure at less than 0.01. Figure 7.10 shows the flow chart of Levenberg Marquardt algorithm.

```
                           ┌──────────────┐
                           │    Start     │
                           └──────────────┘
                                  │
                   ┌──────────────────────────────────┐
                   │ Take an appropriate small value of μ │
                   └──────────────────────────────────┘
                                  │
              ┌──────────────────────────────────────────┐
              │ Compute the sum of the squared errors over all inputs │
              └──────────────────────────────────────────┘
                                  │
                        ◇ Is stopping criterion satisfied?  ── Yes ──▶
                                  │ No
           ┌──────────────────────────────────────────┐
           │ Compute: ΔW = (J J^t + μ I)^{-1} × J^t e   │
           └──────────────────────────────────────────┘
                                  │
              ┌──────────────────────────────────┐
              │ Update the network weights w using Δw │
              └──────────────────────────────────┘
                                  │
           ┌──────────────────────────────────────────┐
           │ Recalculate the sum of squared errors using the updated weights │
           └──────────────────────────────────────────┘
                                  │
    μ = 0.1 μ  ◀── Yes ── ◇ Sum of squared errors decreased
                                  │ No
    Discard the new weights
    μ=10 μ                                        End
```

$\text{Compute: } \Delta W = \left(J\, J^t + \mu\, I\right)^{-1} \times J^t e$

$\mu = 0.1\,\mu$

$\mu = 10\,\mu$
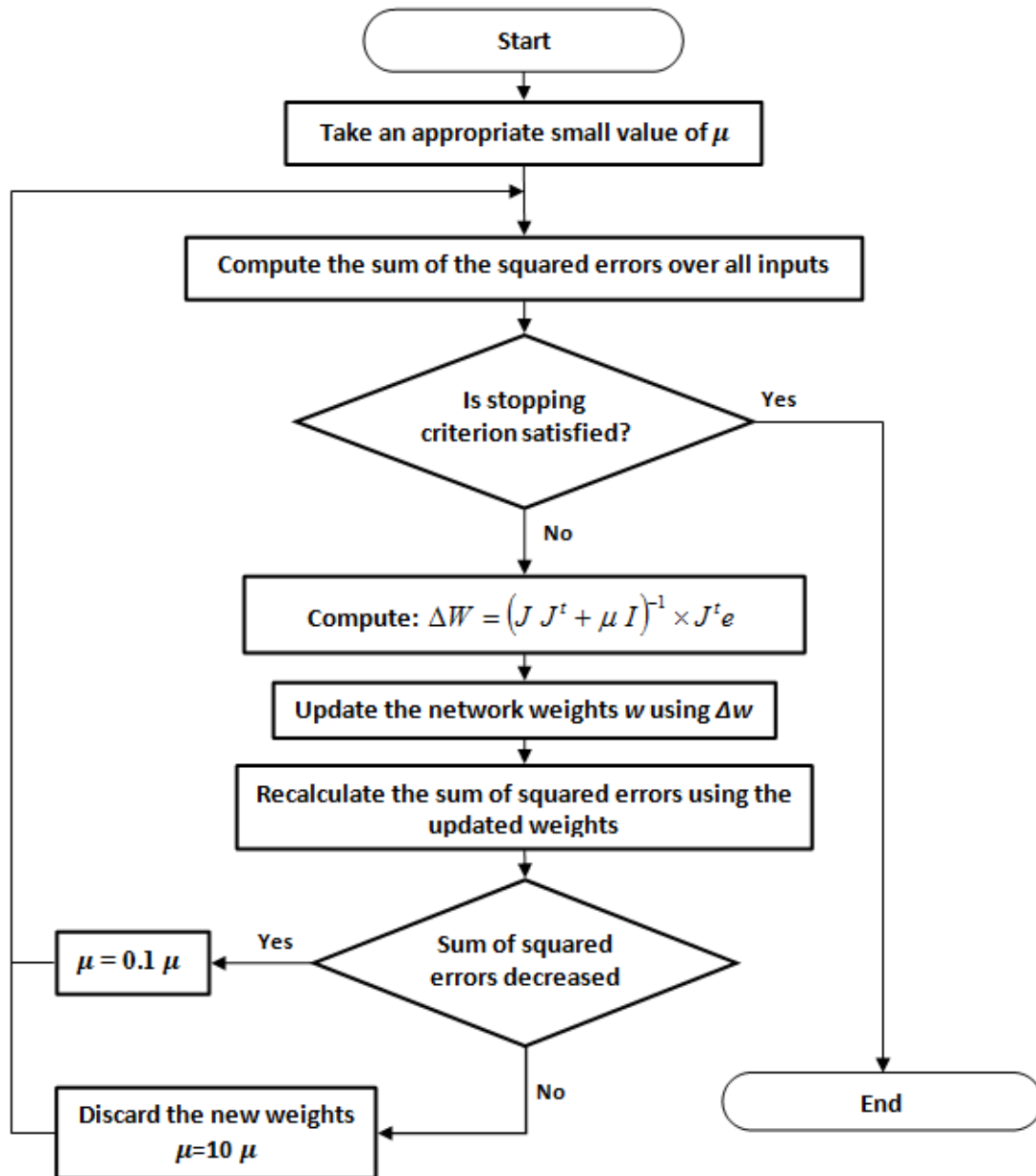
Figure 7.10 - Levenberg Marquardt algorithm flow chart

7.4 Intelligent energy distribution strategy

The energy management strategy (EMS) should determines the split power between the photovoltaic, wind turbine, PEMFC stack and battery while satisfying the load power requirement with respect to dynamic restrictions to the battery and FC stack. In this work, the EMS acts based on certain scenarios, as shown in Figure 7.11.
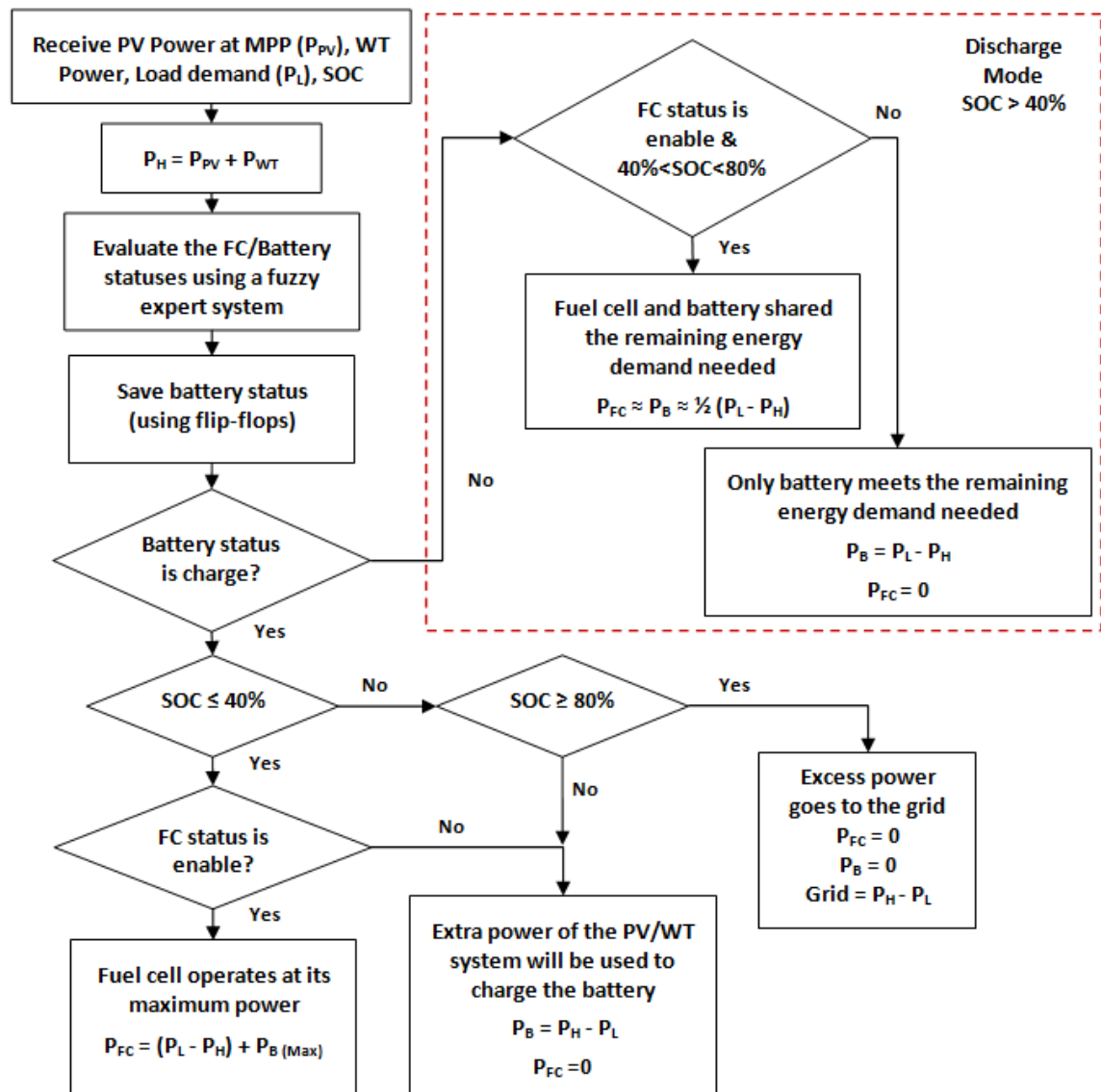
Figure 7.11 - Proposed energy management system algorithm

Frequent power demand variations and unpredictable load profile are unavoidable. Adding to this, the nonlinear subsystems add to the complexity of the structure of hybrid system. Hence, an advance fuzzy expert system according to the weather variations, load demand and battery SOC is presented. Figure 7.12 shows the proposed fuzzy expert system for EMS.
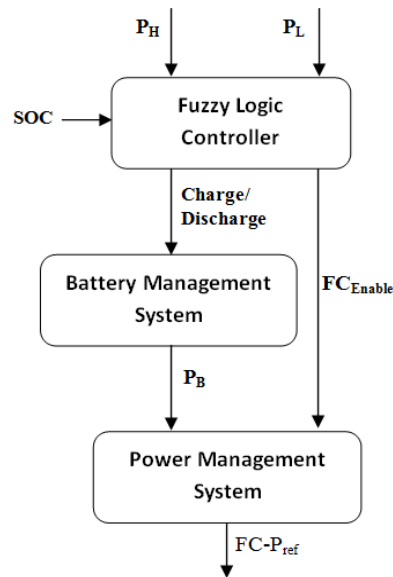
Figure 7.12 - Proposed fuzzy expert system for EMS

A fuzzy logic controller (FLC) is used to decide the optimum operation of the PEMFC/battery system. As shown in Figure 7.11, there are five possible operating modes.

- In grid mode, the excess power of the PV/WT goes to the grid. In this case the back-up power system is off (fuel cell/battery).

- In charge mode, the battery storage is charged by the PV/WT when the load demand is lower than the power generated or/and it's charged by the fuel cell when the SOC is low.

- In battery mode, the power demand is provided only by the battery while the fuel cell is switched off. This mode is suitable for low power demand.

- In hybrid mode, both fuel cell and battery system contributes to fulfil the remaining energy demand needed:

$$P_L(t) - P_H(t) = P_{FC}(t) + P_B(t) \qquad (7.7)$$

This mode is suitable for high power demand.

The FLC and battery management system maintains the SOC at a reasonable level (40-80%). Also, they prevents against voltage collapse by controlling the power required from the battery (P_B) (see Figure 7.11). An S-R type flip-flop has been used for storing battery status (BS), as shown in Figure 7.13.
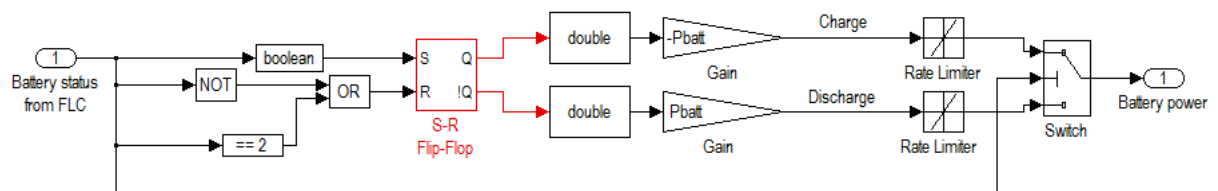
Figure 7.13 - S-R type flip-flop for storing battery status

The power management system controls the reference power of the PEMFC stack (*FC_P$_{ref}$*) by splitting the power demand (P_L) as a function of the available power of the battery and the PV/WT system (P_H) (see Figures 7.11 & 7.14).
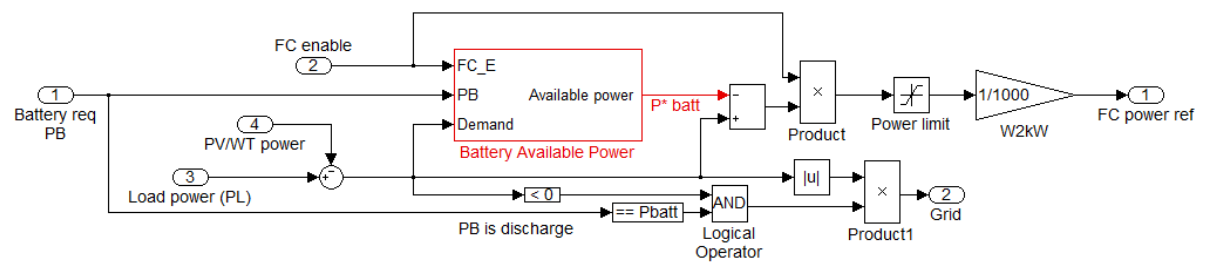
Figure 7.14 – Subsystem implementation of the power management system

7.4.1 Derivation of fuzzy logic controller for EMS

The block diagram of fuzzy logic controller is shown in Figure 7.15.
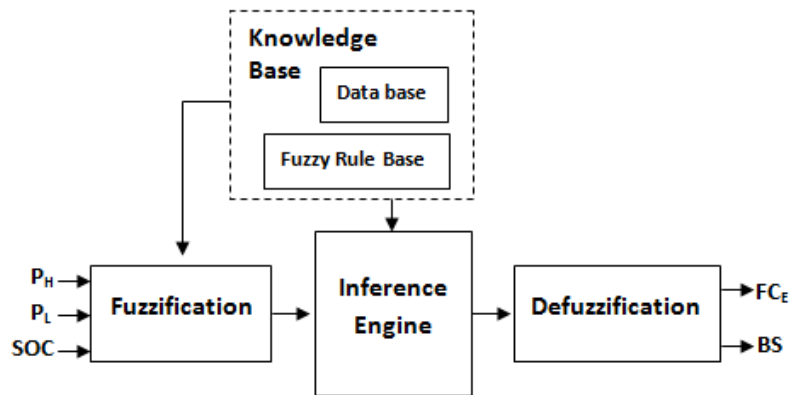
Figure 7.15 – Block diagram of fuzzy logic controller for EMS

The FLC relates the outputs to the inputs using a list of if-then statements called rules. The if-part of the rules describes the fuzzy sets (regions) of the input variables. For ease of computation, the fuzzy variables P_H, P_L, and SOC are described by fuzzy singleton, meaning that the measured value of these variables are used in the interface process without being fuzzified. Specifically the fuzzy rules are in the form:

Rule i: **IF** P_H is A_i and P_L is B_i and SOC is C_i, **THEN** FC_E is D_i and BS is E_i

Where A_i, B_i, and C_i are fuzzy subsets in their universes of discourse, and D_i, E_i are fuzzy singletons. Each universe of discourse is divided into three fuzzy subsets: L (Low), M (Medium), and H (High). The fuzzy subsets and the shape of membership function are shown in Figure 7.16.
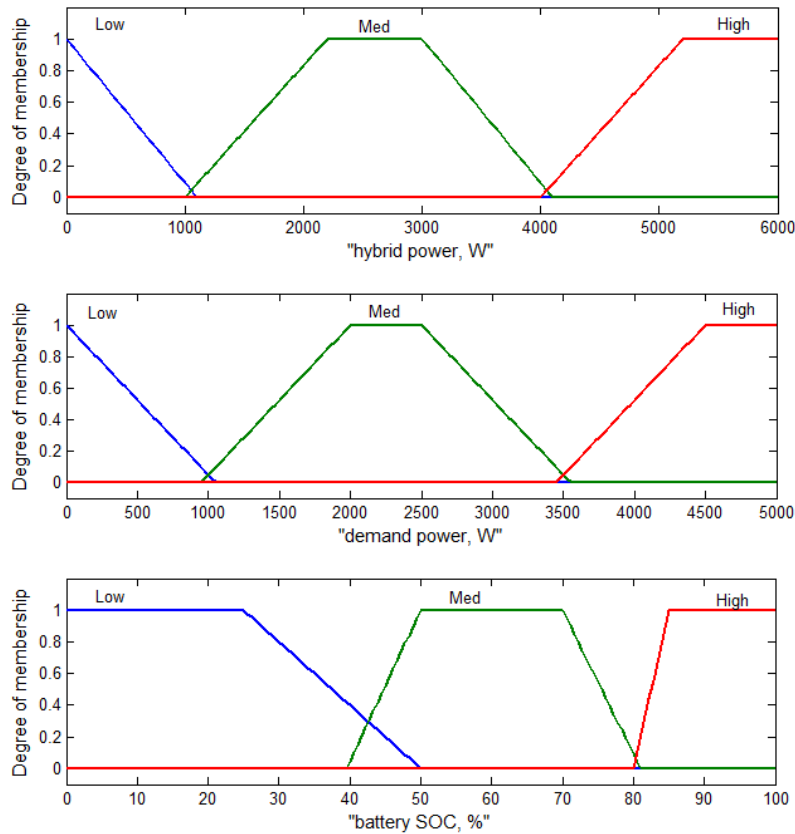
Figure 7.16- Membership functions of the FLC

These degrees of membership are evaluated to obtain the output controller, and the then-parts of all rules are averaged and weighted by these degrees of membership. The core of the rule set of the fuzzy controller is illustrated as follows.

Table 7.2 - Fuzzy logic rules

1-3	IF P_H is L and P_L is L\M\H and SOC is L, THEN FC_E is ON and BS is CO	**4-6**	IF P_H is M and P_L is L\M\H and SOC is L, THEN FC_E is OFF\ON\ON and BS is CO
7-9	IF P_H is H and P_L is L\M\H and SOC is L, THEN FC_E is OFF\OFF\ON and BS is CO	**10-12**	IF P_H is L and P_L is L\M\H and SOC is M, THEN FC_E is OFF\ON\ON and BS is CD
13-15	IF P_H is M and P_L is L\M\H and SOC is M, THEN FC_E is OFF\OFF\ON and BS is CD	**16-18**	IF P_H is H and P_L is L\M\H and SOC is M, THEN FC_E is OFF and BS is CD
19-21	IF P_H is L and P_L is L\M\H and SOC is H, THEN FC_E is OFF and BS is DO	**22-24**	IF P_H is M and P_L is L\M\H and SOC is H, THEN FC_E is OFF and BS is DO
25-27	IF P_H is H and P_L is L\M\H and SOC is H, THEN FC_E is OFF and BS is DO		

Note: CO means charge only, DO means discharge only, and CD means charge or discharge.

For example, if we assumed that P_H, P_L and SOC are 600, 641, and 48.2, respectively. Then from Figure 7.16, P_H, and P_L belongs to L and SOC belongs to L and M (rule 1 and 10). Thus the two possible combinations are: (1) P_H is L, P_L is L and SOC is L (2) P_H is L P_L is L and SOC is M. For each case we calculate the weighting factor using the fuzzy AND operator (product), as shown in Figure 7.17, and obtain the corresponding singleton values D_i and E_i. E_i can be either 0 (DO), 1 (CO) or 2 (CD[19]).

Then, the backup power system (FC/battery) status is computed using the centre of gravity method (Negnevitsky 2004). This gives $FC_E = 0.159 \approx 0$ (off) and $BS = 1.8 \approx 2$ (battery operates in the normal mode; it can discharge or charge. In this case it will discharge 41W to the load).
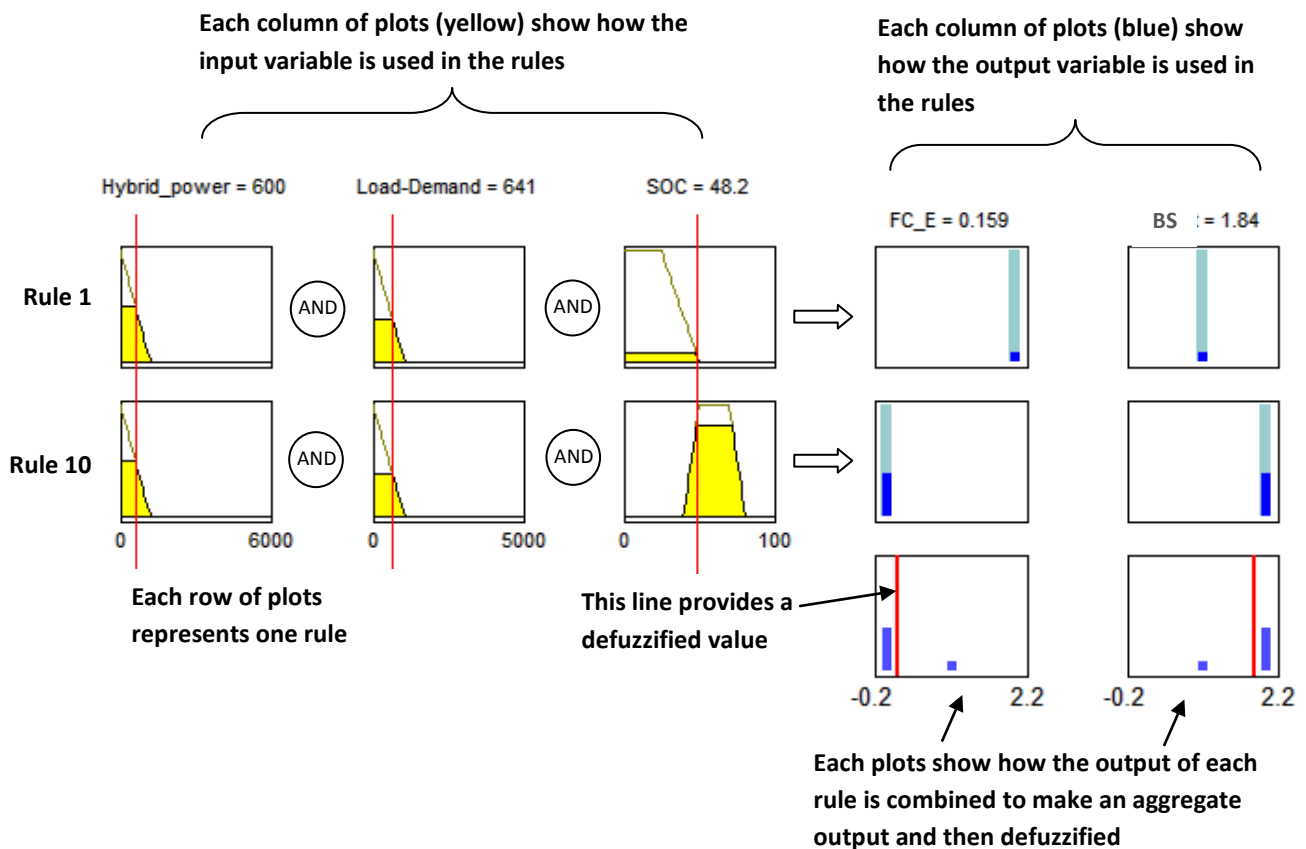
Figure 7.17 - Graphic illustration of inference mechanism

---

[19] Battery SOC is in the desired limit (40<SOC<80), so it can be either charged or discharged.

7.5 PEMFC temperature controller

The operating temperature of the stack is an important controlled variable, which impacts the performance of the PEMFC[20]. Hence, in order to improve the generating performance of the PEMFC and prolong its life, it must be controlled efficiently.

In the last three decades, different approaches have been implemented for solving temperature control system, among these controllers:

- **On/off (switch) control:** an on/off controller is the simplest and least expensive form of control available. For example, it will turn on the cooler (e.g. fan) when the process variable is above the set point and turn it off when the process variable is below the set point. However, although the simplicity is the main feature of this control, the process temperature will be cycling continually, going from below set point to above, and back below as shown in Figure 7.18.
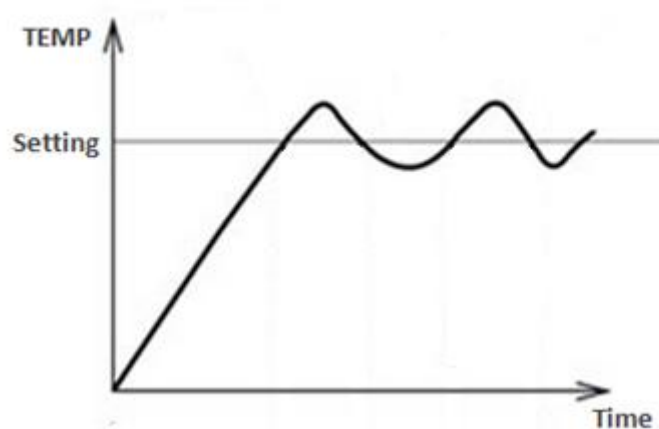
Figure 7.18 - Characteristics of ON/OFF temperature control action (Coulton 2013)

Proportional control: proportional controls are designed to eliminate the cycling associated with on/off control. Hence, with proportional action (P), the controlled object no longer switches as a direct result of the set value. It compares the difference between the set value and the process variable, and then controls the output

---

[20] One of the limitations of the previous FC stack model was the heating and cooling system (Souleman et al. 2009).

proportional to the deviation. This proportional action temperature control is active within user-zone around the set point called the proportional band (Pb). Proper adjustment of the proportional band will result in smooth control. However, it is rare that the temperature stabilizes exactly on the set point, it is usually becomes stable with some deviation called offset, as shown in Figure 7.19.
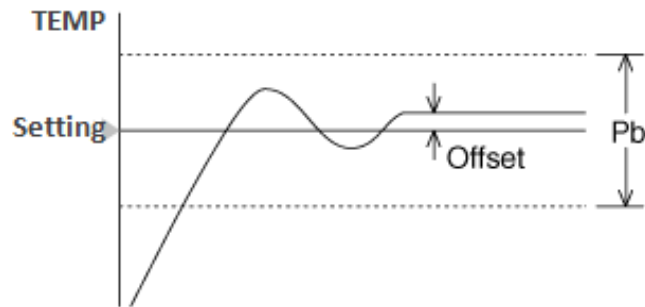
Figure 7.19 - Characteristics of proportional temperature control action (Coulton 2013)

- **PID control:** this controller combines proportional control with two additional adjustments, integral and derivative, which helps the unit automatically compensate for changes in the system. Hence, the purpose of the integral and derivative actions is to automatically compensate for any steady state offset inherent with a proportional controller.

  The controller measures the rate of the temperature increase and moves or resets the proportional band up or down depending on the offset. Figure 7.20 shows the characteristics of PID temperature control action.
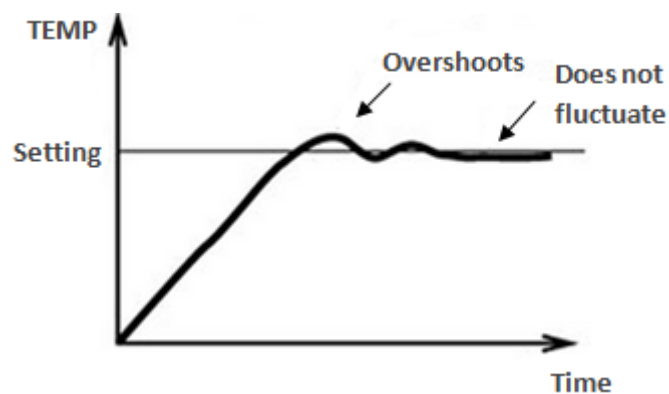
Figure 7.20 - Characteristics of PID temperature control action (Coulton 2013)

- **Fuzzy logic control:** as mention earlier in this chapter, fuzzy logic is a simple way to arrive at a definite conclusion based upon ambiguous, vague, imprecise, or missing input information. It attempts to model our sense of words, our decision making and our common sense. In short fuzzy logic attempts to mimic human thought process.

  Previous studies showed that fuzzy logic provides a more efficient and resourceful way to solve temperature control systems (Underwood 2005). Moreover, fuzzy logic can control nonlinear systems that would be difficult or impossible to model mathematically.

  A temperature controller working with fuzzy logic would compare the set point with the actual temperature to establish how far from the set point the temperature is. Then using the fuzzy rules, the controller would add more or less cool/heat.

  As shown in Figure 7.21, with fuzzy logic, the control output is smooth; despite a wide range of input variations.
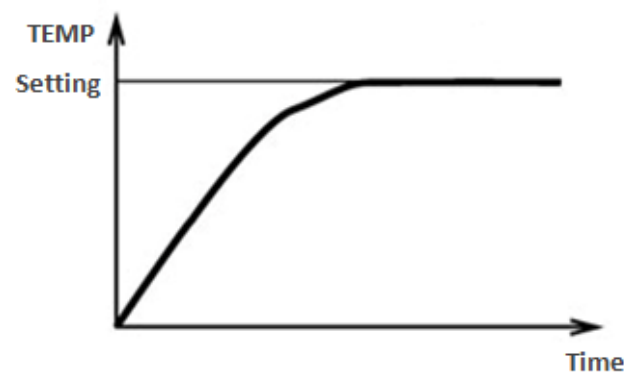
Figure 7.21 - Characteristics of fuzzy temperature control action (Coulton 2013)

Consequently, in this work, the PEMFC stack model described by Souleman (Souleman et al. 2009), is modified to include a fuzzy temperature controller. Scheme of the temperature control system is presented in Figures 7.22 and 7.23.
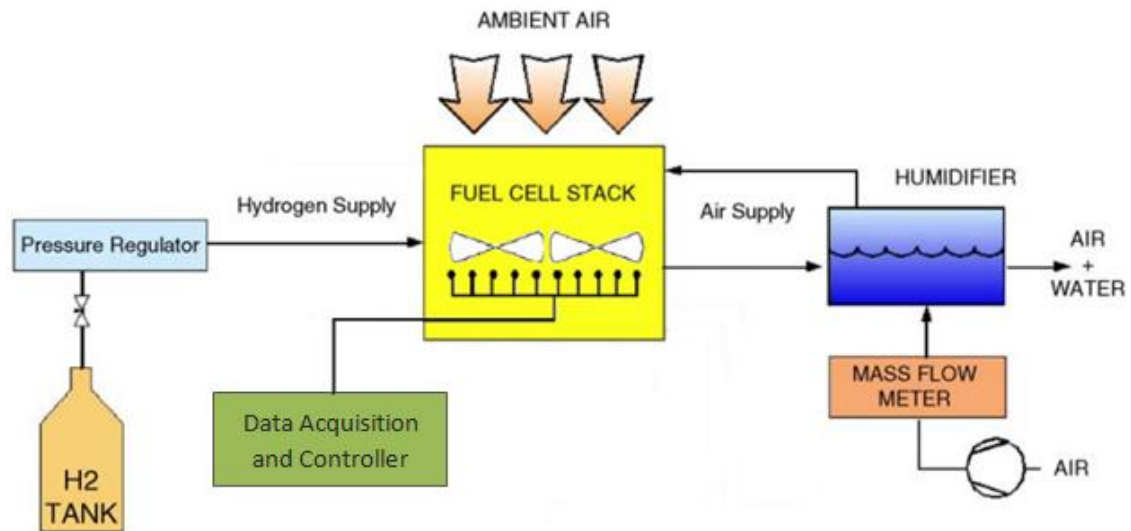
Figure 7.22 - Schematic diagram of the PEMFC system
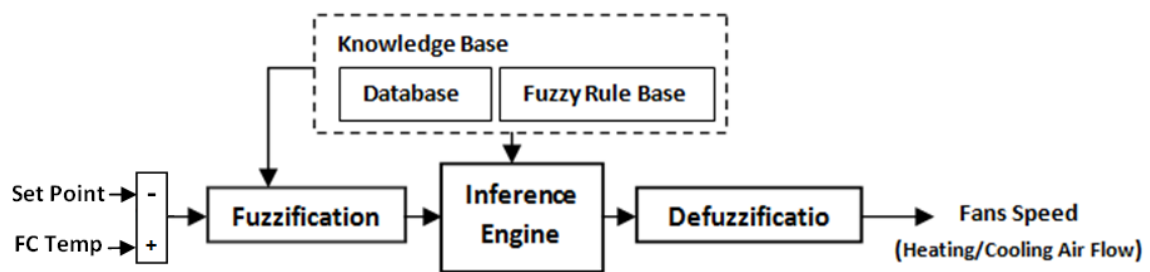
Figure 7.23 - PEMFC temperature control based on fuzzy logic

The main function of this control system is to maintain the temperature stable and equal to the stack operating temperature (e.g. 65°C). The FLC is used to control the airflow from the heater and cooler fans, based on the error temperature[21]. In case of cold start-up (temperature error is large negative), the heater fan (F1) needs to be on. On the contrary, if the stack temperature is hot (temperature error is large positive), the cooler fans (F2) speed needs to be at the high level. Triangular membership functions and centroid defuzzification method are adopted. The membership functions are shown in Figure 7.24.

---

[21] It's the difference between the set point and the actual (stack) temperature.
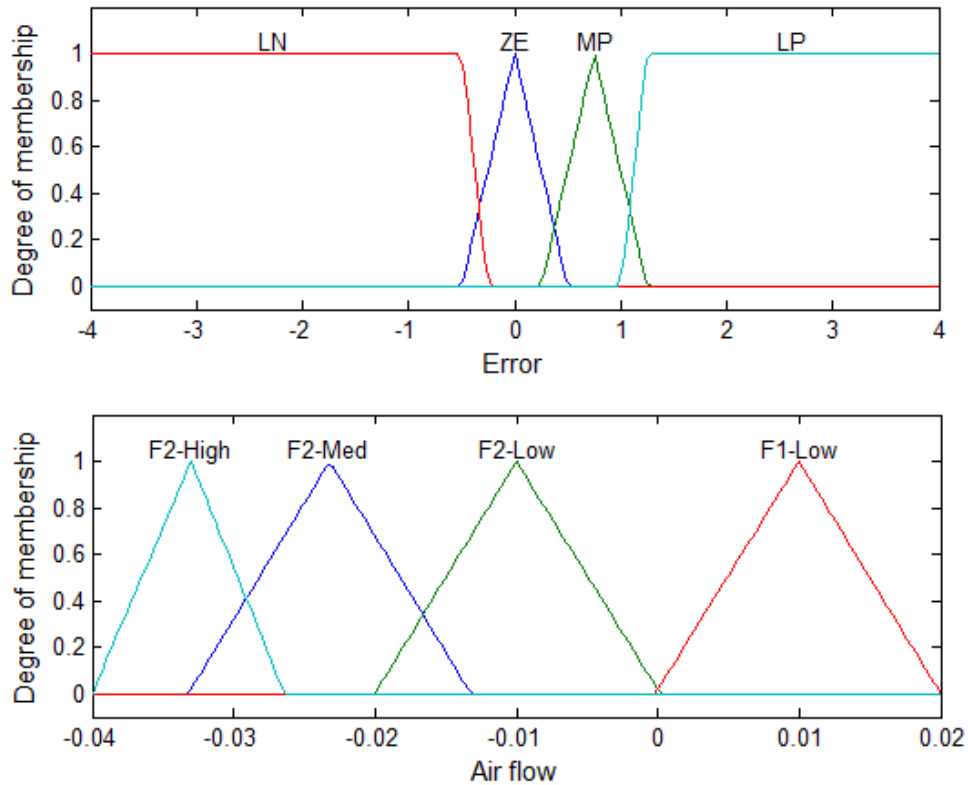
Figure 7.24 - Membership functions of the fuzzy temperature controller

Table 7.3 shows the rule base of the temperature FLC.

Table 7.3 - Fuzzy logic rules for the temperature controller

Temperature Error	Fan Airflow	Temperature Error	Fan Airflow
Large Negative (LN)	F1-Low	Medium Positive (MP)	F2-Medium
Zero Error (ZE)	F2-Low	Large Positive (LP)	F2-High

Over time, the control system calculates the cooling/heating effect inside the stack, taking into account the thermal isolation and cooling/heating activities. And based on these equations the output temperature will be calculated as follow (Natsheh & Albarbar 2013; Larminie & Dicks 2003):

$$\Delta T_{FC} = \left(T_A - T_{FC}\right) \times K_T + \left(T_{FC} \times K_{Fan}\right) + \frac{H}{M \times C_S} \tag{7.8}$$

$$T_{FC}(t) = \int \Delta T_{FC} \, dt \tag{7.9}$$

Where T_A is the ambient temperature, T_{FC} is the FC stack temperature, K_T is the thermal isolation multiplier, K_{Fan} is the cooling/heating factor, H is the heat generated in a fuel cell, M is the whole stack mass, and C_S is the average specific heat capacity of the stack.

To calculate the heat generated in a fuel cell, Equation (7.10) is applied (Larminie & Dicks 2003).

$$H = P_S \left| \frac{1.48}{V_{FC}} - 1 \right| \qquad \textbf{(7.10)}$$

Where Ps is the power produced by the stack, and V_{FC} is the stack voltage.

7.6 Summary

Energy management strategy is one of the important tasks in developing hybrid power system. Hence, this chapter presents a novel adaptive scheme for energy management in stand-alone hybrid power systems. The method introduces an on-line energy management by using a hierarchical controller between four energy sources: photovoltaic (PV) panels, wind turbine, battery storage, and proton exchange membrane fuel cell (PEMFC). The proposed method includes

▪ A feed-forward, back-propagation neural network controller in the first layer, which is added in order to achieve the maximum power point (MPP) for the different types of PV panels. Here, a training set of 2000 cases were obtained from four different PV panels namely: Lorentz mono-crystalline, Sharp's-NUS0E3E, BP-485J, and Astronergy-CHSM6610P. This data set has covered different solar radiation and temperature conditions that could possibly take place.

▪ In the second and third layer, an advanced fuzzy expert system has been developed to optimize performance by distributing the power inside the hybrid system and by managing the charge and discharge of the current flow. Here,

Sugeno fuzzy logic controller is used to decide the optimum operation of the PEMFC/battery system. As shown in Figure 7.11, there are five possible operating modes: grid mode, PV-charge mode, FC-charge mode, battery mode, and hybrid mode.

- Finally, and in the third layer, Mamdani fuzzy logic controller is presented to control the airflow from the heater and cooler fans, based on the error temperature. The main function of this control system was to maintain the stability of the PEMFC temperature ($65^{o}C$).

Next, to demonstrate the effectiveness of the proposed strategy, Chapter 8 presents and discusses the simulation results which derived from the proposed hybrid system model.

Chapter 8

Simulation Results & Discussion

*In the **previous chapters** the **dynamics** simulation **models** for each of the: PV array, wind turbine, PEM fuel cell, and Li-Ion battery were explained and shown. Afterward, in **Chapter 7**, an optimized **energy management** based on a **hierarchical controller** has been implemented to satisfy important objectives such as: **optimal operation of PV panel, battery charge balance, optimal operation of FC, and load following**.*

*In **this chapter** the **simulation results** of the **proposed hybrid system** and its **control strategy** shown in **Figure 7.1** will be discussed. Here, **P&O algorithm** with linear and non-linear controllers are provided for a comparison with the **proposed MPPT controller** system. Moreover, a **case study** will be presented in Section 8.2 for **monitoring** a 28.8kW **solar power plant** located in central Manchester.*

8.1 Evaluating the proposed MPPT

Training neural networks is considered a very important stage in developing the network system model, the output usually depends on the parameter settings of the network and the type of inputs which is fed to the network, any misuse in sitting configuration or input may give incorrect prediction output. Hence, to insure network accuracy, the network must be tested on a continuous basis and should be monitored during the training and testing operations. Once the neural network is trained, as shown in Section 7.3.2, the next step is to test the network to judge its performance and to determine whether the prediction results confirm with the actual results. Using the 400 cases allocated for the testing set, the model input parameters were entered consecutively for each case and a prediction for the optimal V_{ref} was obtained. Table 8.1 shows, a portion of these cases that were used in the testing process.

Table 8.1 - Portion of the testing set

Astronergy CHSM6610P Open-circuit voltage at (25°C, 1kW/m²) (36.88V)			Sharp's NUS0E3E Open-circuit voltage at (25°C, 1kW/m²) (30V)			Lorentz mono-crystalline Open-circuit voltage at (25°C, 1kW/m²) (20.6V)		
Case #	Solar radiation (W/m²)	Cell temperature (°C)	Case #	Solar radiation (W/m²	Cell temperature (°C)	Case #	Solar radiation (W/m²)	Cell temperature (°C)
4	700	35	18	640	80	26	500	65
7	550	10	19	550	50	27	680	50
8	480	13	20	400	10	28	540	75
9	240	17	35	500	20	29	700	88
10	1000	25	39	900	45	30	470	64

The prediction results were then compared with the actual results of the 400 cases. The statistical analysis of these results indicates that the R^2 value (coefficient of

determination[22]) for the testing set was 0.99. This result demonstrate that the MPPT-NNC model developed in this work can predict the optimal V_{ref} for any trained PV panels, at any environmental conditions with high accuracy. The graphical results of the first 31 cases in the testing set are shown in Figure 8.1.
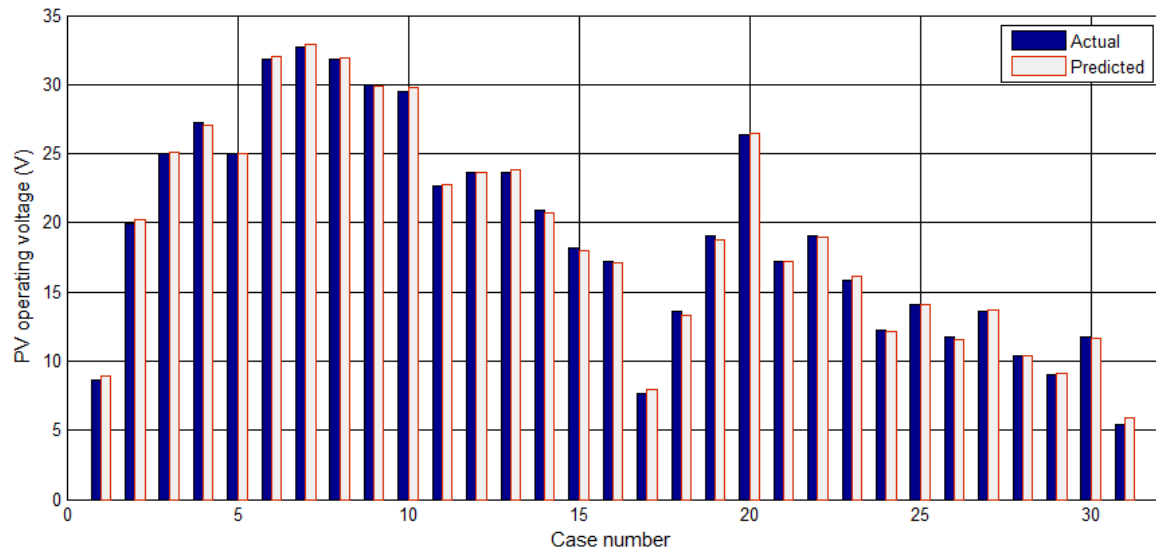
Figure 8.1 - Actual and predicted PV operating voltage for the first 31 cases in the testing set

8.1.1 A comparison between P&O and ANN

The simulation results of the PV system using an ANN and classical P&O algorithm are discussed in this section. Figure 8.2 compares the optimum PV power (P_{mpp}) obtained from the classical P&O and the proposed NNC algorithm.

From Figure 8.2(a, b), it's shown that by using the ANN the optimum power will be more steady and close to the theoretical power as compared to the classical P&O algorithm[23].

---

[22] In statistics, the coefficient of determination indicates how well a model predicts future outcomes (Di Bucchianico 2008).

[23] Despite the P&O algorithm is easy to implement it has a common problem. The array terminal voltage is perturbed every MPPT cycle; therefore when the MPP is reached, the output power oscillates around the maximum, resulting in power loss in the PV system. This is especially true in constant or slowly-varying atmospheric conditions (see Figure 8.2 (a)).
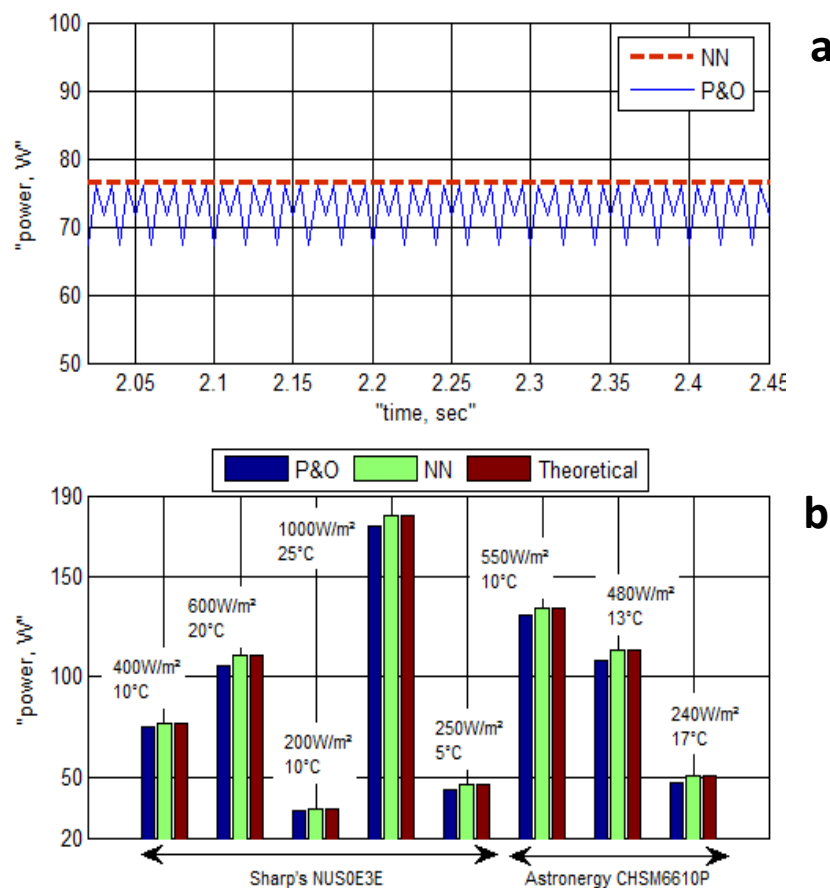
Figure 8.2 (a) P_{mpp} at 400W/m^2, 10°C (Sharp's) **(b)** P_{mpp} at different conditions

Moreover, to evaluate the performance of the proposed PV control system, a comparison between the P&O[24] (with PI and PBC), and the proposed NNC is carried out for a set of solar radiation. The comparison is made in a system comprises: PV panels, MPPT control, battery, and DC-DC converter. The rated power of the PV system is 680W. During the comparison, solar irradiance, load profiles and models parameters are equal to those presented in reference (Tofighi & Kalantar 2011).

If the reference voltage (V_r) is assumed at 100V and the SOC is at 70%, the system response to changes in solar irradiance and load resistance is given in the following

---

[24] In P&O technique (indirect method), the output voltage reference is used as the control parameter in conjunction with a controller (e.g. PI controller) to remove power fluctuates.

figures. Figure 8.3 shows the PV system voltage and current, which were obtained based on the MPPT-NNC algorithm.
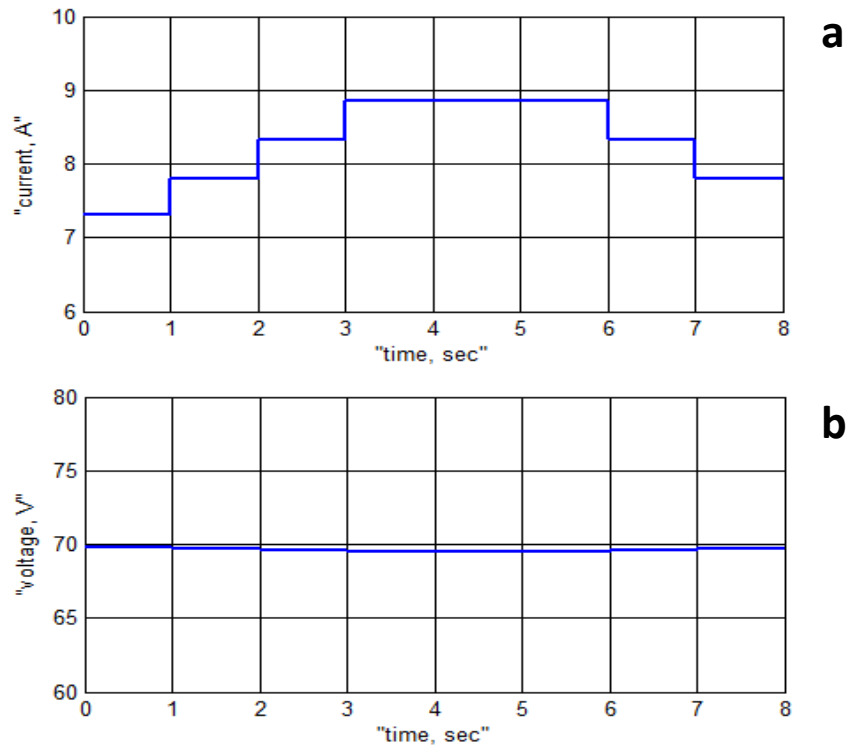
Figure 8.3 (a) PV (BP 485J) system current at MPP **(b)** PV (BP 485J) system voltage at MPP

The PV, battery and load power under the change in solar irradiance and load resistance are shown in Figure 8.4.
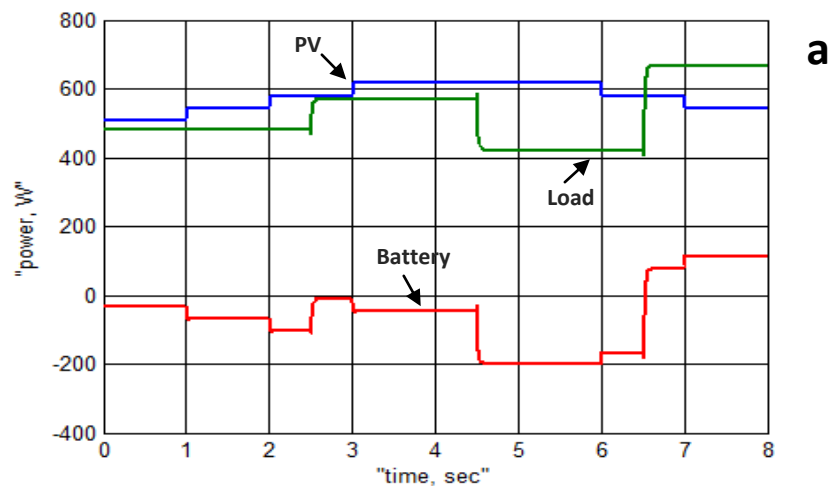
Figure 8.4 (a) PV, battery and load power using the proposed NNC
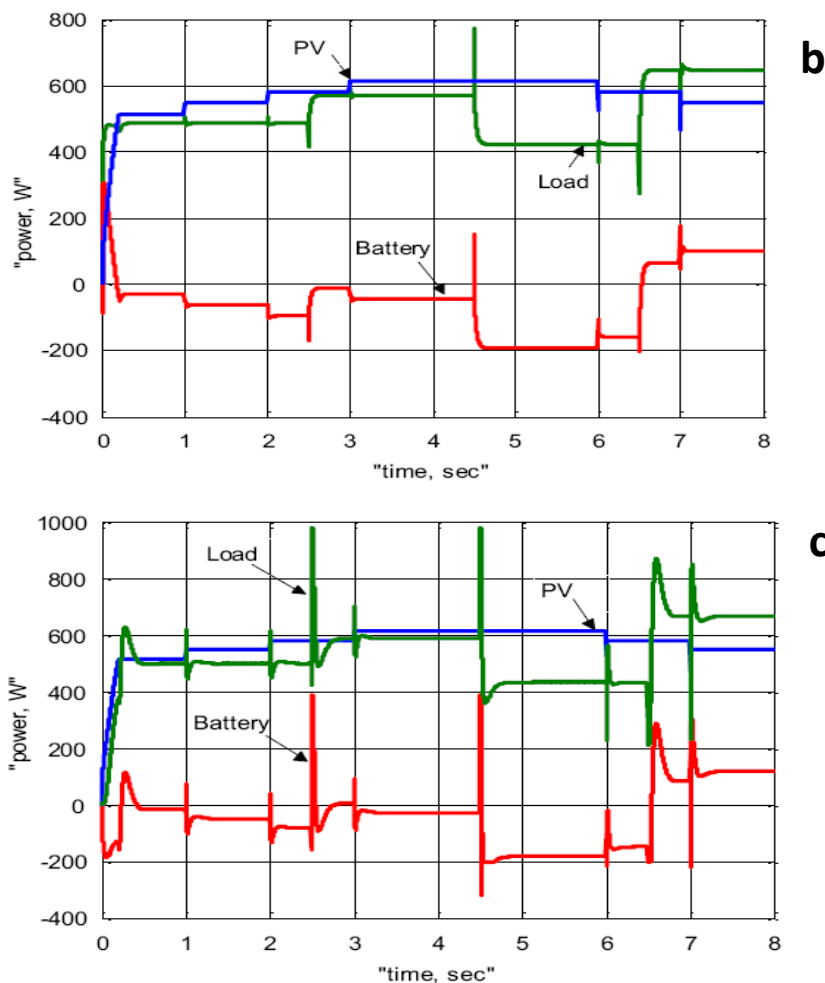
Figure 8.4 – PV, battery and load power (**b**: PBC (Tofighi & Kalantar 2011), **c**: PI (Tofighi & Kalantar 2011))

As shown, linear PI controller has shown its instability in handling various rapid changes in solar radiation[25], though the change was only from 750W/m^2-900W/m^2. While non-linear PBC even if it has a few power fluctuations, the simulation results of the proposed NNC show better transient performance, with low overshoot, short settling time and zero steady-state error.

Figure 8.5 presents the SOC of the battery storage to demonstrate the charge and discharge modes. In this case, the initial SOC of the battery storage is 70. The battery

---

[25] This prove that the operation control of hybrid power system is not a linear problem (Tofighi & Kalantar 2011; Rodolfo & Jose´ 2005) due to the uncertain renewable energy supplies, load demands and the non-linear characteristics of some components.

will be in the discharge mode between (6.5s and 8s), since the load power exceeds the generated power of PV system; which is evident in Figure 8.4.
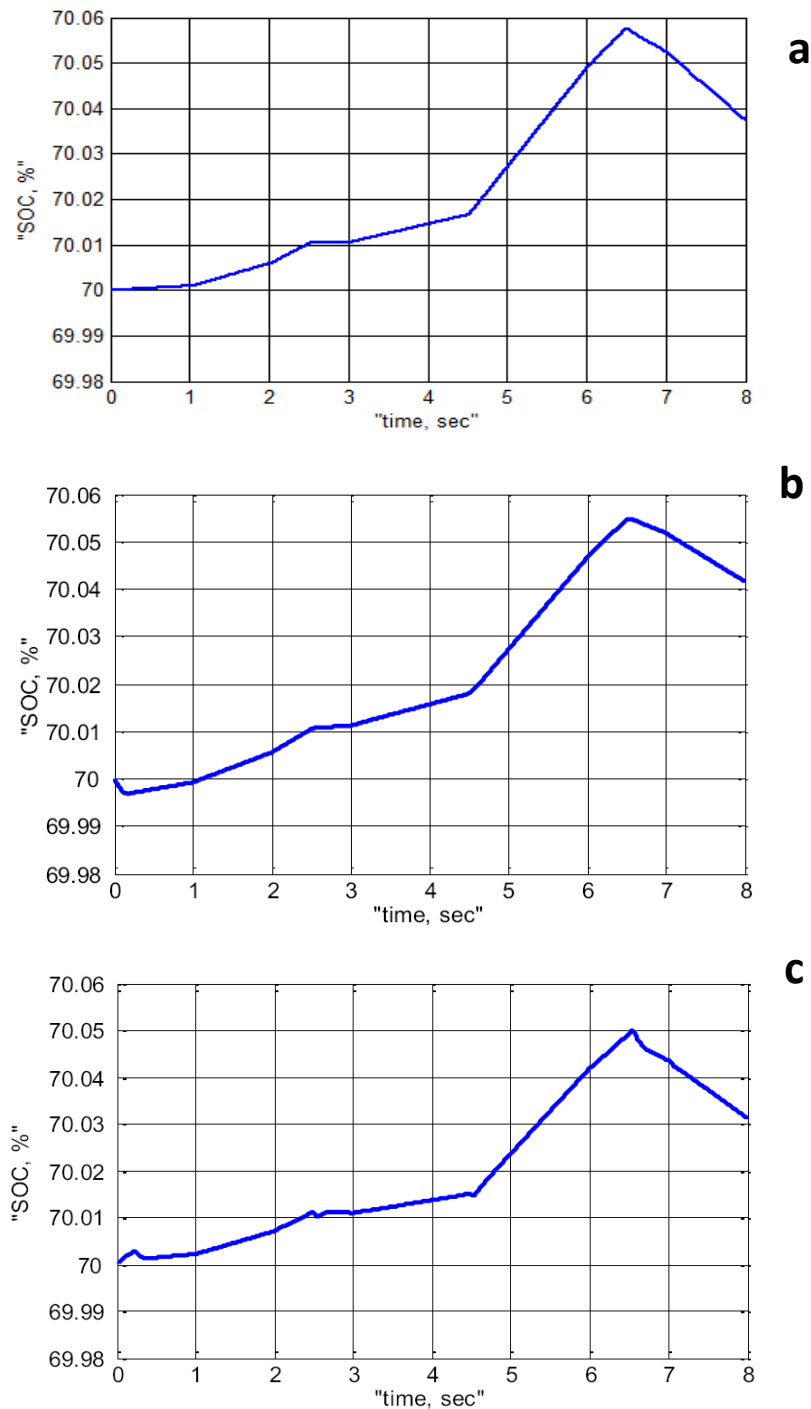
Figure 8.5 – Battery state-of-charge (**a**: NNC, **b**: PBC (Tofighi & Kalantar 2011), **c**: PI (Tofighi & Kalantar 2011))

8.2 Case study: performance of PV power stations in Manchester

PV system owners must be assured that their photovoltaic system operates well and that their investment will pay off. Regardless of which system they operate, plant parks, individual systems or private systems, failures and defects must be detected and repaired immediately. This could be achieved by and only by optimizing these system performance and eliminate any degradation at early stage.

Consequently, in this section, a new approach is proposed for PV system monitoring. The block diagram of the developed system is shown in Figure 8.6.
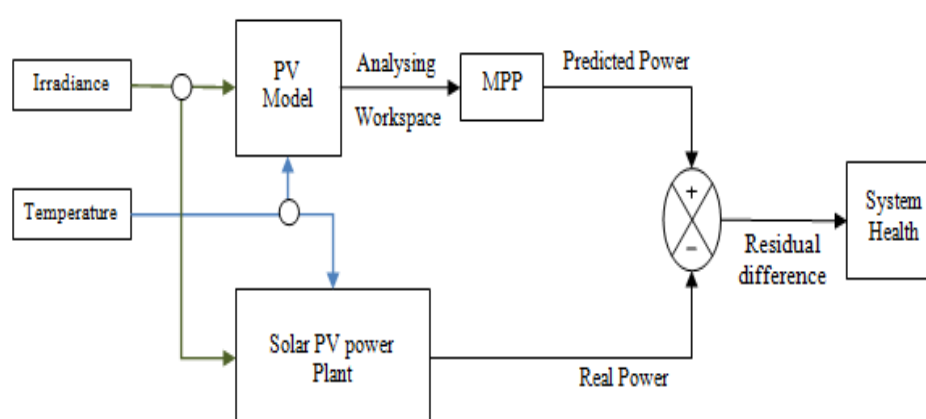
Figure 8.6 - PV Array fault detection block diagram (Natsheh & Albarbar 2011)

As shown in Figure 8.6, the developed monitoring system enables early system degradation to be identified via the calculation of the residual difference in power generation between the computer model[26] and the actual PV panels. In this study, irradiance, temperature and system output power are gathered from a 28.8kW grid connected solar power system.

---

[26] The implementation and design for the proposed PV model has been addressed previously in Chapter 6.

8.2.1 Solar power plants in central Manchester: description

In 2009, Manchester Metropolitan University (MMU) installed three PV power stations on its campus in Manchester with a combined maximum power of 55.8kW (enough power to light 7200 100-watt light bulbs, power 960 student laptops, boil 40 kettles or supply electricity to 10 houses). Figure 8.7(a), shows the 28.8kW PV power plant designated as (All Saints building) PV array 1. Figure 8.7(b) shows the (All Saints building) PV array 2. Both power stations use the Sharp NU-180 (E1) PV panels and they were placed at an inclination angle of 10°, and azimuth angle of 30°.

Figure 8.7 (a) All Saints building PV array 1

Figure 8.7 (b) All Saints building PV arrays 2

As shown in Figure 8.7, the solar power plant is divided into two buildings. Building 1 has its PV system located on the sixth floor with a total of 160 PV panels. Building 2 has its array spread over two floors (floor 6 and 4). There are 150 panels in total, 78 PV panels on floor 6 and 72 on floor 4. Table 8.2 shows the PV system plant profile.

Table 8.2 - PV system plant profile

	MMU All Saints Building 1	MMU All Saints Building 2
Location	Manchester, UK	Manchester, UK
Commissioning	8th July 2009	6th July 2009
System power	28.80kWp	27.00kWp
Anticipated annual output kWh	17250	16063
PV modules	160 Sharp NU-180 (E1)	150 Sharp NU- 180 (E1)
Azimuth angle	30°	30°
Angle of inclination	10°	10°
Active area	185.7043 m^2	174.0978 m^2

Table 8.3 shows the specifications for Sharp NU-180 PV panel, which has been used in the PV power stations.

Table 8.3 - Sharp NU-180 specifications (1kW/m^2, 25° C)

Maximum power (P_m)	180W	Temp coefficient for P_m	- 0.485% / °C
Open circuit voltage (V_{oc})	30V	Temp coefficient for V_{oc}	-104 mV / °C
Voltage at P_m (V_{amp})	23.7V	Temp coefficient for I_{sc}	+ 0.053% / °C
Short circuit current (I_{sc})	8.37A	No. of cells and connections	48 in series
Current at P_m (I_{amp})	7.6A		

The total power delivered to the national grid by the PV systems since their commissioning back in 2009, is shown in Figure 8.8. Due to the weather, one might think that PV arrays in Manchester would not produce much power, however as these results show that is not the case.
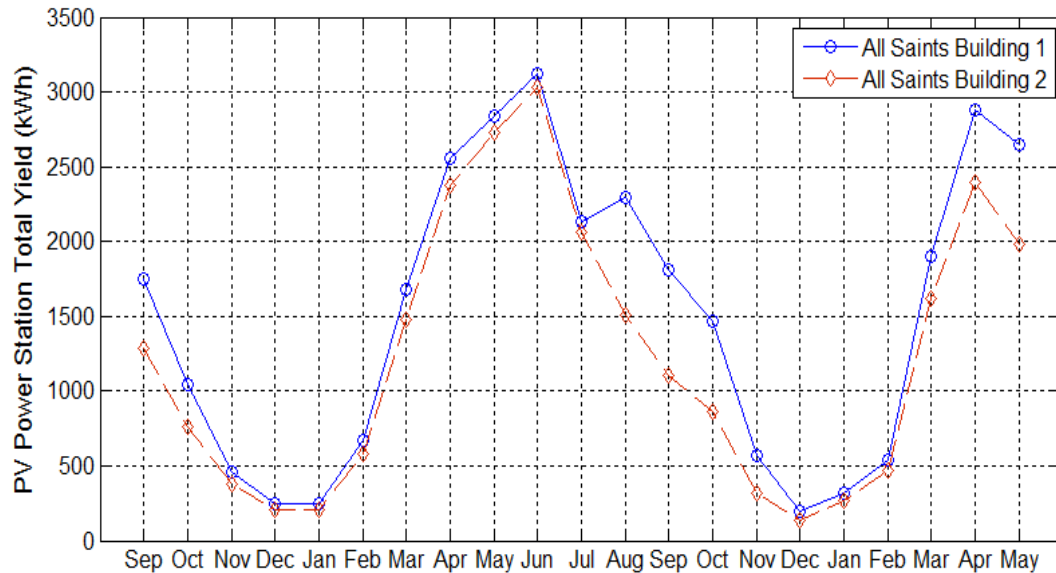
Figure 8.8 - PV systems total yield (Sep 2009 – May 2011)

8.2.2 Metrological data

The main input parameters for the PV power stations are solar radiation and cell temperature. The daily average solar radiation and temperature data for Manchester were collected from monitoring on the 28.8kW grid connected solar power system located on tower block within MMU campus, data were collected over 21 month's period as monthly average data. The daily average data obtained from the mentioned source can be used further to find the incident solar irradiation on the PV arrays. This data set was started back in 2009 when the systems were commissioned. The solar irradiation and panel temperature distributions throughout the 21 month's period for Manchester are illustrated in Figure 8.9.
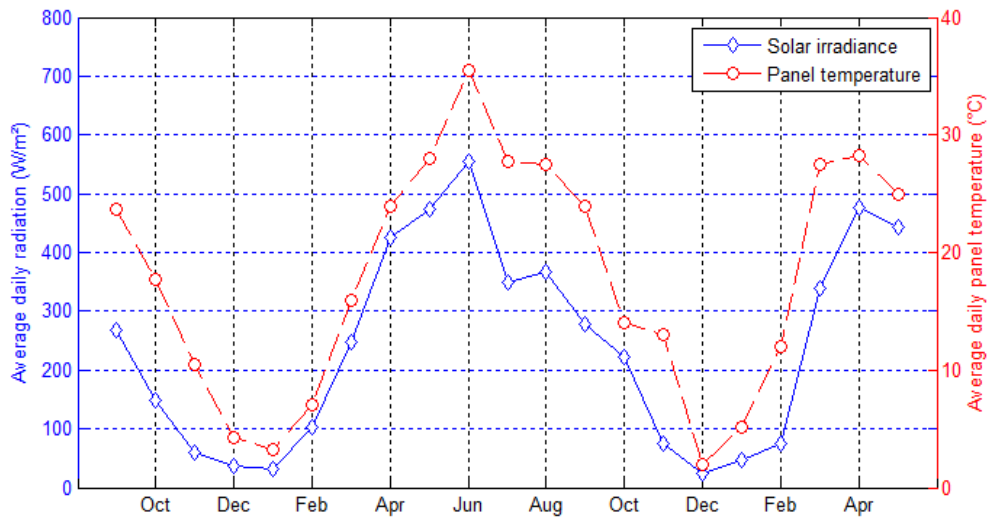
Figure 8.9 – Solar irradiation and panel temperature distribution during the 21 month's period for Manchester (2009/2011)

8.2.3 Results and comments

The proposed PV model was simulated using MatLab to monitor the 28.8kW grid connected PV power station by calculating the residual difference between the model predicted and the actual measured power parameters (Natsheh & Albarbar 2012). Measurements were taken over 21 month's period; using hourly average irradiance and cell temperature. These real-time parameters are used as inputs of the developed PV model. The performance of the system is shown in Figure 8.10(a) and 8.10(b).
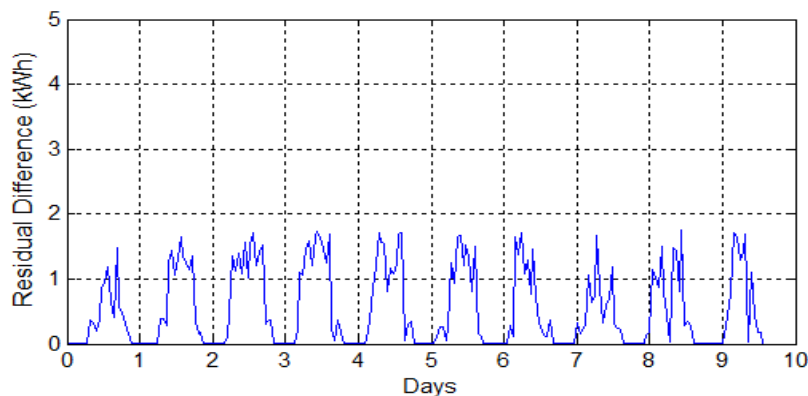
Figure 8.10 (a) System performances during 10 day of Jun 2010
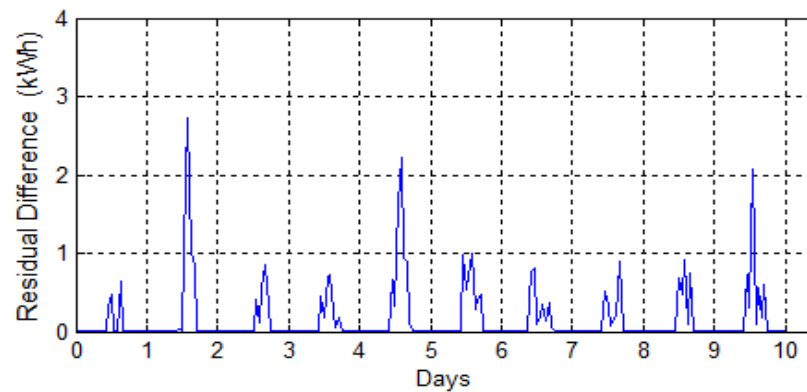
Figure 8.10 (b) System performances during 10 day of Dec 2010

It was found from Figure 8.10(a) that the system has a good performance, since the residual difference between the model prediction and the actual power is less than 1.70kW. The difference caused due to the clouds, dust, wire, and aging. Ageing had small effect on data measurement because the system was purchased in July 2009 and hence is still relatively new. Also it can be observed from Figure 8.10(b) that system degradation will be indicated when the residual difference is above 1.90kW; due to shading, snow cover and panel fault.

8.3 The proposed hybrid system and its control strategy

The simulation results of the PV/WT/PEMFC/battery hybrid system using ANN and fuzzy logic are discussed in this section. Simulation results are obtained by developing a detailed MatLab/Simulink software package, as shown in Figure 8.11.
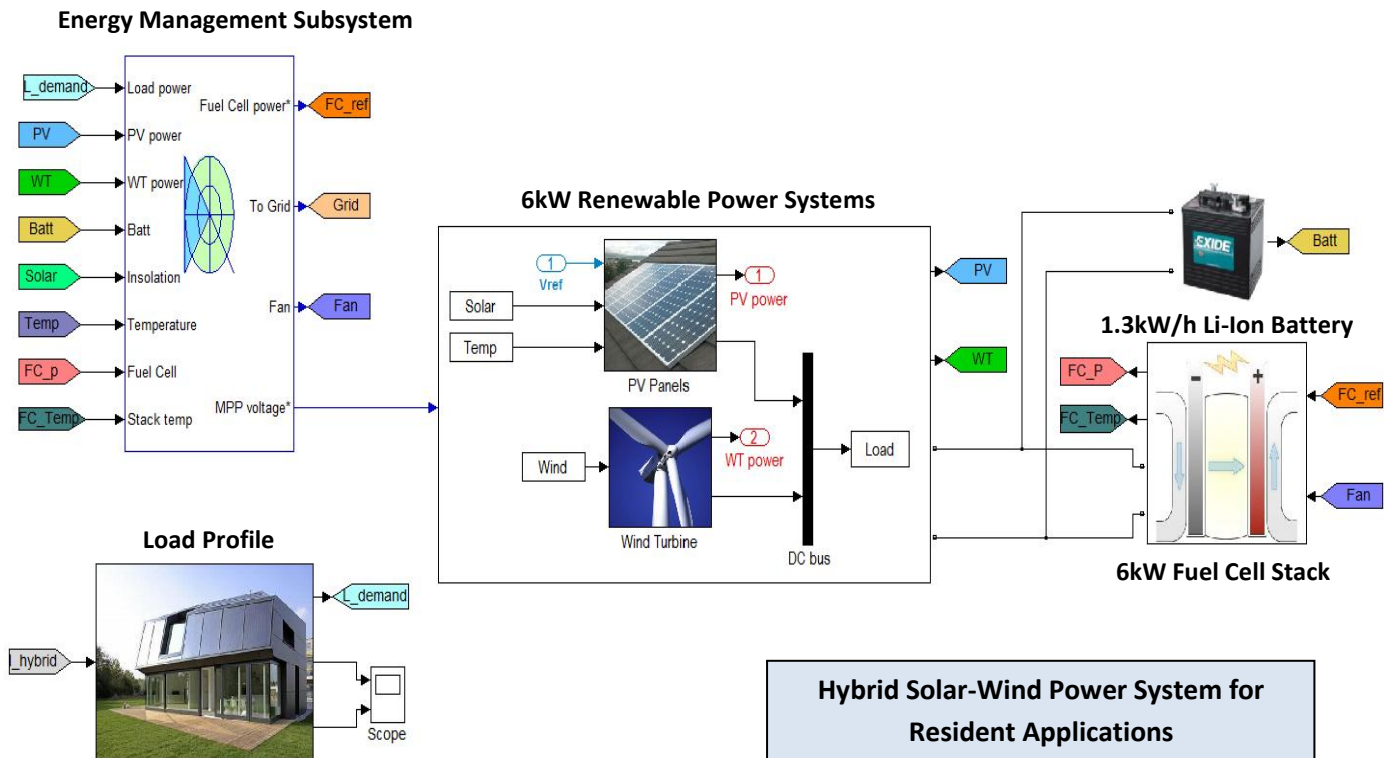
Figure 8.11 - Hybrid power system simulation model

The specifications of the renewable power sources used are given in Table 8.4.

Table 8.4 - PV/WT system specifications

PV Sharp's (NU-180) at (1kW/m^2, 25° C)		Wind turbine	
Maximum power (P_m)	180 (W)	Peak Output Power	3200 (W)
Open circuit voltage	30 (V)	Base wind speed	11 (m/s)
Voltage at P_m	23.7 (V)	Base rotational speed	520 (rad/s)
Short circuit current	8.37 (A)		
Current at P_m	7.6 (A)		

The specifications of the PEMFC stack and Li-Ion battery system are given in Table 8.5 and 8.6.

Table 8.5 - PEMFC stack parameters

Voltage at 0A and 1A	65 (V), 63 (V)
Nominal operating point	133.3 (A), 45 (V)
Maximum operating point	225 (A), 37 (V)
Number of cells	65
Operating temperature	65 (^{o}C)
Nominal Air flow rate	300 (l/m)
Nominal supply pressure [Fuel , Air]	1.5(bar), 1 (bar)
Nominal composition [H_2, O_2, H_2O(Air)]	99.95, 21, 1 (%)

Table 8.6 - Li-Ion battery parameters

Nominal [voltage, capacity]	200 (V), 5.8783 (Ah)
Fully charged voltage	232.8 (V)
Maximum capacity	6.5 (Ah)
Internal resistance	0.307 (Ω)
Exponential zone [voltage, capacity]	216.07 (V), 0.319 (Ah)

Finally, Table 8.7 shows the power conditioning units' parameters include DC-DC and DC-ac converters.

Table 8.7 - Power conditioning units' parameters

DC-DC Converter	
Resistance	0.2 (Ω)
Capacitance	3300 (μF)
Inductance	200 (μH)
DC-AC Inverter	
AC line RMS voltage	120 (V)
AC line frequency	60 (Hz)
Output port series resistance	0.8 (Ω)
Switching loss current	0.04 (A)

In the simulation process, the aim is to observe the proposed system behaviour under different operating condition. The solar radiation, panel temperature, wind speed and user load profiles are all used to test the performance of the proposed hybrid system model, as shown in Figure 8.12 (a), (b), and (c).
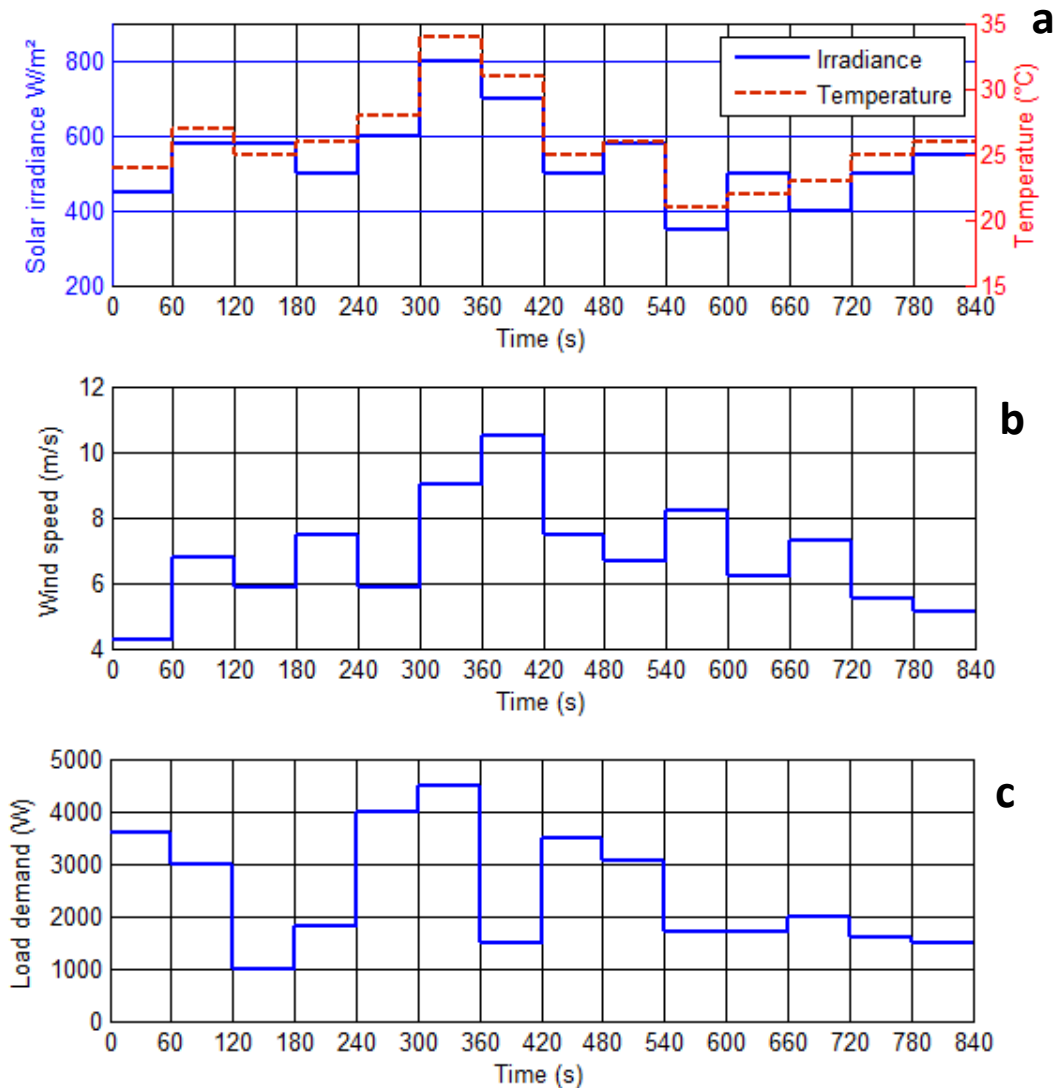
Figure 8.12 (a) Solar radiation and panel temperature profiles **(b)** Wind speed profile **(c)** Load demand profile.

As shown, simulation results are obtained for the time interval between 0 and 840 sec. The power demand profile has a significant effect on determining the EMS. In this study, a practical load profile for two family members in resident application (Dursun & Kilic 2012) is established, as shown in Figure 8.12 (c). From this load profile it is

evident that the average power demand is less than 2.4kW. The load profile during peak load periods (0 to 120 sec, 240 to 360 sec, and from 420 to 540 sec) varies from 3 to 4.5kW, as illustrated in Figure 8.12 (c). However, due to weather condition, the output power of the PV/WT system varies from 1.3 to 3.5kW, as shown in Figure 8.13. Therefore, a PEM fuel cell with a reversible ESS was added to the renewable power system. The battery bank system is capable of sustaining the extra load of 1.3kW for 1h during peak load demand periods. While, the 6kW PEMFC can meets the remaining extra power and protect the battery from over-discharging.
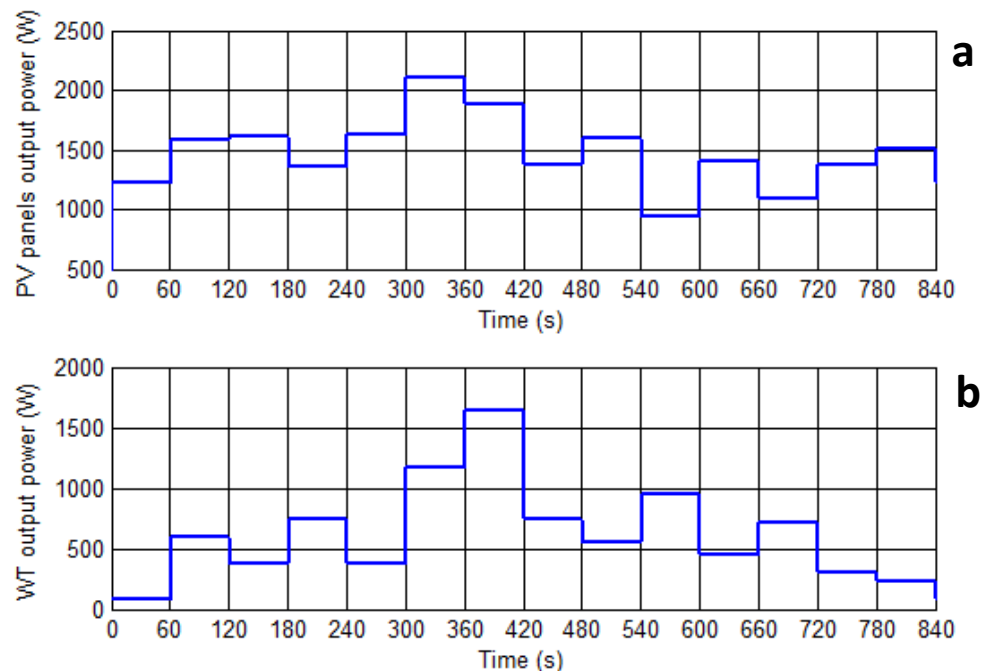
Figure 8.13 (a) Total power of the solar power plant **(b)** Total power of the wind Turbine

Moreover, according to the proposed EMS algorithm, which shown in Section 7.4, battery SOC level is determining the operation of the PEM fuel cell, during peak load demand periods. Hence when the:

- SOC is low ($\leq 40.5\%$), the remaining energy is satisfied by the PEMFC stack, and the extra power will be used to charge the battery (SOC goes high).

- SOC is high ($\geq$ 80%), the remaining energy is satisfied by the battery bank only. At this time, the battery bank discharge current is very high and the battery bank terminal voltage drops significantly.

- SOC is between 40.5% and 80%, the remaining energy is satisfied by either the battery bank or by the hybrid PEMFC/battery system.

Therefore in the following subsections two cases have been tested during the simulation. The rated power of the PV/WT system is 6kW; the solar radiation, wind speed and user load profiles are the same for the three cases (Figure 8.12).

8.3.1 First case

The initial SOC of the battery storage is 33%. Hence, when the SOC is low (time intervals 0 to 120sec), the peak load demand is satisfied by the PEMFC stack, and the extra power will be used to charge the battery (SOC goes high), as shown in Figure 8.15. However, during that time, the PEMFC stack power is very high. Consequently, in order to maintain the stack temperature stable and equal to the stack operating temperature (65°C), a fuzzy logic temperature controller has been added, as shown in Section 7.5. Figure 8.16 shows the stack temperature during that period.
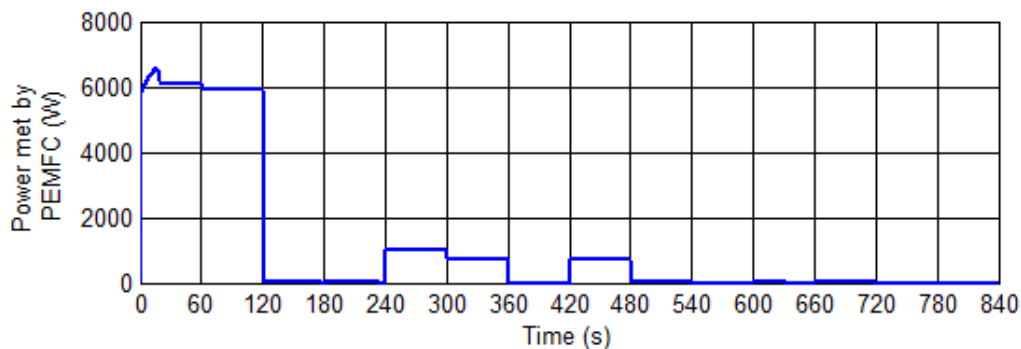
Figure 8.15 - Power satisfied by PEMFC
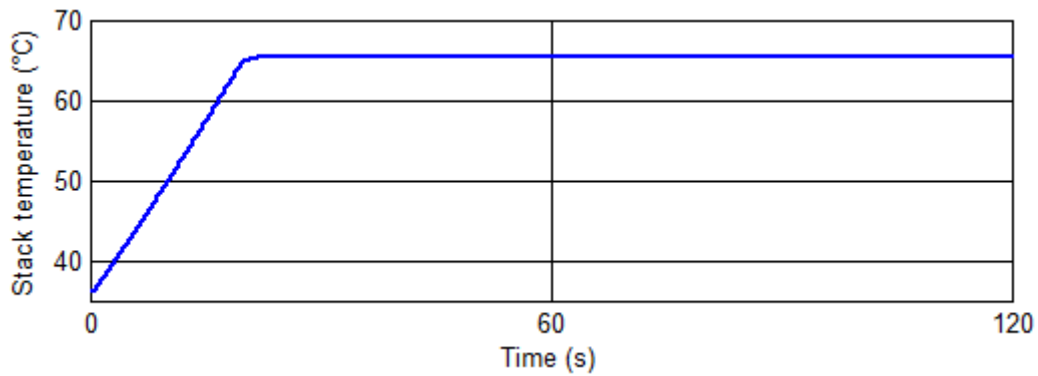
Figure 8.16 – PEMFC stack operating temperature

On the other hand, when the SOC is above 40.5%, then the remaining energy is satisfied by either the battery bank (480 to 540sec, and from 660 to 720sec) or by the hybrid PEMFC/battery system (240 to 360sec, and from 420 to 480sec)[27], as shown in Figures 8.15 and 8.17
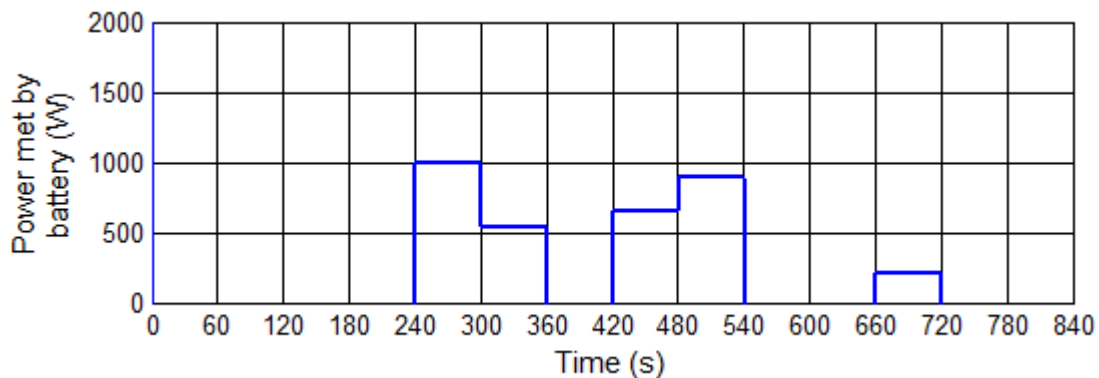
Figure 8.17 - Power satisfied by battery

The power met by the battery introduces a current change at the battery bank terminal as depicted in Figure 8.18 (a). When the battery current is positive (time intervals 240 to 360sec, 420 to 540sec, and from 660 to 720sec), energy is transferred to the load by the battery bank. When the battery current is negative, the battery bank is recharged. Figure 8.18 (b), shows the SOC of the battery during the simulation.

---

[27] To increase the life time of the back-up system, both FC and battery system contributes to fulfil the remaining energy demand needed. This mode is suitable for high power demand (hybrid mode); see Section 7.4.

Simulation Results & Discussion   **153**
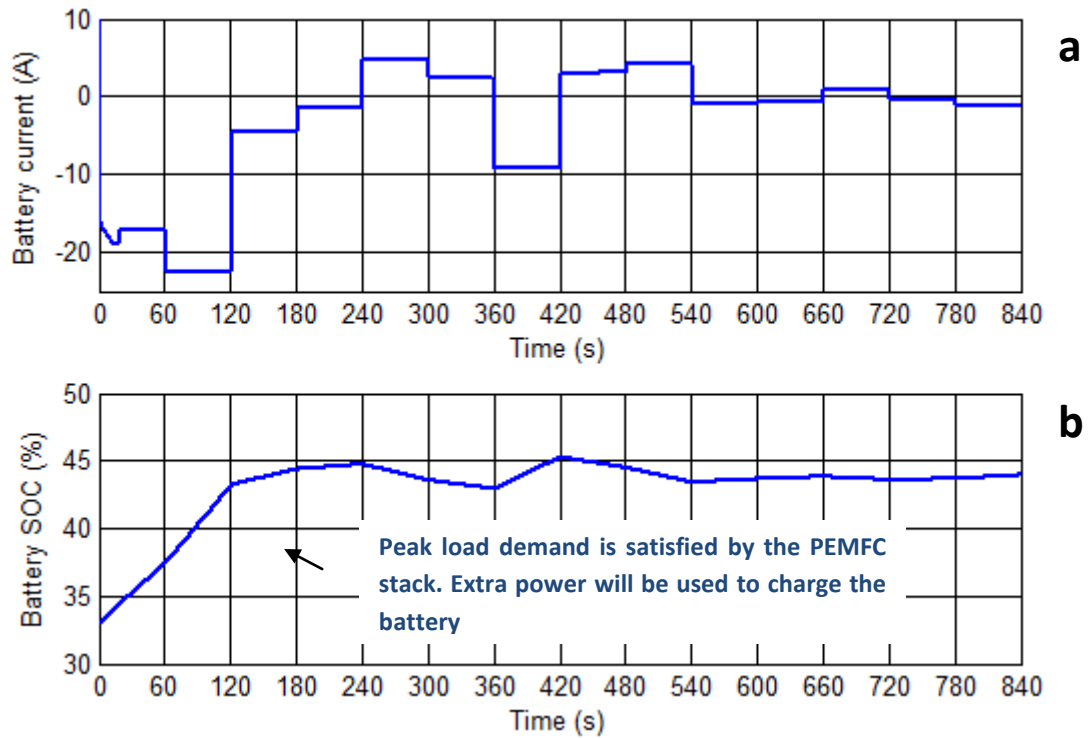
Figure 8.18 - System response during the first case (a) Battery current change with respect to load profile (b) Battery SOC

8.3.2 Second case

The initial SOC of the battery storage is 89%. The system response to changes in solar irradiance and load profile is presented in the following figures.

The peak load demand is satisfied by the battery bank as shown in Figure 8.19.

During this case the PEMFC is off; since the battery SOC is high.
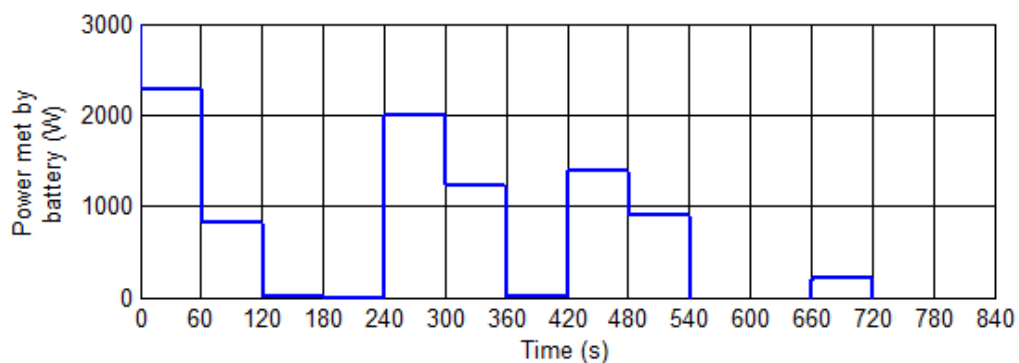
Figure 8.19 - Power satisfied by battery

Figure 8.20(a), shows the variation of the battery bank current between positive and negative according to the required load demand. From Figures 8.19 and 8.13, it is evident that the PV/WT system and battery bank together share this load requirement. Figure 8.20(b), shows the SOC of the battery during the simulation.
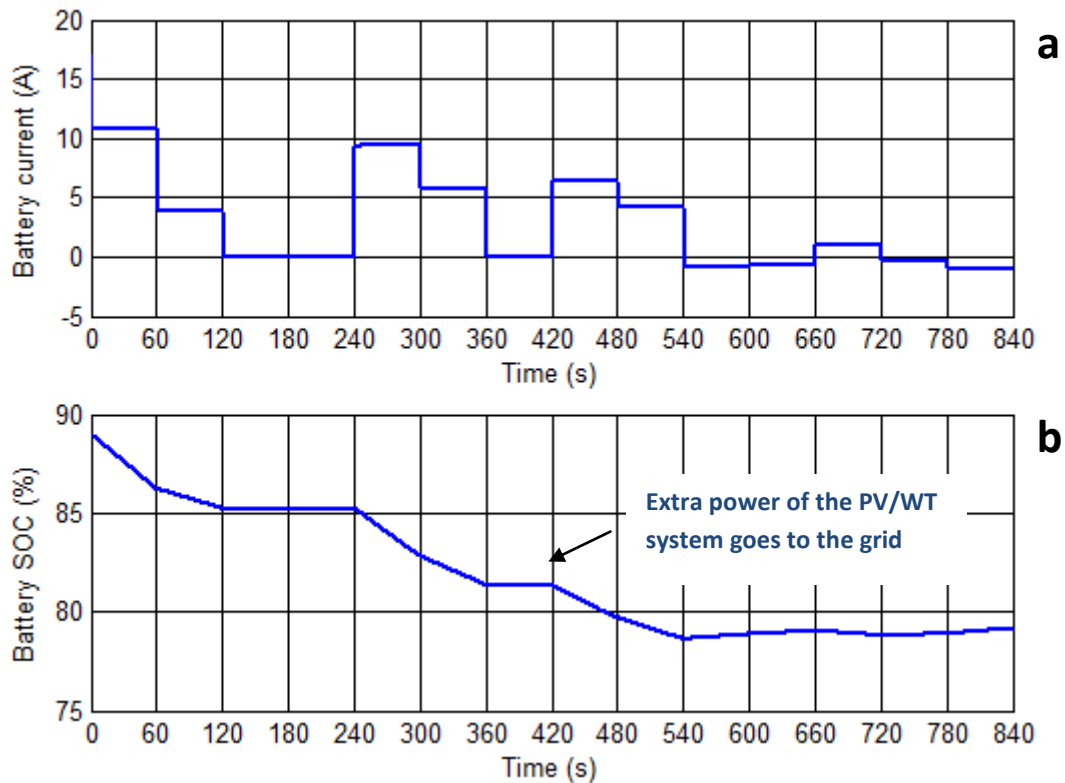
Figure 8.20 - System response during the second case **(a)** Battery current change with respect to load profile **(b)** Battery SOC

Consequently, from the previous Figures (8.19 and 8.20), it's clear that during peak load demand (load power requirement is higher than the power generated by the PV/WT system) the PV/WT system supplies the available power and the battery bank supplies the remaining extra power (0 to 120sec, 240 to 360sec, 420 to 540sec, and from 660 to 720sec). On the other hand, when the produced power by the PV/WT system is more than the required power of load, and the SOC of the battery is below 80%, the extra power of the PV/WT will be used to charge the battery and the SOC goes high (540 to 660sec and from 780 to 840sec). Otherwise, if the SOC is above

80%, based on the EMS it is not in the safe charge mode. In this case the excess power goes to the grid as shown in Figure 8.21(a).
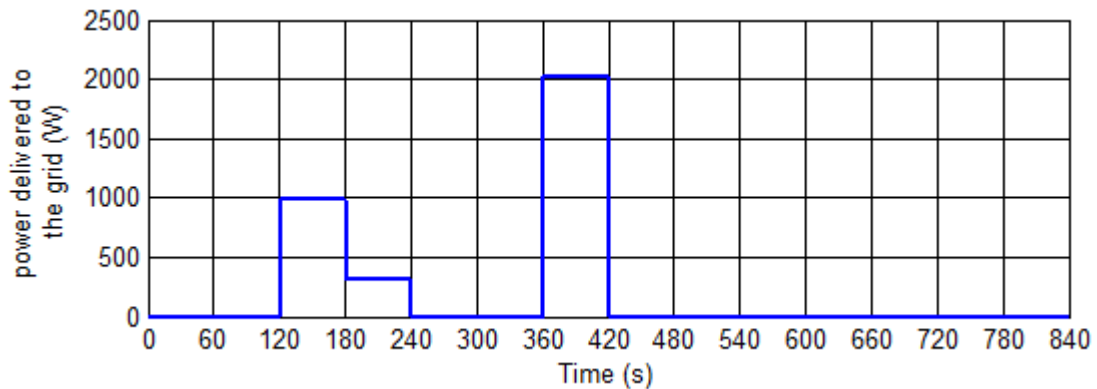
Figure 8.21(a) - Power delivered to the grid

The simulated grid side inverter voltage and current waveforms are shown in Figure 8.21(b). It can be seen that the line current is pure sinusoidal and in phase with the grid voltage.
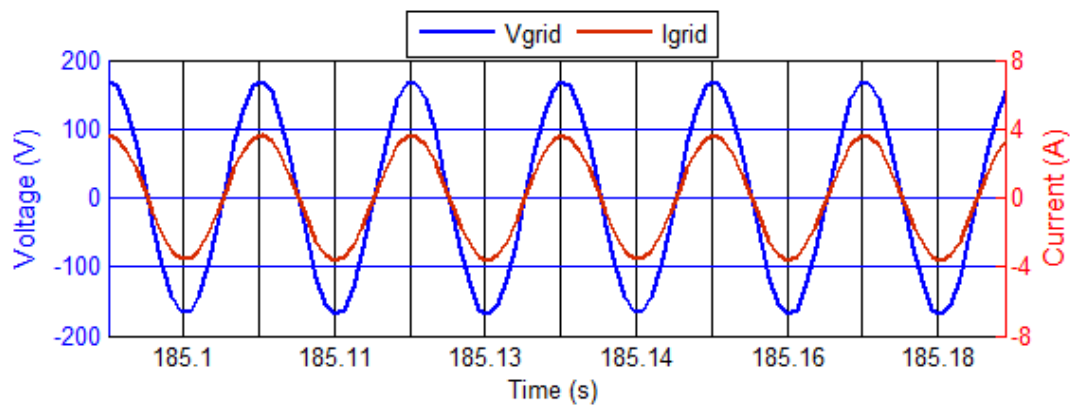
Figure 8.21(b) - Voltage and current waveforms in the grid side

From the first and second cases the results show that the proposed model and its control strategy illustrate excellent performance under various operating conditions, and maintained the state-of-charge at a reasonable level.

8.4 Summary

The results presented in this Chapter demonstrate the robustness of the developed hybrid system model. It was found that the hybrid topology exhibits excellent performance under various operating conditions, and maintain the SOC between 40% - 80%. Moreover, to investigate the validity of the proposed MPPT controller system, P&O algorithm with linear and non-linear controllers were provided. The results of the proposed system have low overshoot, short settling time and zero steady-state error compared with those of the P&O controller results.

On the other hand, this Chapter presents a new approach for PV system monitoring; by calculating the residual difference between the model predicted and the actual measured power parameters. Measurements were taken over 21 month's period; using hourly average irradiance and cell temperature. Good agreement was achieved between the theoretical simulation and the real time measurement taken the online grid connected solar power plant. With this system it is possible to identify PV generation problems quickly and improve long term system health and efficiency.

Chapter 9

Conclusions & Future Work

*Following is a **summary and conclusion** of the proposed **stand-alone hybrid power system**. Also, some of the **future research** that can be done in this subject will be given.*

9.1 Summary

This thesis presents a novel adaptive scheme for energy management in stand-alone hybrid power systems. The proposed management system was designed to manage the power flow between the hybrid power system and energy storage elements in order to satisfy the load requirements based on artificial neural network (ANN) and fuzzy logic controllers.

9.1.1 PV MPPT based on neural network

Tracking the maximum power point (MPP) of a photovoltaic (PV) array is an essential part of a PV system. As such, many maximum power point tracking (MPPT) techniques have been developed and implemented. Among these techniques, hill-climbing MPPT such as perturb and observe (P&O), which is a simple algorithm that does not require previous knowledge of the PV generator characteristics and is easy to implement with analogue and digital circuits. However, the main problem of this technique can be seen when solar radiation rapidly change. In addition, P&O technique may cause many oscillations around the MPP, and this slows down the response of the system. In the literature there are two ways for implementing P&O algorithm: direct method (duty ratio perturbation) and indirect method (reference voltage/current perturbation). In the direct methods, the MPP is searched by continuously perturbing the duty cycle of the DC-DC converter. Although the simplicity is the main feature of this method, it has a slower transient response compared to the indirect method and worse performance at rapidly changing irradiance. In this study, as illustrated in Section 7.3.2, intelligent control technique using artificial neural network was associated to an MPPT controller in order to increase the tracking response and consequently increase the tracking efficiency.

The neural network controller was employed to achieve the MPP for different types of PV panels, based on Levenberg Marquardt learning algorithm. Here, a training set of 2000 cases were obtained from four different PV panels namely: Lorentz mono-crystalline, Sharp's NUS0E3E, BP-485J, and Astronergy CHSM6610P. This training data set covers the different solar radiation and temperature conditions that could possibly take place.

9.1.2 Advanced fuzzy expert system

Frequent power demand variations and unpredictable load profile are unavoidable. Adding to this, the nonlinear subsystems add to the complexity of the structure of hybrid system. Hence, an advanced fuzzy expert system according to the weather variations, load demand and battery SOC, was developed to distribute the power among the hybrid system and to regulate the fuel cell/battery set points to reach best performance. Here, a fuzzy logic controller was used to decide the optimum operation of the fuel cell/battery system. As shown in Figure 7.11, there are five possible operating modes: grid mode, PV-charge mode, fuel cell-charge mode, battery mode, and hybrid mode.

- In grid mode, the excess power of the PV/WT goes to the grid. In this case the back-up power system is off (fuel cell/battery).

- In charge mode, the battery storage is charged by the PV/WT when the load demand is lower than the power generated or/and it's charged by the fuel cell when the SOC is low.

- In battery mode, the power demand is provided only by the battery while the fuel cell is switched off. This mode is suitable for low power demand.

- In hybrid mode, both fuel cell and battery system contributes to fulfil the remaining energy demand needed. This mode is suitable for high power demand.

9.1.3 Dynamic modelling of hybrid system

To develop an overall energy management strategy for the system and to investigate the system performance, dynamic models for the main components in the proposed hybrid system have been developed as mentioned in Chapter 6. The models are as the following:

a) **Photovoltaic model**

A generalized PV model which is representative of all photovoltaic cell, module, and array has been developed as shown in Section 6.1.1. The proposed model takes cell temperature and solar irradiance as its input parameters and outputs the power under different conditions. The P-V characteristic curves of the PV model under different irradiances (at 25 ∘C) are given in Figure 6.5 (a). It is noted from the figure that the higher the irradiance, the larger are the short-circuit current and the open-circuit voltage. As a result, the larger will be the output PV power. Temperature also plays an important role in the PV performance because the two parameters (I_{gc}, I_{ds}) in Equation (3.2). The effect of the temperature on the PV model performance is illustrated in Figure 6.5 (c). It is noted from the figure that the lower the temperature, the higher is the maximum power and the larger the open circuit voltage.

Afterward, the outcome of the developed model is further validated and supported by a case study carried out through monitoring a 28.8kW solar power plant located in central Manchester. Measurements were taken over 21 month's period; using hourly average irradiance and cell temperature. It was found that system

degradation could be clearly monitored by determining the residual (the difference) between the output power predicted by the model and the actual measured power parameters. With this novel approach (Natsheh & Alhussein 2012) it is possible to identify PV generation problems quickly and improve long term system health and efficiency (see Section 8.2).

b) Wind turbine model

The amount of power that a wind turbine can extract from the wind depends on the turbine design. Factors such as the wind speed and the rotor diameter affect the amount of power that a turbine can extract from the wind. The wind turbine was modelled using the mathematical equations shown in Chapter 3. In this model, whereas the inputs are the wind speed, pitch angle, and generator speed, the output is the torque applied to the generator shaft. The pitch angle, as shown in Figure 6.11, is controlled in order to limit the generator output power to its nominal value for high wind speeds.

The built-in SimPowerSystem block model of a DC machine is used as a power generator driven by the wind turbine. The proposed wind turbine DC generator model is implemented as shown in Figure 6.9.

c) Li-Ion battery model

The model of the Li-Ion battery is implemented in MatLab/Simulink using several standard Simulink blocks as well as some of the SimPowerSystem blocks. In this model, the output is a vector containing three signals: state-of-charge, battery current and voltage. The model is implemented as shown in Figure 6.13.

In previous work (Tremblay & Dessaint 2009), the dynamic behaviour of the battery model has been validated with respect to current variation and the battery

SOC. Results shows that the error between the real voltage and the simulated voltage is within 5%, for SOC between 20% - 100%, during the discharge and the charge mode. When the SOC decreases below 20%, the error of the simulation model is around 10%. This is quite acceptable, since the desired SOC limits is between 40% - 80%.

d) Proton exchange membrane fuel cell (PEMFC) model

PEMFC is an electrochemical device that converts chemical energy into electrical energy. They show great performance in residential applications due to the low working temperature and fast start-up. In this work, the PEMFC stack model described by Souleman (Souleman et al. 2009), is modified to include a fuzzy temperature controller. Scheme of the temperature control system is presented in Figures 7.22 and 7.23. The main function of this control system was to maintain the temperature stable and equal to the stack operating temperature.

Hence, the modified fuel cell model (see Figure 6.16) combines the features of chemical and electrical models, and it has two important dynamic properties. These properties are fuel/air flow and temperature. State of these dynamic properties will change according to any disturbances on surrounding operating conditions and load changes.

As shown in Figure 8.11, the proposed hybrid system model has been implemented using the MatLab/Simulink software package, and designed with dialog boxes like those used in the Simulink block libraries. Such a model is easy to be used for the implementation on MatLab/Simulink modelling and simulation platform, especially, when there is now a solar-wind-hydrogen energy system model which can be used for modelling, analysing and teaching in the field of renewable energy conversion systems.

9.2 Conclusion

The analysis of simulation results has shown that the adaptive algorithm developed is suitable for stand-alone hybrid power systems. This control algorithm is capable of:

- Extracting maximum power from the PV panels with tracking efficiency exceed 94.5%.

- Splitting the power between the power sources to sustain the efficiency of the system.

  - Regulating the PEMFC on/off status according to external environmental changes and to load demand expectation

- Optimizing the generating performance of the PEMFC by maintaining the temperature stable and equal to the stack operating temperature (e.g. 65%).

Simulation results were obtained by developing a detailed dynamic hybrid system model. Real-time measured parameters and practical load profile for two family members in resident application have been used as inputs for the developed algorithm. Results show that the proposed hybrid system exhibits excellent performance under various operating conditions, and maintained the battery SOC at a reasonable level 40% - 80%. Hence, from the results, it's clear that during peak load demand when the SOC is:

- Low, the remaining required energy is satisfied by the PEMFC stack, and the extra power will be used to charge the battery.

- High, the remaining required energy is met by the battery bank only.

- Medium, based on the PV/WT power level, the remaining required energy is satisfied by either the battery bank or by the hybrid PEMFC/battery system.

On the other hand, simulation results show that when the produced power by the PV/WT system is more than the required power of load, and the SOC of the battery is

below 80%, the extra power of the PV/WT will be used to charge the battery and the SOC goes high. Otherwise, if the SOC is above 80%, based on the EMS it is not in the safe charge mode. In this case the excess power goes to the grid.

Moreover to investigate the validity of the proposed MPPT controller system, P&O algorithm with two different controllers' techniques, linear PI and non-linear passivity-based controller (PBC) were provided. The comparison is made in a system comprises: PV panels, MPPT control, battery, and DC-DC converter. The comparison demonstrate that linear PI controller proven it's instability in handling various (rapidly) changes in solar radiation; although it was only from $750W/m^2$-$900W/m^2$. While non-linear PBC even if it has a few power fluctuations, the simulation results of the proposed neural network controller shows better transient performance, with low overshoot, short settling time and zero steady-state error.

9.3 Contribution to knowledge

This research work has made the following contributions to knowledge:

- Developed an automated tool for optimizing hybrid power system performance, such as that used in smart-house or electric car applications.

- Presents a new approach for PV system monitoring, by calculating the residual difference between the model predicted and the actual measured power parameters.

- Developed an adaptive scheme for energy management in stand-alone hybrid power systems based on artificial neural network and fuzzy logic controllers.

9.4 Future Works

Although the proposed system was proven, by simulation, there are still many areas which could benefit from additional research and development activity before this technology can be feasible for industrial application. Most of these areas are targeted at improving efficiency and increasing overall energy yields. Among them, besides constructing a hardware prototype, photovoltaic/wind turbine monitoring systems.

Photovoltaic or wind turbine system owners must be assured that their system operates well and that their investment will pay off. Regardless of which system they operate, plant parks, individual systems or private systems, failures and defects must be detected and repaired immediately. This could be achieved by and only by optimizing these system performance and eliminate any degradation at early stage.

In this study a novel approach has been proposed for PV system monitoring (Natsheh & Albarbar, 2011); by calculating the residual difference between the model predicted and the actual measured power parameters (see Section 8.2). However, this approach can be enhanced by including the artificial intelligent. A feed-forward back-propagation neural network model can be trained to predict the generated power of PV or WT. Then the residual different can be calculated using sensors and microcontroller. Moreover, in case the residual exceeded the healthy threshold a text message can be sent from the microcontroller to the owner handset.

References

Ahmed, N.A., Al-Othman, A.K., & Al-Rashidi, M.R. (2011) *Development of an Efficient Utility Interactive Combined Wind/Photovoltaic/Fuel Cell Power System with MPPT and DC Bus Voltage Regulation*, Electric Power Systems Research, 81, (5), pp. 1096–1106

Ahmed, N.A., Miyatake, M., & Al-Othman, A.K. (2008) *Power Fluctuations Suppression of Standalone Hybrid Generation Combining Solar PV/Wind Turbine and Fuel Cell Systems*, Energy Conversion and Management, 49, (10), pp. 2711-2719.

Al-Alawi, A., Al-Alawi, S.M., & Islam, S.M. (2007) *Predictive Control of an Integrated PV-Diesel Water and Power Supply System Using an Artificial Neural Network*, Renewable Energy, 32, (8), pp. 1426-1439.

Bagul, A.D., Salameh, Z.M., & Borowy, B. (1996) *Sizing of a Stand-Alone Hybrid Wind Photovoltaic System using a Three-Event Probability Density Approximation*, Solar Energy, 56, (4), pp. 323–35.

Baring-Gould, E.I., Manwell, J.F., & Van Dijk, V.A.P. (1996) *HYBRID 2: The Hybrid Power System Simulation Model,* NREL.

Battery University [BU], Retrieved Nov 11, 2012, from http://batteryuniversity.com/learn/article/whats_the_best_battery

Behave, A.G., (1999) *Hybrid Solar–Wind Domestic Power Generating System: a Case Study*. Renewable Energy, 17, (3), pp. 355–358.

Black Global Enterprises [BGE], Retrieved May 6, 2012, from http://photovoltaic-solar-power.com/apps/home_apps/Roof%20Tiles/index.html

Bodine Electric Company [BEC], Retrieved Feb 6, 2013, from http://gearmotorblog.wordpress.com/2013/01/15/pmdc-gearmotors-dc-motors/

Borowy, B.S., & Salameh, Z.M. (1994) *Optimum Photovoltaic Array Size for a Hybrid Wind/ PV System*, IEEE Trans. Energy Conversion, 9, (3), pp. 482–488.

Borowy, B.S., & Salameh, Z.M. (1996) *Methodology for Optimally Sizing the Combination of a Battery Bank and PV Array in a Wind/PV Hybrid System*, IEEE Trans. Energy Conversion, 11, (2), pp. 367–373.

Bucciarelli Jr, L.L. (1984) *Estimating Loss-of-Power Probabilities of Standalone Photovoltaic Solar Energy Systems*, Solar Energy, 32, (2), pp. 205–209.

Caudill, M. (1991) *Neural Network Training Tips and Techniques*, AI Expert, 6, (1), pp. 56-61.

Celik, A.N. (2003) *Techno-Economic Analysis of Autonomous PV–Wind Hybrid Energy Systems using Different Sizing Methods*, Energy Conversion and Management, 44, (12), pp. 1951-1968.

Chayawatto, N., Kirtikara, K., Monyakul, V., Jivacate, C., & Chenvidhya, D. (2009) *DC–AC Switching Converter Modelling of a PV Grid Connected System under Islanding Phenomena*, Renewable Energy, 34, (12), pp. 2536-2544.

Coulton, Retrieved Jan 16, 2013, from http://www.coulton.com/QandA_controller

Cox, E. (1999) *The Fuzzy Systems Handbook: a Practitioner's Guide to Building*, *using, and Maintaining Fuzzy Systems*, 2nd edn., Academic Press, San Diego, CA.

Das, D., Esmaili, R., Longya, X., & Nichols, D. (2005) *An Optimal Design of a Grid Connected Hybrid Wind/Photovoltaic/Fuel Cell System for Distributed Energy Production*, 31st Annual Conference of IEEE, Industrial Electronics Society, Raleigh, NC.

Dell, R.M., & Rand, D.A.J. (2001) *Understanding Batteries*, Royal Society of Chemistry.

Di Bucchianico, A. (2008) *Coefficient of Determination (R^2) -* Encyclopedia of Statistics in Quality and Reliability, John Wiley and Sons, Inc.

Dihrab, S., & Sopian, K. (2010) *Electricity Generation of Hybrid PV/Wind Systems in Iraq*, Renewable Energy, 35, (6), pp. 1303-1307.

Dursun, E., & Kilic, O. (2012) *Comparative Evaluation of Different Power Management Strategies of a Standalone PV/Wind/PEMFC Hybrid Power System*, Electrical Power and Energy Systems, 34, (1), pp. 81-89.

Elgendy, M.A., Zahawi, B., & Atkinson, D.J. (2012) *Assessment of Perturb and Observe MPPT Algorithm Implementation Techniques for PV Pumping Applications*, IEEE Trans. Sustainable Energy, 3, (1), pp. 21-33.

Elhadidy, M.A., & Shaahid, S.M. (2000) *Parametric Study of Hybrid (Wind + Solar + Diesel) Power Generating Systems*, Renewable Energy, 21, (2), pp. 129–139.

El-Sharkh, M.Y., Rahman, A., Alam, M.S., Byrne, P.C., Sakla, A.A., & Thomas, T. (2004) *A Dynamic Model for a Standalone PEM Fuel Cell Power Plant for Residential Applications*, 138, (1–2), pp. 199–204.

Energy Efficiency and Renewable Energy [EERE], Retrieved Nov 15, 2012, from http://www1.eere.energy.gov/hydrogenandfuelcells/fuelcells/fc_types.html

Erdem, Z.B. (2010) *The Contribution of Renewable Resources in Meeting Turkey's Energy-Related Challenges*, Renewable and Sustainable Energy Reviews, 14, (9), pp. 2710-2722.

Erickson, R.W., Maksimovic, D. (2000) *Fundamentals of Power Electronics*, 2nd edn., Springer.

Esram, T., Urbana, I.L., Chapman, P.L. (2007) *Comparison of Photovoltaic Array Maximum Power Point Tracking Techniques*, IEEE Trans. Energy Conversion, 22, (2), pp. 439 – 449.

European Photovoltaic Industry Association [EPIA], Retrieved Aug 9, 2012, from http://www.solarplaza. com/article/solar-photovoltaics-2010-a-record-year-in-all-res

Four Winds Energy [FWE], Retrieved Sep 22, 2012, from http://www.four-winds-energy.com/wind.html

Gipe, P. (1993). *Wind Power for Home & Business*. Chelsea Green Publishing Company.

Gipe, P. (2004). *Wind Power: Renewable Energy for Home, Farm, and Business*. Chelsea Green Publishing Company.

Gordon, J.M. (1987). *Optimal Sizing of Standalone Photovoltaic Solar Power Systems, Solar Cells*, 20, (4), pp. 295–313.

Gow, J.A., & Manning, C.D. (1999) *Development of a photovoltaic array model for use in power-electronics simulation studies*, Electric Power Applications, IEE Proceedings, 146, (2), pp. 193-200.

Guyon, I.P. (1991) *Applications of Neural Networks to Character Recognition*, International Journal of Pattern Recognition and Artificial Intelligence, 5, (1-2), pp. 353–382.

Hagan, M., & Bemuth, B. (1996) *Neural Network Design*, PWS Pub. Co., Boston, USA.

Hajizadeh, A., & Golkar, M.A. (2007) *Intelligent Power Management Strategy of Hybrid Distributed Generation System*. International Journal of Electrical Power & Energy Systems, 29, (10), pp. 783–795.

Hau, E. (2006). *Wind Turbines: Fundamentals, Technologies, Application, Economics*, 2nd edn. Springer, Berlin, Germany.

Haykin, S. (1998) *Neural Networks: a Comprehensive Foundation*, Prentice Hall.

How Stuff Works [HSW], Retrieved Nov 11, 2012, from http://electronics.howstuffworks.com/everyday-tech/lithium-ion-battery1.htm

H-Tec Education [HTE], Retrieved May 6, 2012, from http://www.h-tec.com/fileadmin/content/edu/Lehrmaterialien/Transparencies.pdf

Hugo, E.M.L. (2007) *Maximum Power Tracking Control Scheme for Wind Generator Systems, MSc* Thesis, Texas A&M University.

Hwas, A., & Katebi, R. (2012) *Wind Turbine Control using PI Pitch Angle Controller,* IFAC Conference on Advances in PID Control, Brescia, Italy.

Ipsakis, D., Voutetakis, S., Seferlis, P., Stergiopoulos, F., & Elmasides, C. (2009) *Power Management Strategies for a Standalone Power System using Renewable Energy Sources and Hydrogen Storage*, International Journal of Hydrogen Energy, 34, (16), pp. 7081-7095.

Jacobson, M.Z., & Delucchi, M.A. (2009) *A Path to Sustainable Energy by 2030*, Scientific American, 301, (5), pp. 58–65.

Jacobson, M.Z., & Delucchi, M.A. (2011) *Providing all Global Energy with Wind, Water, and Solar Power, Part I: Technologies, Energy Resources, Quantities and Areas of Infrastructure, and Materials*, Energy Policy, 39, (3), pp. 1154–1169.

Kalogirou, S.A. (2004) *Optimization of Solar Systems using Artificial Neural-Networks and Genetic Algorithms*, Applied Energy, 77, (4), pp. 383–405.

Karaki, S.H., Chedid, R.B., & Ramadan, R. (1999) *Probabilistic Performance Assessment of Autonomous Solar–Wind Energy Conversion Systems*, IEEE Trans. Energy Conversion, 14, (3), pp. 766–772.

Kellogg, W.D. et al. (1998) *Generation Unit Sizing and Cost Analysis for Stand-Alone Wind, Photovoltaic and Hybrid Wind/PV Systems*, IEEE Trans. Energy Conversion, 13, (1), pp. 70-75.

Kerr, M.J., & Cuevas, A. (2003) *Generalized Analysis of the Illumination Intensity vs. Open Circuit Voltage of PV Modules*, Solar Energy, 76, (1–3), pp. 263–267.

Khan, M.J., & Iqbal, M.T. (2005) *Pre-feasibility Study of Standalone Hybrid Energy Systems for Applications in Newfoundland*, Renewable Energy 30, (6), pp. 835–854.

Kim, I.S., & Youn, M.J. (2005) *Variable-Structure Observer for Solar Array Current Estimation in a Photovoltaic Power-Generation System*, Electric Power Applications, IEE Proceedings, 152, (4), pp. 953–959.

Kim, M., Sohn, Y.-J., Lee, W.-Y., & Kim, C.-S. (2008) *Fuzzy Control Based Engine Sizing Optimization for a Fuel Cell/Battery Hybrid Mini-Bus*. Journal of Power Sources, 178, (2), pp. 706-710.

Kim, S.K., Jeon, J.H., Cho, C.H., Kim, E.S., & Ahn, J.B. (2009) *Modeling and Simulation of a Grid-Connected PV Generation System for Electromagnetic Transient Analysis*, Solar Energy, 83, (5), pp. 664- 678.

Koutroulis, E. et al. (2006) *Methodology for Optimal Sizing of Standalone Photovoltaic/Wind-Generator Systems using Genetic Algorithms*, Solar Energy 80, (9), pp. 1072–1088.

Larminie, J., & Dicks, A. (2003) *Fuel Cell Systems Explained*, 2nd edn., John Wiley & Sons Ltd.

Li, X., Xu, L., Hua, J., Lin, X., Li, J., & Ouyang, M. (2009) *Power Management Strategy for Vehicular-Applied Hybrid Fuel Cell/Battery Power System*, Journal of Power Sources, 191, (2), pp. 542-549.

Lubosny, Z. (2003) *Wind Turbine Operation in Electric Power Systems,* Springer, *Berlin*, Germany.

Mahmoudi, H., Abdul-Wahab, S.A., Goosen, M.F.A., Sablani, S.S., Perret, J., & Ouagued, A. (2008) *Weather Data and Analysis of Hybrid Photovoltaic-Wind Power Generation Systems Adapted to a Seawater Greenhouse Desalination Unit Designed for Arid Coastal Countries*. Desalination, 222, (1-3), pp. 119-127.

Mamdani, E.H., & Assilian, S. (1975) *An Experiment in Linguistic Synthesis with a Fuzzy Logic Controller*, International Journal of Man–Machine Studies, 7, (1), pp. 1–13.

Manwell, J.F., McGowan, J.G., & Rogers, A.L. (2002) *Wind Energy Explained: Theory, Design and Application*, John Wiley & Sons Ltd.

 Markvart, T. (1996) *Sizing of Hybrid PV–Wind Energy Systems*. Solar Energy, 59, (4), pp. 277–281.

Mathew, S. (2006) *Wind Energy Fundamentals Resources Analysis and Economics*, Springer.

MathWorks, Documentation Center, 2012
http://www.mathworks.co.uk/help/physmod/powersys/ref/dcmachine.html

Miller, R. (2002) *Worlds Beyond the Sun*, Twenty-First Century Books.

Mohamed, F.A., and Koivo, H.N. (2010) *System Modelling and Online Optimal Management of Micro-Grid using Mesh Adaptive Direct Search*, International Journal of Electrical Power and Energy Systems, 32, (5), pp. 398–407.

Muljadi. E., & Butterfield, C.P. (2001) *Pitch-Controlled Variable-Speed Wind Turbine Generation,* IEEE Trans. Industry Applications, 37, (1), pp. 240– 246.

Musgrove, P. (1976) *Windmills Change Direction*, New Scientist, 72, ISSN 0262-4079.

National Renewable Energy Laboratory [NREL], Retrieved May 6, 2012, from
http://www.nrel.gov/solar/

Natsheh, E.M., & Albarbar, A. (2013) *Hybrid Power Systems Energy Controller Based on Neural Network and Fuzzy Logic*, Smart Grid and Renewable Energy, 4, (2), pp. 187-197.

Natsheh, E.M., & Albarbar, A. (2012) *Solar Power Plant Performance Evaluation: Simulation and Experimental Validation*, Journal of Physics: Conference Series, 364, (1), pp. 1-13.

Natsheh, E.M., & Albarbar, A. (2011) *Photovoltaic Model with MPP Tracker for Standalone /Grid-Connected Applications*, IET Conference on Renewable Power Generation, Edinburgh, UK.

Natsheh, E.M., Albarbar, A., & Yazdani, J. (2011) *Modelling and Control for Smart Grid Integration of Solar/Wind Energy Conversion System*, 2nd IEEE PES International Conference and Exhibition on Innovative Smart Grid Technologies, Manchester, UK.

Negnevitsky, M. (2004) *Artificial Intelligence: a Guide to Intelligent Systems*, Addison Wesley, Essex.

Newquay Weather Station [NWS], Retrieved Sep 15, 2012, from
http://www.newquayweather.com/wxsolarmap.php

Nishioka, K. et al. (2003) *Field-Test Analysis of PV System Output Characteristics Focusing on Module Temperature*, Solar Energy Mater PV Modules, 75, (3–4), pp. 665–671.

Notton, G., Muselli, M., Poggi, P., & Louche, A. (1996) *Autonomous Photovoltaic Systems: Influences of Some Parameters on the Sizing: Simulation Time-Step, Input and Output Power Profile*, Renewable Energy, 7, (4), pp. 353–369.

Onar, O.C., Uzunoglu, M., & Alam, M.S. (2008) *Modelling, Control and Simulation of an Autonomous Wind Turbine/PV/Fuel Cell/Ultra-Capacitor Hybrid Power System*, Journal of Power Sources, 185, (2), pp. 1273–1283.

Onar, O.C., Uzunoglua, M., & Alam, M.S. (2006) *Dynamic Modeling, Design and Simulation of a Wind/Fuel Cell/Ultra-Capacitor-Based Hybrid Power Generation System. Journal of Power Sources*, 161, (1), pp. 707-722.

Patel, M. (2006) *Wind and Solar Power Systems*, 2nd edn, Taylor & Francis Group.

Phang, J.C.H., Chan, D.S.H., & Philips, J.R. (1984) *Accurate Analytical Method for the Extraction of Solar Cell Model Parameter*, IEEE Electronics Letters, 20, (10), pp.406-408.

Price, T.J. (2004) *Blyth, James (1839–1906), Oxford Dictionary of National Biography* (Online ed.), Oxford University Press. doi:10.1093/ref:odnb/100957

Qiuli, Y., Srivastava, A.K., Choe, S.-Y., Gao, W. (2006) *Improved Modeling and Control of a PEM Fuel Cell Power System for Vehicles*, SoutheastCon, 2006. Proceedings of the IEEE, pp. 331 - 336.

Ramirez-Rosado, I.J., & Bernal-Agustin, J.L. (1998) *Genetic Algorithms Applied to the Design of Large Power Distribution Systems,* IEEE Trans. Power System, 13, (2), pp. 696-703.

Reddy, K.N., & Agarwal, V. (2007) *Utility Interactive Hybrid Distributed Generation Scheme with Compensation Feature*. IEEE Trans. Energy Conversion, 22, (3), pp. 666-673.

Reichling, J.P., & Kulacki, F.A. (2008) *Utility Scale Hybrid Wind-Solar Thermal Electrical Generation: a Case Study for Minnesota. Energy*, 33, (4), pp. 626-638.

Renewable Energy Policy Network for the 21st Century [REN21], Retrieved April 25, 2012, from http:// sustainablejohn.com/?p=213

Renewable Solution [RES]*,* Retrieved Sep 26, 2012, from http://www.renewablesolutionconsultancy.co.uk/index.php/renewable-energy-training/14-training-information/69-wind-turbine-facts

Richmond, R. (2012) *The use of Lithium Ion Batteries for Off-Grid Renewable Energy Applications*, http://www.righthandeng.com/rhe_mref_2012_li-ion.pdf

Rivera, M.R. (2008) *Small Wind / Photovoltaic Hybrid Renewable Energy System Optimization,* MSc Thesis, University of Puerto Rico.

Rodolfo, D.-L, & José, L.B.-A. (2005) *Design and Control Strategies of PV-Diesel Systems using Genetic Algorithms,* Solar Energy, 79 (1), pp. 33-46.

Rogowsky, R.A. (2009) *Wind Turbines Industry and Trade Summary*, Retrieved May 9, 2011, from http://www.readbag.com/usitc-publications-332-its-2

Runtz, K.J., Lyster, M.D. (2005) *Fuel Cell Equivalent Circuit Models for Passive Mode Testing and Dynamic Mode Design*, Canadian Conference on Electrical and Computer Engineering, Saskatoon, Sask.

Sandia National Laboratories (1995) *Standalone Photovoltaic Systems: a Handbook of Recommended Design Practices*, Daystar, Inc. Las Cruces, New Mexico.

Serway, R.A., & Vuille, C. (2011) College Physics, 9th ed. Brooks/Cole.

Shakya, B.D., Aye, L., & Musgrave, P. (2005) *Technical Feasibility and Financial Analysis of Hybrid Wind– Photovoltaic System with Hydrogen Storage for Cooma*, International Journal of Hydrogen Energy, 30, (1), pp 9–20.

Sharaf, A.M., Elbakush, E., & Altas, I.H. (2007) *Novel Control Strategies for Photovoltaic Powered PMDC Motor Drives*, IEEE Electrical Power Conference, Montreal, Quebec, Canada.

Shepherd, C.M. (1965) *Design of Primary and Secondary Cells - Part 2: An equation describing battery discharge*, Journal of Electrochemical Society, 112, pp. 657-664

Siegfried, H. (1998) *Grid Integration of Wind Energy Conversion Systems*, John Wiley & Sons Ltd, ISBN 0-471-97143-X.

Sills, B. (2011) *Solar May Produce Most of World's Power by 2060, IEA Says,* Retrieved April 25, 2012, from http://www.bloomberg.com/news/2011-08-29/solar-may-produce-most-of-world-s-power-by-2060-iea-says.html

Solar Energy International (2007) *Photovoltaic Design and Installation Manual*, New Society Publishers.

Souleman, N.M., Tremblay, O., & Dessaint, L.-A. (2009) *A Generic Fuel Cell Model for the Simulation of Fuel Cell Power Systems,* IEEE Power & Energy Society General Meeting, pp. 1-8.

Sugeno, M. (1985) *Industrial Applications of Fuzzy Control*, North-Holland, Amsterdam

Tina, G., Gagliano, S., & Raiti, S. (2006) *Hybrid Solar/Wind Power System Probabilistic Modelling for Long-Term Performance Assessment*. Solar Energy, 80, (5), pp. 578-588.

Tofighi, A., & Kalantar, M. (2011) *Power Management of PV/Battery Hybrid Power Source via Passivity-Based Control*, Renewable Energy, 36, (9), pp. 2440-2450.

Tremblay, O., & Dessaint, L.-A. (2009) *Experimental Validation of a Battery Dynamic Model for EV Applications, World Electric Vehicle Journal,* 3, ISSN 2032-6653 2009 AVERE, EVS24 Stavanger, Norway.

Tremblay, O., Dessaint, L.-A., & Dekkiche, A.-I. (2007) *A Generic Battery Model for the Dynamic Simulation of Hybrid Electric Vehicles*, IEEE Vehicle Power and Propulsion Conference, Arlington, TX.

Tsai, H.L. (2010) *Insolation-Oriented Model of Photovoltaic Module using Matlab/Simulink*, Solar Energy, 84, (7), pp. 1318-1326.

Underwood, C.P. (2005) *A Fuzzy Logic Controller for Temperature Control of Air Handling Plant*, CSTB 3rd Matlab/Simulink Building and HVAC Simulation Workshop, Paris.

Villalva, M.G., Gazoli, J.R., & Filho, E.R. (2009) *Comprehensive Approach to Modeling and Simulation of Photovoltaic Arrays*, IEEE Trans. Power Electronics, 24, (5). pp 1198–1208.

Virginia Tech [VT], Retrieved Nov 11, 2012, from
http://www.ece.vt.edu/news/ar08/livinglab.html

Wang, C., & Nehrir, M.H. (2008) *Power Management of a Stand-alone Wind/PV/Fuel Cell Energy System*. IEEE Trans. Energy Conversion, 23, (3), pp. 957-967.

Wang, Y., Chen, K.S., Mishler, J., Cho, S.C., and Adroher, X.C. (2011) A *Review of Polymer Electrolyte Membrane Fuel Cells: Technology, Applications, and Needs on Fundamental Research*, Applied Energy, 88, (4), pp. 981-1007.

Wind Turbine Swept Area [WTSA], Retrieved Oct 6, 2012, from
http://www.daviddarling.info/encyclopedia/S/AE_swept_area.html

Wind Energy - The Facts [WindFacts], Retrieved May 9, 2011, from http://www.wind-energy-the-facts.org/en/part-i-technology/chapter-3-wind-turbine-technology/evolution-of-commercial-wind-turbine-technology/growth-of-wind-turbine-size.html

Yang, H.X., & Lu, L. (2004) *Study of Typical Meteorological Years and Their Effect on Building Energy and Renewable Energy Simulations*, ASHRAE Trans, 110, (2), pp. 424–431.

Yang, H.X., Lu, L., & Zhou, W. (2007) *A Novel Optimization Sizing Model for Hybrid Solar–Wind Power Generation System*, Solar energy, 81, (1), pp. 76–84.

Yang, H.X., Zhou, W., & Lou, C.Z. (2009) *Optimal Design and Techno-Economic Analysis of a Hybrid Solar–Wind Power Generation System*, Applied Energy, 86, (2), pp. 163–169.

Yang, H.X., Zhou, W., Lu, L., & Fang, Z.H. (2008) *Optimal Sizing Method for Standalone Hybrid Solar–Wind System with LPSP Technology by using Genetic Algorithm,* Solar Energy. 82, (4), pp. 354–367.

Zadeh, L. (1965) *Fuzzy sets.* Information and Control, 8(3), pp. 338–353.

Zadeh, L. (1973) *Outline of a new approach to the analysis of complex systems and decision processes*, IEEE Trans. Systems, Man, and Cybernetics, SMC-3, (1), pp. 28–44.

Zhang, J., & Lee, J. (2011) *A Review on Prognostics and Health Monitoring of Li-Ion Battery,* Journal of Power Sources, 196, (15), pp. 6007-6014.

Zhou, W., Lou, C., Li, Z., Lu, L., & Yang, H. (2010) *Current Status of Research on Optimum Sizing of Standalone Hybrid Solar–Wind Power Generation Systems,* Applied Energy. 87, (2), pp. 380-389.

Zhou, W., Yang, H.X., & Fang, Z.H. (2007) *A Novel Model for Photovoltaic Array Performance Prediction*, Applied Energy, 84, (12), pp. 1187–1198.

Zhou, W., Yang, H.X., & Fang, Z.H. (2008) *Battery Behaviour Prediction and Battery Working States Analysis of a Hybrid Solar–Wind Power Generation System*, Renewable Energy, 33, (6), pp. 1413–1423.

Zoulias, E.I., & Lymberopoulos, N. (2007) *Techno-Economic Analysis of the Integration of Hydrogen Energy Technologies in Renewable Energy Based Standalone Power Systems*, Renewable Energy, 32, (4), pp. 680–696.

Appendix

Appendix A: Coefficient of determination (R^2)

In statistics, the coefficient of determination (denoted R^2 and pronounced R-square) indicates how well a model predicts future outcomes. R-square can take on any value between 0 and 1, with a value closer to 1 indicating that a greater proportion of variance is accounted for by the model. For example, an R-square value of 0.9234 means that the fit explains 92.34% of the total variation in the data about the average. R-square is defined as follow:

$$R^2 = 1 - \frac{SS_R}{SS_T} \tag{A-1}$$

$$SS_R = \sum_{i=1}^{n} (y_i - f_i)^2 \tag{A-2}$$

$$SS_T = \sum_{i=1}^{n} (y_i - x)^2 \tag{A-3}$$

Where SS_R is the sum of squares of the regression, SS_T is the total sum of squares, y is the original value, x is the mean of the original data, and f is the predicted value.

Appendix B: Articles published from my work

- Intelligent Controller for Managing Power Flow within Standalone Hybrid Power Systems
- Hybrid Power Systems Energy Controller Based on Neural Network and Fuzzy Logic
- Solar Power Plant Performance Evaluation: Simulation and Experimental Validation
- Photovoltaic Model with MPP Tracker for Stand-alone/Grid-Connected Applications
- PV System Monitoring and Performance of a Grid Connected PV Power Station Located in Manchester-UK
- Modelling and Control for Smart Grid Integration of Solar/Wind Energy Conversion System